Title
Genetic Circuits Specifying the Lifetime and Speed of Biological Rhythms

Author
Mushtaqh Ali, Ruhi

Publication Date
2020

Peer reviewed|Thesis/dissertation

UNIVERSITY OF CALIFORNIA

Los Angeles

Genetic Circuits Specifying the Lifetime and Speed of Biological Rhythms

A dissertation submitted in partial satisfaction of the requirements for the degree Doctor of Philosophy in Biological Chemistry

by

Ruhi Mushtaqh Ali

2020

Genetic Circuits Specifying the

Lifetime and Speed of Biological Rhythms

by

Ruhi Mushtaqh Ali

Doctor of Philosophy in Biological Chemistry

University of California, Los Angeles, 2020

Professor Alison R. Frand, Chair

Biological rhythms are ubiquitous in nature. Examples include daily cycles of rest and activity observed among most living organisms and annual cycles of hibernation and migration observed among animals and birds. However, the timekeeping mechanisms that underlie the vast majority of biological rhythms are not well understood. I chose the molting cycle of *C. elegans* as a scientific model to study this problem. *C. elegans* molt 4 times at regular time intervals. Each life stage of the animal consists of the intermolt, a 6 – 8 h period of feeding and locomotion, which is followed by the molt, and a 2 h period of sleep-like quiescence and remodeling of the exoskeleton.

I found that transcriptional–post-transcriptional feedback loops among the conserved nuclear hormone receptor NHR-23 and the *let-7* family of miRNAs govern both the pace of the molting cycle and the total number of molts. The negative feedback loop acts within a genetic

oscillator – the molting cycle timer – to schedule the timing of reiterative molts and within an hourglass timer to schedule the extinction of the molting cycle in adulthood. Knockdown of *nhr-23* slowed down the pace of the cycle, whereas forced expression of *nhr-23* or inactivation of *let-7s* accelerated the pace of the cycle. Interactions between NHR-23 and *let-7s* drive the cyclical expression of *nhr-23*, *let-7s* and scores of downstream targets necessary for the process of molting. I also found that the oscillatory expression of *nhr-23* is dampened in regular increments over the course of larval development; the dampening was dependent upon the activity of *let-7s*. Moreover, forced expression of *nhr-23* was sufficient to trigger extra molts in sexually mature animals. I propose that the incremental dampening brings the levels of *nhr-23* below a critical threshold, preventing entry into another molt. Both the core components and *cis*-regulatory elements of this timekeeping mechanism are conserved from nematodes to humans.

Going further, I identified additional genes and molecules that either act upstream of NHR-23 and *let-7s* or in independent pathways to control the number of molts in *C. elegans*. An as-yet-unidentified hormone is thought to control molting by acting as a ligand for NHR-23. Consistent with this model, I show that dietary supplementation of cholesterol is necessary for forced expression of NHR-23 to trigger extra molts. Thus, cholesterol or a cholesterol-derivative might act as a native ligand for NHR-23. Using a reverse genetics approach, I also uncovered genes that might act in pathways for synthesis of the ligand. My findings might lead to discovery of a hormone that promotes molting in *C. elegans*—a long-standing question in the field. Further examination of how the molecular and genetic interactions uncovered in this thesis regulate the molting cycle could lead to a better understanding of developmental clocks, as well as the circadian clock and related sleep, metabolic and psychiatric disorders.

The dissertation of Ruhi Mushtaqh Ali is approved

John K Kim

Hilary Ann Coller

Tracy L Johnson

Feng Guo

Steven Erik Jacobsen

Alison Renee Frand, Committee Chair

University of California, Los Angeles

2020

For my wonderful husband, Sanjeet Patel, and my loving parents, Myrtle and Mushtaqh Ali.

Thank you for always believing in me.

TABLE OF CONTENTS

ABBREVIATIONS

ATP	Adenosine Triphosphate
BLAST	Basic Local Alignment Search Tool
CBI	Cholesterol Biosynthetic Intermediates
CCG	Clock-Controlled Gene
CGC	*Caenorhabditis* Genetics Center
ChIP	Chromatin Immunoprecipitation
CRY	Cryptochrome
CRISPR	Clustered Regularly Interspersed Short Palindromic Repeats
DSPD	Delayed Sleep Phase Disorder
ECM	Extracellular Matrix
GFP	Green Fluorescent Protein
HSD	Hydroxysteroid Dehydrogenase
let-7s	*let-7* Family of MicroRNAs
LBD	Ligand-Binding Domain
LCS	*let-7* Complementary Sequence
miRNA	microRNA
Mlt	Molting Cycle Defective
MIH	Molt-Inhibiting Hormone
NHR	Nuclear Hormone Receptor
ROR	Retinoid-Related Orphan Receptor
RNAi	RNA-interference
UTR	Untranslated Region

ACKNOWLEDGEMENTS

I would first like to thank Dr. Alison Frand for being a wonderful mentor and for training me to think deeply about scientific questions, design rigorous experiments and communicate the results clearly. Dr. Frand's creativity has been a constant source of inspiration for me. Besides scientific training, Dr. Frand has cared deeply for my health and well-being. The last few months have particularly stressful and Dr. Frand's support never wavered. This past year was also one of my favorites because I got to work so closely with Dr. Frand, both at the bench and on our paper, and I have learnt a lot.

I was fortunate to have been trained by not just one, but two talented scientists. I am deeply grateful to Dr. John Kim for co-mentoring me since 2016. Dr. Kim knew exactly when to be supportive and when to be critical. The Skype meetings with Dr. Kim and Dr. Frand will be among my favorite memories from grad school. Dr. Kim pushed me to use CRISPR when the method had never been done in the lab before, and the resulting reagent became a critical part of my thesis. I also find the way that he approaches a scientific question from a lot of different angles with seemingly endless energy inspiring.

Next, I want to thank my doctoral committee, Dr. Hilary Coller, Dr. Tracy Johnson, Dr. Feng Guo and Dr. Steve Jacobsen, for their constant support and enthusiasm for this project. My committee recognized the findings that were novel and interesting and showed me the right path. The project has grown to what it is today because of their guidance.

I also want to thank the Frand lab alumni – also known as my lab family – Hannah Maul-Newby, Trisha Chong, Chloe Maybrun, Sophie Katz, Jackie Lopez, Sophie Shay and Rita Shrestha. I treasure our discussions—scientific and otherwise! The years that we spent together in the lab were some of my *happiest* and I learned so much from each of them.

I also want to thank Dr. Gabriela Monsalve, a graduate from the Frand lab, who discovered the role of *lin-42* in timing the molting cycle and began to consider auxiliary components of the molting timer. Dr. Monsalve has continued to help with my career over the past six months.

I am grateful to Dr. Ann E. Rougvie for taking the time to thoroughly read and provide invaluable critique for the manuscript detailed in Chapter II.

My husband Sanjeet has a wonderful quality of making any obstacle seem easier to overcome after I speak with him about it. Only he truly has this effect on me.

My mother and father taught me to work hard and persevere and all of my accomplishments are a direct result of their love and support. I am also grateful to my brother Dyan and my Aunt Sheila and Uncle Jai, for always celebrating my little wins with such joy and enthusiasm.

Thanks to Beth and Kenny, for always being interested in the worms and for letting me decompress whenever I needed it. Thanks also to Jenn for being my favorite partner and for always challenging me. I also want to express my gratitude to Keith, Justine and Daniel, for enriching my life deeply

over the last 3 years and for, despite being outside of science, teaching me skills that have transferred over so well.

Chapter II of this thesis was peer-reviewed at *eLife* and is currently under revision. A version appears on the pre-print server BioRxiv. Full copyright is retained by Ruhi Mushtaqh Ali and Alison R. Frand. The author list is as follows: Ruhi Patel, Himani A. Galagali, John K. Kim and Alison R. Frand (corresponding author).

The American Cancer Society (RSG-12-149-01-DDC to ARF) and the National Science Foundation (IOS1258218 to ARF) supported this research.

VITA

EDUCATION

2008–2012 Bachelor of Technology, Biotechnology, Anna University, India.

RESEARCH WORK AND TRAINING

2012–2020 School of Medicine, University of California, Los Angeles

2014–2020: Doctoral Research
Mentor: Dr. Alison Frand
Thesis: Genetic Circuits Specifying the Lifetime and Speed of Biological Rhythms

2013–2014: Pre-doctoral Research
Mentor: Dr. Kathrin Plath
Project: Chromosome folding dynamics during development

2012 Honors Thesis for undergraduate research
National Center for Biological Sciences, TIFR, Bangalore.
Mentor: Dr. Aswin Sai Narain Seshasayee
Title: Regulation of DNA methylation in *E. Coli K-12*

2011 European Bio-Informatics Institute (EMBL-EBI), Hinxton, UK.
Undergraduate Research
Mentor: Dr. Nicholas Luscombe
Project: A Pipeline for ChIP-Seq Data Analysis. ChIP-Seq pipeline

2010 European Bio-Informatics Institute (EMBL-EBI), Hinxton, UK
Undergraduate Research
Mentor: Dr. Nicholas Luscombe
Project: Comparative genomics of antibiotic resistance in bacteria

2009–2010 Undergraduate Research
Department of Biochemistry, Anna University, Chennai
Mentor: Dr. Gautam Pennathur
Project 1: Extraction of lipases from microorganisms in industrial sludge
Project 2: Live cell imaging using fluorescent porphyrin derivatives.

PUBLICATIONS

1. **Patel, R.**, Galagali, H.A., Kim, J.K. and Frand, A.R. (2020). Feedback among a Retinoid-Related Nuclear Receptor and *let-7* miRNAs Controls the Pace and Number of Molts in *C. elegans*. Submitted to *eLife*, peer-reviewed and now under revision.

2. **Mushtaqh Ali, R.**, Cavalli, F.M.G., Vaquerizas, J.M., and Luscombe, N.M. (2012). A

Pipeline for ChIP-Seq Data Analysis. *http://www.epigenesys.eu/en/protocols/bio-informatics/411-a-pipeline-for-chip-seq-data-analysis*

3. Prieto, A.I., Kahramanoglou, C., **Mushtaqh Ali, R.**, Fraser, G.M., Seshasayee, A.S., and Luscombe, N.M. (2012). Genomic analysis of DNA binding and Gene Regulation by Homologous Nucleoid-Associated Proteins IHF and HU in *Escherichia coli K12*. *Nucleic Acids Research*, 40(8):3524-37. PMID: 22180530.

HONORS AND AWARDS

1. Individual Fellowship from the California Institute for Regenerative Medicine (TG2-01169), Declined.

PRESENTATIONS

Oral Presentations

1. **Mushtaqh Ali, R**. Biological Chemistry Monday Seminar Series, UCLA, November 9, 2015.
2. **Mushtaqh Ali, R.** and Frand, A.R. UCLA-MBI Annual Retreat and Research Conference, Lake Arrowhead. April 22–24, 2016.
3. **Mushtaqh Ali, R.** and Frand, A.R. Cold Spring Harbor Laboratory (CSHL) Meeting on Regulatory and Non-coding RNAs, New York. August 23–27, 2016.
4. **Patel, R**. Biological Chemistry Monday Seminar Series, UCLA, May 1, 2017.
5. **Patel, R**. Biological Chemistry Monday Seminar Series, UCLA, April 8, 2019.
6. **Patel, R.** and Frand, A.R. 22nd International *C. elegans* Conference, Los Angeles. June 20–24, 2019.

Poster Presentations

1. **Mushtaqh Ali, R**. and Frand, A.R. Genetic Circuitry of a Developmental Timer. 20th International *C. elegans* Meeting, Los Angeles. June 24–28, 2015.

2. **Mushtaqh Ali, R.** and Frand, A.R. Molecular Circuitry of an Ultradian Behavioral and Developmental Clock in *C. elegans*. Gordon Research Conference on Chronobiology, Girona, Spain. June 28–July 3, 2015.

TEACHING EXPERIENCE

1. Teaching Assistant for Dr. Michael Grunstein, Dr. John Colicelli and Dr. Ke Shuai. Course: Cell Cycle. Spring 2014.

2. Teaching Assistant for Dr. Pei Yun Lee. Course: Developmental Biology. Winter 2015.

CHAPTER I

Biological Timekeeping Mechanisms in Metazoans

Biological rhythms and related timekeeping mechanisms are ubiquitous and vital features of animal development and physiology. The detected periods of biological rhythms range from 0.1 seconds to 1 year (Rapp, 1979). Infradian rhythms have a period greater than 24 h and include circannual rhythms such as courtship and singing behavior in song sparrows and hibernation in squirrels, as well as monthly rhythms like the estrous cycle (Schwartz and Andrews, 2013). Circadian rhythms have a period of 24 h; sleep-wake and feeding-fasting are some well-studied examples. Ultradian rhythms have a period less than 24 h; the 35 – 75-s rhythm in full-body movement in the chick embryo, the 120-min rhythm in formation of somites in the mouse embryo and the 8-h rhythm in deposition of dentin in the growing molars of mice are some examples (Gomez et al., 2008; Hamburger and Balaban, 1963; Ono et al., 2019). The timekeeping mechanisms that underlie the lifetime and speed of the vast majority of rhythms are not well defined.

Mutations in genes that govern developmental rhythms are associated with life-threatening birth defects. For example, the congenital skeletal disorder spondylocostal distosis – characterized by a misshapen spine, malformed ribs and fused vertebrae – is associated with mutations in components of the Notch signaling pathway, which controls the regular formation of somites (Shifley and Cole, 2007; Sparrow et al., 2007). Both mice and humans born with severely malformed ribs often die soon after birth, likely due to related difficulties in breathing.

Mutations in genes that govern physiological rhythms are associated with sleep, metabolic and psychiatric disorders. For example, a deletion in the human *CRY1* gene is associated with production of a dominant negative protein product that increases the period of sleep-wake cycles by thirty minutes (Patke et al., 2017). As a result, carriers of this mutation go to bed later every night, relative to the preceding night—a syndrome called delayed sleep phase disorder (DSPD)

that can cause chronic sleep deprivation. Mutations in other clock genes such as *BMAL1* and *PER3* are associated with bipolar disorder (Mansour et al., 2006; Nievergelt et al., 2006). Furthermore, desynchronization of the internal circadian clock relative to external time-givers, such as light-dark cycles or nutrition, which arises from shift work or social jet lag is associated with obesity and cancer (Roenneberg et al., 2012; Roenneberg and Merrow, 2016). Social jet lag manifests due to differences in the times at which people sleep and wake up between weekdays and weekends and was reported among 87% of a sample of day workers.

Biological Timekeeping Mechanisms: Two Paradigms

One major type of biological timekeeping mechanism is the hourglass timer, which schedules singular events relative to one another (Johnson and Day, 2000). Therein, accrual or depletion of specific molecules above or below a critical concentration triggers an event. In *Xenopus* embryos, an hourglass timer likely controls the degradation of Cyclin E five hours after fertilization, at the same time as the mid-blastula transition (Howe and Newport, 1996). Additionally, *in vitro* studies have shown that accumulation of the cyclin-dependent kinase (CDK) inhibitor p27 past a concentration threshold partly triggers the differentiation of oligodendrocyte precursor cells (OPCs) into oligodendrocytes eight days after initial exposure to platelet-derived growth factor (PDGF) (Durand and Raff, 2000). Genetic inactivation of p27 delays the differentiation of OPCs, relative to controls (Durand et al., 1998).

The other major type of biological timekeeping mechanism is the genetic oscillator, which schedules recurring events (Johnson and Day, 2000). Genetic oscillators comprise interconnected feedback loops among transcriptional activators and both transcriptional and post-transcriptional repressors. The net result of the interactions is cyclical expression of core clock genes, as well as

many downstream targets—called clock-controlled genes (CCGs). The waves in gene expression drive rhythmic cellular and behavioral processes.

In theory, hourglass timers, which are based on concentration thresholds, can operate within more complex genetic oscillators (Johnson and Day, 2000). This model may explain how rhythmic expression of core clock genes generates rhythmic expression of CCGs, and by extension, rhythmic cellular and organismal behaviors. For example, a repressor protein within a genetic oscillator may only effectively repress expression of target genes upon surpassing a critical concentration. Some functions of the circadian clock protein PER2 are dependent upon concentration and this is discussed in more detail below (Song and Rogulja, 2017; Takahashi, 2017).

A Developmental Rhythm and the Related Genetic Oscillator

Rhythmic budding of somites, which give rise to vertebrae and skeletal muscle, from the immature pre-somitic mesoderm (PSM) is one example of a cyclic developmental process (Pourquie, 2011). In developing embryos, somites bud off from the anterior end of the PSM. While somites continue to form, expansion of the PSM occurs in the posterior direction as the embryo elongates. The rate at which somites are formed ultimately controls the number of vertebrae in the mature animal, with as few as 10 vertebrae detected in frogs and as many as 315 in corn snakes (Gomez et al., 2008).

Formation of a new somite boundary is controlled by interactions between the segmentation clock and the maturation wavefront (Pourquie, 2011). The segmentation clock, composed of interconnected feedback loops among components of the Notch, FGF and Wnt signaling pathways, causes cells within the PSM to switch between “permissive” and “non-

permissive" states. The maturation wavefront consists of the signaling molecules Fgf8, Wnt3a and Retinoic acid. There is a gradient in the level of these molecules, with levels of Fgf8 and Wnt3a highest at the posterior end of the embryo and the levels of Retinoic acid highest at the anterior end. Fgf8 and Wnt3a both preserve the PSM in the immature form, while Retinoic acid promotes maturation into somites in part by causing downregulation of *Fgf8* expression. Thus, a new somite boundary is formed when the cells in the PSM are in the permissive state and when levels of secreted Fgf8 and Wnt3a are below a critical concentration.

There are several rhythmic processes in development, however, the genetic oscillators that underlie many of the rhythms are not known (Rapp, 1979). Furthermore, the extent to which components of developmental timers regulate the speed and duration of physiological rhythms are also not well understood. The work done in this thesis will help address these scientific questions.

Circadian Rhythms and the Circadian Clock

Circadian rhythms are defined as biological rhythms with a 24-h period that are temperature compensated, meaning that the rhythm occurs at the same time every day within a range of physiological temperatures, and can be entrained or adjusted by external light-dark cycles. Circadian rhythms in animal behavior and physiology include the sleep-wake and feeding-fasting cycles, diurnal changes in body temperature, blood pressure and metabolism (Farhud and Aryan, 2018). Circadian rhythms in cellular behavior have also been detected, such as cycles in production of ATP, biosynthesis of collagen and assembly of collagen fibrils (Chang et al., 2020; Reinke and Asher, 2019). The circadian clock governs all of the abovementioned rhythms.

The core circadian clock consists of the transcriptional activators BMAL1 (brain and muscle ARNT-like 1) and CLOCK (circadian locomotor output cycles kaput) and the repressor

proteins PER (period) and CRY (cryptochrome) (Takahashi, 2017). During the daytime in diurnal organisms, BMAL1-CLOCK heterodimers bind to E-box elements within the promoters of the *PER* and *CRY* genes and activate transcription (Song and Rogulja, 2017; Takahashi, 2017). The PER and CRY proteins accumulate in the cytoplasm throughout the day. At nighttime, PER and CRY proteins form heteromeric complexes, translocate into the nucleus, interact with BMAL1-CLOCK heterodimers and repress expression of *PER* and *CRY* genes (Song and Rogulja, 2017; Takahashi, 2017). The protein levels of PER and CRY subsequently fall. The cycle resets every morning. Cyclical expression of *BMAL1* is under control of the nuclear hormone receptors ROR (retinoic acid receptor-related orphan receptor) and REV-ERB. Both nuclear receptors compete with each other for binding to the same site – the retinoid-related orphan receptor response element RORE – within the promoter of *BMAL1*, with ROR acting as a transcriptional activator and REV-ERB, a transcriptional repressor. The genes encoding both ROR and REV-ERB also cycle in expression—cyclical expression is regulated by transcription factors BMAL1, DBP (D-box binding protein) and NFIL3 (nuclear factor, interleukin-3 regulated). Thus, multiple interconnected feedback loops among activators and repressors drive waves in expression of core clock genes.

MicroRNAs are emerging as important regulators of the expression of the core clock genes and rhythmic behaviors. Knockout of *Dicer*, which encodes an endoribonuclease that is essential for the production of mature miRNAs, in mice reduced the period of rest-activity rhythms by 2 h and increased the rate of PER2 protein accumulation relative to control mice (Chen et al., 2013). Moreover, the miRNAs *mir-24* and *mir-30a* together repress the expression of *Per2* in mouse embryonic fibroblasts. The period of rest-activity rhythms and the amplitude of *Per2* expression of a mutant mouse strain lacking the endogenous *Per2* 3′UTR were both significantly higher than

controls (Yoo et al., 2017). Fruit flies that lack the miRNA *bantam* undergo cycles of rest and activity significantly faster than control animals (Kadener et al., 2009). Furthermore, *bantam* represses the expression of the *clock* gene in insect cell lines. However, the extent to which miRNAs act as core components of the circadian clock is not well understood.

Post-translational modifications regulate the period and phase of circadian rhythms by controlling the accumulation rates of core clock proteins (Song and Rogulja, 2017; Takahashi, 2017). For example, the kinases CK1δ and CK1ε phosphorylate and promote the degradation of PER proteins in the cytoplasm. Similarly, the ubiquitin ligase FBXL21 polyubiquitinates CRY proteins in the cytoplasm, targeting them for degradation. During the day, the relatively fast degradation rates of PER and CRY prevent the proteins from reaching sufficient concentrations to translocate into the nucleus. The accumulation rate of PER and CRY proteins finally outpaces the degradation rate in the evening, allowing the formation of PER-CRY complexes in the cytoplasm. The multiprotein complexes translocate into the nucleus and repress gene expression.

The core clock proteins regulate the expression of target genes that are required for metabolic processes such as glucose homeostasis, production of ATP, autophagy, as well as behavioral processes such as sleep and mating (Allada and Chung, 2010; Reinke and Asher, 2019). Importantly, rhythmic cellular and behavioral outputs of the circadian clock also control the expression level and activity of core clock components. Feedback from cellular and behavioral rhythms can therefore fine-tune the phase of expression of the core oscillator to better anticipate daily cycles of feeding-fasting and light-dark.

Post-translational modification of core clock proteins is one mechanism that couples the clock to the levels of nutrients and ATP, and intracellular redox conditions, among other cues (Reinke and Asher, 2019). For example, the enzyme *O*-GlcNAc transferase (OGT) catalyzes the

addition of β-D-N-acetylglucoasmine (GlcNAc) to BMAL1 and CLOCK (Li et al., 2013). Glycosylation of BMAL1 and CLOCK interferes with ubiquitination and slows the rate of turnover of the proteins. The levels of Uridine diphosphate N-acetylglucosamine, the donor of the GlcNAc group, is sensitive to intracellular levels of nutrients such as glucose and glutamine (Hanover et al., 2012). Additionally, the protein AMP kinase – which is sensitive to the intracellular ratio of AMP to ATP – phosphorylates and targets CRY1 for degradation (Lamia et al., 2009).

Findings from this thesis add to the growing body of work showing that miRNAs play a central role in regulating the speed of biological rhythms. The known and proposed core components of the molting cycle timer as well as the *cis*-regulatory elements, which are both described later, are conserved from nematodes to humans. Thus, my work may refine the current model of the circadian clock. The findings also imply that core circadian clock components could control developmental rhythms.

The Molting Cycle of *C. elegans*: A Model for Developmental Timing

C. elegans molt four times at regular 8 – 10 h intervals under standard culture conditions (Frand et al., 2005; Monsalve et al., 2011; Singh and Sulston, 1978). Animals move and feed during the intermolt, and then enter the molts, when foraging ceases, a new exoskeleton or cuticle is made and the old one is shed. Early in the intermolt, the epidermal stem cells or seam cells of the worm switch from a quiescent state to a dividing one for 1 or 2 rounds of cell division (Sulston and Horvitz, 1977). Later in the intermolt, the seam cells, differentiated epidermis (hyp7) and other tissues synthesize temporary extracellular matrices. The matrices include the sheath, which surrounds the body and the plugs, which fill in openings such as the mouth, vulva and anus (Katz et al., 2018; Maul-Newby et al., 2018). Because internal body pressure could otherwise cause the

animal to implode, the sheath and plugs are necessary to keep the animal intact while the old exoskeleton is released, and the new cuticle is made. During the molt, animals enter a temporary state of behavioral quiescence, termed lethargus, when locomotion is reduced and pumping of the pharynx, the feeding apparatus, is undetectable. The collagenous cuticle is remodeled at this time. Worms ecdyse or shed the pre-existing cuticle by undertaking a set of distinctive behaviors that include flipping—abrupt 180° rotations around the long axis of the body (Schwarz and Bringmann, 2017; Tramm et al., 2014). Moreover, roughly 14% of the *C. elegans* genome oscillates in expression throughout larval development (Hendriks et al., 2014; Kim et al., 2013).

I asked two questions about the molting cycle of *C. elegans*. First, how do specific genetic and molecular circuits determine the frequency of the molting cycle (Chapter II)? Second, how do the specific genes and molecules control the total number of molts (Chapters II and III)? I addressed these questions by combining behavioral studies with molecular-genetic and bioinformatic approaches.

Control of the Pace of Molting: The Molting Cycle Timer

Previous work from the Frand lab showed that LIN-42, which is similar in sequence to mammalian PER, sustains the pace and rhythm of the molting cycle in *C. elegans* (Monsalve, 2013). The *lin-42* genomic locus, as annotated in WormBase WS274, produces at least seven distinct mRNA and protein isoforms; three isoforms – LIN-42A, LIN-42B and LIN-42C – have been shown to regulate the pace of molting. Specifically, the pace of the molting cycle of *lin-42(ok2385)* mutants, which do not express both *lin-42a* and *lin-42b* transcripts, are longer and more arrhythmic than wild-type animals. Additionally, increasing the dosage of *lin-42c*, by using extrachromosomal arrays, extended the duration of the molting cycle relative to wild-type animals

(Monsalve, 2013). Forced expression of *lin-42a* is sufficient to induce molting and lethargy. Moreover, the expression of the *lin-42* gene cycles throughout larval development, with peak levels of transcripts and proteins detected late in the intermolt. Additional components of this PER-based oscillator were not yet known. In Chapter II of my thesis, I will uncover novel components of the molting cycle timer.

The nuclear hormone receptor NHR-23 was a key candidate component of the molting cycle timer. NHR-23 is similar in sequence to mammalian ROR, a core component of the circadian clock (Sluder and Maina, 2001; Sluder et al., 1999; Takahashi, 2017). The abundance of *nhr-23* transcripts rise and fall throughout larval development, with peaks mid-way through each larval stage (Hendriks et al., 2014; Kim et al., 2013; Kostrouchova et al., 2001). Genetic inactivation of *nhr-23* results in a molting cycle defective phenotype (Mlt) wherein animals are unable to fully shed their old cuticle (Kostrouchova et al., 1998, 2001). Moreover, NHR-23 activates the expression of several genes necessary for execution of the molts (Frand et al., 2005; Kouns et al., 2011).

The *let-7* family of miRNAs were additional key candidate components of the PER-based molting cycle timer. The levels of primary transcripts of *let-7*, as well as three paralogs – *mir-84*, *mir-48* and *mir-241* – all cycle throughout larval development (McCulloch and Rougvie, 2014; Van Wynsberghe et al., 2011). Moreover, LIN-42 binds to the promoter of *let-7* and represses transcription of the *let-7* family members (McCulloch and Rougvie, 2014; Perales et al., 2014; Van Wynsberghe et al., 2014). Also, loss-of-function mutations in *lin-42* partially suppress the heterochronic phenotypes of *let-7* and vice versa, showing genetic interaction between the two genes (Tennessen et al., 2006). The action of *let-7* mutants in the heterochronic pathway are described below.

Control of the Number of Molts: The Heterochronic Pathway and Newly Identified Pathways

Genes in the heterochronic pathway of *C. elegans* control the temporal identity of the seam cells, as well as other tissues, during each life stage (Rougvie and Moss, 2013). The seam cells undergo stereotypical divisions during each larval stage: an asymmetric division in both L1 and L3; a symmetric and an asymmetric division in L2; and an asymmetric division in L4 followed by terminal differentiation (Rougvie and Moss, 2013). Terminal differentiation of the seam during the L4 is characterized by exit of seam cells from the cell cycle, fusion of seam cells with each other, and the subsequent formation of three alae, which are longitudinal ridges in the adult cuticle. Furthermore, terminal differentiation of the epidermis is accompanied by cessation of the molting cycle in wild-type adults. Two classes of heterochronic mutants have been identified: precocious heterochronic mutants, which skip divisions typical of a given larval stage; and retarded heterochronic mutants, which reiterate divisions typical of a given larval stage (Ambros and Horvitz, 1984).

The *let-7* family mutants are in the class of retarded heterochronic mutants. The *let-7* gene promotes the transition from L4 to Adulthood (Reinhart et al., 2000). The epidermis of *let-7(n2853)* mutants fails to terminally differentiate during the L4 stage; the seam cells of sexually mature *let-7(n2853)* animals undergo cell divisions and the cuticles lack alae, unlike wild-type adults (Reinhart et al., 2000). Similarly, the *let-7* sisters – *mir-48*, *mir-84* and *mir-241* – promote the transition of the seam cells from the L2 fate to the L3 fate (Abbott et al., 2005). Moreover, both *let-7(n2853)* single and *let-7(mg279) mir-84(tm1304)* double mutants undergo supernumerary molts (Hayes et al., 2006; Reinhart et al., 2000). Supernumerary molts also occur when other genes

that promote terminal differentiation of the epidermis, such as *lin-29* and *mab-10*, are mutated (Ambros and Horvitz, 1984; Chalfie et al., 1981; Harris and Horvitz, 2011). However, the mechanisms that restrict the number of molts to four are not well understood. In Chapter II of my thesis, I will show that an hourglass timer based on the levels of NHR-23 counts down the number of molts.

Additional, independent pathways may also control the number of molts in *C. elegans*. The gene *pqn-47/myrf-1* was isolated from a forward genetic screen for adult animals that molt (Russel et al., 2011). A translational fusion for MYRF-1 is expressed in the seam cells and several neurons in the head, among other tissues (Russel et al., 2011). Another study in *C. elegans* showed that a distinct MYRF-1 fusion gene is cleaved in the Endoplasmic Reticulum (ER) into an N terminal fragment, which translocates to the nucleus and likely acts as a transcription factor, and a C terminal fragment, which localizes to the ER (Meng et al., 2017). MYRF-1 promotes maturation of dorsal neurons (DD) at the L1-L2 transition by promoting rewiring of the synapses (Meng et al., 2017). However, the role of MYRF-1 in the cessation of molts is not yet fully defined. Perhaps, at the L4-Adult transition, MYRF-1 promotes the maturation or rewiring of neurons that normally trigger molting in larvae.

Neuroendocrine Control of Molting in Insects and *C. elegans*

Neuroendocrine control of molting is well-established in insects (Danielsen et al., 2013; Di Cara and King-Jones, 2013). The sterol-derived hormone ecdysone promotes entry into the molts in many insect species, including *D. melanogaster* and *M. sexta*. Production of ecdysone is under control of prothoracicotropic hormone (PTTH), a neuropeptide released from the brain, as well as pathways sensitive to nutrient levels such as the insulin-signaling and TOR pathways (Danielsen

et al., 2013). Moreover, juvenile hormone (JH) controls the quality of the molt i.e. when larval-to-larval molts occur when titers of JH are relatively high, whereas a larval-to-adult molt occurs when titers of JH are relatively low. Although similar molecules have not been detected in *C.* elegans, molting in *C. elegans* may also be under neuroendocrine control.

C. elegans are auxotrophic for cholesterol and require cholesterol supplementation in the diet for growth and development (Kurzchalia and Ward, 2003; Yochem et al., 1999). Molting defects manifest in the second generation when animals are grown on media lacking cholesterol for two consecutive generations (Yochem et al., 1999). Additionally, inactivation of the gene encoding LRP-1, which is similar in sequence to mammalian low-density lipoprotein receptor-related proteins, also causes molting defects (Yochem et al., 1999). The LRP-1 protein is detectable in one of the tissues that NHR-23 is expressed in—the epidermis. It is therefore possible that LRP-1 normally endocytoses a steroid-based hormone that acts as a ligand for NHR-23 and promotes molting (Yochem et al., 1999). In Chapter III of my thesis, I will describe efforts to uncover the identity of such a hormone. I will also identify pathways that may synthesize or degrade a hormone that promotes molting.

A Unified Timekeeping Mechanism Controls the Speed and the Lifetime of the Molting Cycle

In Chapter II, I will describe a transcriptional–post-transcriptional feedback loop between NHR-23 and the *let-7* family of miRNAs that unites two distinct timekeeping mechanisms – a genetic oscillator and an hourglass timer – to control both the frequency and number of molts in *C. elegans*. Knockdown of *nhr-23* slows progression of the molting cycle, whereas genetic inactivation of *let-7s* or forced expression of *nhr-23* speeds up the cycle. During each intermolt, NHR-23 binds to response elements within the promoter of *let-7s* and activates transcription.

While animals transit the molts, *let-7s* binds to a complementary site (the LCS) in the 3′UTR of *nhr-23* and represses the expression. Bio-informatics analyses show that co-regulation by NHR-23 and *let-7s* is a signature of genes linked to molting that cycle throughout larval development. My findings suggest that reciprocal interactions between the NHR-23 and *let-7s*, as well as regulation of expression of multiple target genes by both gene regulatory molecules, schedule the reiterative transitions through the molts. Moreover, *let-7* dampens the expression of *nhr-23* over the course of larval development. Increasing the gene dosage of *nhr-23* or deleting the LCS from the 3′UTR are sufficient to reanimate the molting cycle in adults. Together, these data indicate that *let-7*–mediated dampening of *nhr-23* schedules extinction of the molting cycle in adulthood.

In Chapter III, I show evidence that either cholesterol or a derivative of cholesterol is necessary for supernumerary molts, likely by binding to NHR-23 and promoting transcriptional activity. I find that several key residues that mediate binding of *H. sapiens* RORα with cholesterol and oxysterols are conserved to NHR-23. By utilizing a reverse genetic approach, I identify a distinct set of P450s that are necessary for the supernumerary molts of *let-7(mg279) mir-84(tm1304)* mutants. Many hits from the screen likely synthesize the as-yet-unidentified ligand that binds NHR-23.

The studies on the molting cycle presented in this thesis improve our understanding of the genetic and molecular circuits that together regulate the speed and lifetime of biological rhythms. Both the core components and *cis*-regulatory elements of the molting cycle timer are conserved from nematodes to humans. Thus, my findings could refine our model of the circadian clock, and further our comprehension of related rhythms, in both normal and pathological conditions. In theory, factors such as the availability of cholesterol/cholesterol biosynthetic intermediates (CBIs) and heme, which are ligands for ROR and REV-ERB, respectively, could influence the period,

phase and amplitude of circadian rhythms (Kallen et al., 2004; Kallen et al., 2002; Raghuram et al., 2007; Santori et al., 2015). However, this has not been fully investigated before. My research shows that both a sterol-based molecule and several conserved sterol-modifying enzymes control the onset of extra molts, implying that similar molecules and genes could govern circadian rhythms in mammals.

REFERENCES

Abbott, A.L., Alvarez-Saavedra, E., Miska, E.A., Lau, N.C., Bartel, D.P., Horvitz, H.R., and Ambros, V. (2005). The let-7 MicroRNA family members mir-48, mir-84, and mir-241 function together to regulate developmental timing in Caenorhabditis elegans. Dev Cell *9*, 403-414.

Allada, R., and Chung, B.Y. (2010). Circadian organization of behavior and physiology in Drosophila. Annu Rev Physiol *72*, 605-624.

Ambros, V., and Horvitz, H.R. (1984). Heterochronic mutants of the nematode Caenorhabditis elegans. Science *226*, 409-416.

Chalfie, M., Horvitz, H.R., and Sulston, J.E. (1981). Mutations that lead to reiterations in the cell lineages of C. elegans. Cell *24*, 59-69.

Chang, J., Garva, R., Pickard, A., Yeung, C.C., Mallikarjun, V., Swift, J., Holmes, D.F., Calverley, B., Lu, Y., Adamson, A.*, et al.* (2020). Circadian control of the secretory pathway maintains collagen homeostasis. Nat Cell Biol *22*, 74-86.

Chen, R., D'Alessandro, M., and Lee, C. (2013). miRNAs are required for generating a time delay critical for the circadian oscillator. Curr Biol *23*, 1959-1968.

Danielsen, E.T., Moeller, M.E., and Rewitz, K.F. (2013). Nutrient signaling and developmental timing of maturation. Curr Top Dev Biol *105*, 37-67.

Di Cara, F., and King-Jones, K. (2013). How clocks and hormones act in concert to control the timing of insect development. Curr Top Dev Biol *105*, 1-36.

Durand, B., Fero, M.L., Roberts, J.M., and Raff, M.C. (1998). p27Kip1 alters the response of cells to mitogen and is part of a cell-intrinsic timer that arrests the cell cycle and initiates differentiation. Curr Biol *8*, 431-440.

Durand, B., and Raff, M. (2000). A cell-intrinsic timer that operates during oligodendrocyte development. Bioessays *22*, 64-71.

Farhud, D., and Aryan, Z. (2018). Circadian Rhythm, Lifestyle and Health: A Narrative Review. Iran J Public Health *47*, 1068-1076.

Frand, A.R., Russel, S., and Ruvkun, G. (2005). Functional genomic analysis of C. elegans molting. PLoS Biol *3*, e312.

Gomez, C., Ozbudak, E.M., Wunderlich, J., Baumann, D., Lewis, J., and Pourquie, O. (2008). Control of segment number in vertebrate embryos. Nature *454*, 335-339.

Hamburger, V., and Balaban, M. (1963). Observations and experiments on spontaneous rhythmical behavior in the chick embryo. Dev Biol *6*, 533-545.

Hanover, J.A., Krause, M.W., and Love, D.C. (2012). Bittersweet memories: linking metabolism to epigenetics through O-GlcNAcylation. Nat Rev Mol Cell Biol *13*, 312-321.

Harris, D.T., and Horvitz, H.R. (2011). MAB-10/NAB acts with LIN-29/EGR to regulate terminal differentiation and the transition from larva to adult in C. elegans. Development *138*, 4051-4062.

Hayes, G.D., Frand, A.R., and Ruvkun, G. (2006). The mir-84 and let-7 paralogous microRNA genes of Caenorhabditis elegans direct the cessation of molting via the conserved nuclear hormone receptors NHR-23 and NHR-25. Development *133*, 4631-4641.

Hendriks, G.J., Gaidatzis, D., Aeschimann, F., and Grosshans, H. (2014). Extensive oscillatory gene expression during C. elegans larval development. Mol Cell *53*, 380-392.

Howe, J.A., and Newport, J.W. (1996). A developmental timer regulates degradation of cyclin E1 at the midblastula transition during Xenopus embryogenesis. Proc Natl Acad Sci U S A *93*, 2060-2064.

Johnson, M.H., and Day, M.L. (2000). Egg timers: how is developmental time measured in the early vertebrate embryo? Bioessays *22*, 57-63.

Kadener, S., Menet, J.S., Sugino, K., Horwich, M.D., Weissbein, U., Nawathean, P., Vagin, V.V., Zamore, P.D., Nelson, S.B., and Rosbash, M. (2009). A role for microRNAs in the Drosophila circadian clock. Genes Dev *23*, 2179-2191.

Kallen, J., Schlaeppi, J.M., Bitsch, F., Delhon, I., and Fournier, B. (2004). Crystal structure of the human RORalpha Ligand binding domain in complex with cholesterol sulfate at 2.2 A. J Biol Chem *279*, 14033-14038.

Kallen, J.A., Schlaeppi, J.M., Bitsch, F., Geisse, S., Geiser, M., Delhon, I., and Fournier, B. (2002). X-ray structure of the hRORalpha LBD at 1.63 A: structural and functional data that cholesterol or a cholesterol derivative is the natural ligand of RORalpha. Structure *10*, 1697-1707.

Katz, S.S., Maybrun, C., Maul-Newby, H.M., and Frand, A.R. (2018). Non-canonical apical constriction shapes emergent matrices in C. elegans. bioRxiv preprint.

Kim, D., Grun, D., and van Oudenaarden, A. (2013). Dampening of expression oscillations by synchronous regulation of a microRNA and its target. Nat Genet *45*, 1337-1344.

Kostrouchova, M., Krause, M., Kostrouch, Z., and Rall, J.E. (1998). CHR3: a Caenorhabditis elegans orphan nuclear hormone receptor required for proper epidermal development and molting. Development *125*, 1617-1626.

Kostrouchova, M., Krause, M., Kostrouch, Z., and Rall, J.E. (2001). Nuclear hormone receptor CHR3 is a critical regulator of all four larval molts of the nematode Caenorhabditis elegans. Proc Natl Acad Sci U S A *98*, 7360-7365.

Kouns, N.A., Nakielna, J., Behensky, F., Krause, M.W., Kostrouch, Z., and Kostrouchova, M. (2011). NHR-23 dependent collagen and hedgehog-related genes required for molting. Biochem Biophys Res Commun *413*, 515-520.

Kurzchalia, T.V., and Ward, S. (2003). Why do worms need cholesterol? Nat Cell Biol *5*, 684-688.

Lamia, K.A., Sachdeva, U.M., DiTacchio, L., Williams, E.C., Alvarez, J.G., Egan, D.F., Vasquez, D.S., Juguilon, H., Panda, S., Shaw, R.J.*, et al.* (2009). AMPK regulates the circadian clock by cryptochrome phosphorylation and degradation. Science *326*, 437-440.

Li, M.D., Ruan, H.B., Hughes, M.E., Lee, J.S., Singh, J.P., Jones, S.P., Nitabach, M.N., and Yang, X. (2013). O-GlcNAc signaling entrains the circadian clock by inhibiting BMAL1/CLOCK ubiquitination. Cell Metab *17*, 303-310.

Mansour, H.A., Wood, J., Logue, T., Chowdari, K.V., Dayal, M., Kupfer, D.J., Monk, T.H., Devlin, B., and Nimgaonkar, V.L. (2006). Association study of eight circadian genes with bipolar I disorder, schizoaffective disorder and schizophrenia. Genes Brain Behav *5*, 150-157.

Maul-Newby, H.M., Maybrun, C., and Frand, A.R. (2018). Temporary Atresia and Corsetry are Essential for Worms to Molt. Paper presented at: EMBO Workshop: *C elegans* development, cell biology and gene expression (Barcelona, Spain).

McCulloch, K.A., and Rougvie, A.E. (2014). Caenorhabditis elegans period homolog lin-42 regulates the timing of heterochronic miRNA expression. Proc Natl Acad Sci U S A *111*, 15450-15455.

Meng, J., Ma, X., Tao, H., Jin, X., Witvliet, D., Mitchell, J., Zhu, M., Dong, M.Q., Zhen, M., Jin, Y.*, et al.* (2017). Myrf ER-Bound Transcription Factors Drive C. elegans Synaptic Plasticity via Cleavage-Dependent Nuclear Translocation. Dev Cell *41*, 180-194 e187.

Monsalve, G.C. (2013). Unifying mechanisms of developmental timing genetic and molecular analysis of the molting cycle timer of Caenorhabditis elegans (Los Angeles: University of California, Los Angeles,), pp. 1 online resource (xiv, 96 p.

Monsalve, G.C., Van Buskirk, C., and Frand, A.R. (2011). LIN-42/PERIOD controls cyclical and developmental progression of C. elegans molts. Curr Biol *21*, 2033-2045.

Nievergelt, C.M., Kripke, D.F., Barrett, T.B., Burg, E., Remick, R.A., Sadovnick, A.D., McElroy, S.L., Keck, P.E., Jr., Schork, N.J., and Kelsoe, J.R. (2006). Suggestive evidence for association of the circadian genes PERIOD3 and ARNTL with bipolar disorder. Am J Med Genet B Neuropsychiatr Genet *141B*, 234-241.

Ono, R., Koike, N., Inokawa, H., Tsuchiya, Y., Umemura, Y., Yamamoto, T., Kanamura, N., and Yagita, K. (2019). Incremental Growth Lines in Mouse Molar Dentin Represent 8-hr Ultradian Rhythm. Acta Histochem Cytochem *52*, 93-99.

Patke, A., Murphy, P.J., Onat, O.E., Krieger, A.C., Ozcelik, T., Campbell, S.S., and Young, M.W. (2017). Mutation of the Human Circadian Clock Gene CRY1 in Familial Delayed Sleep Phase Disorder. Cell *169*, 203-215 e213.

Perales, R., King, D.M., Aguirre-Chen, C., and Hammell, C.M. (2014). LIN-42, the Caenorhabditis elegans PERIOD homolog, negatively regulates microRNA transcription. PLoS Genet *10*, e1004486.

Pourquie, O. (2011). Vertebrate segmentation: from cyclic gene networks to scoliosis. Cell *145*, 650-663.

Raghuram, S., Stayrook, K.R., Huang, P., Rogers, P.M., Nosie, A.K., McClure, D.B., Burris, L.L., Khorasanizadeh, S., Burris, T.P., and Rastinejad, F. (2007). Identification of heme as the

ligand for the orphan nuclear receptors REV-ERBalpha and REV-ERBbeta. Nat Struct Mol Biol *14*, 1207-1213.

Rapp, P.E. (1979). An atlas of cellular oscillators. J Exp Biol *81*, 281-306.

Reinhart, B.J., Slack, F.J., Basson, M., Pasquinelli, A.E., Bettinger, J.C., Rougvie, A.E., Horvitz, H.R., and Ruvkun, G. (2000). The 21-nucleotide let-7 RNA regulates developmental timing in Caenorhabditis elegans. Nature *403*, 901-906.

Reinke, H., and Asher, G. (2019). Crosstalk between metabolism and circadian clocks. Nat Rev Mol Cell Biol *20*, 227-241.

Roenneberg, T., Allebrandt, K.V., Merrow, M., and Vetter, C. (2012). Social jetlag and obesity. Curr Biol *22*, 939-943.

Roenneberg, T., and Merrow, M. (2016). The Circadian Clock and Human Health. Curr Biol *26*, R432-443.

Rougvie, A.E., and Moss, E.G. (2013). Developmental transitions in C. elegans larval stages. Curr Top Dev Biol *105*, 153-180.

Russel, S., Frand, A.R., and Ruvkun, G. (2011). Regulation of the C. elegans molt by pqn-47. Dev Biol *360*, 297-309.

Santori, F.R., Huang, P., van de Pavert, S.A., Douglass, E.F., Jr., Leaver, D.J., Haubrich, B.A., Keber, R., Lorbek, G., Konijn, T., Rosales, B.N.*, et al.* (2015). Identification of natural RORgamma ligands that regulate the development of lymphoid cells. Cell Metab *21*, 286-298.

Schwartz, C., and Andrews, M.T. (2013). Circannual transitions in gene expression: lessons from seasonal adaptations. Curr Top Dev Biol *105*, 247-273.

Schwarz, J., and Bringmann, H. (2017). Analysis of the NK2 homeobox gene ceh-24 reveals sublateral motor neuron control of left-right turning during sleep. Elife *6*.

Shifley, E.T., and Cole, S.E. (2007). The vertebrate segmentation clock and its role in skeletal birth defects. Birth Defects Res C Embryo Today *81*, 121-133.

Singh, R.N., and Sulston, J.E. (1978). Some observations on moulting in Caenorhabditis elegans. Nematologica *24*, 63-71.

Sluder, A.E., and Maina, C.V. (2001). Nuclear receptors in nematodes: themes and variations. Trends Genet *17*, 206-213.

Sluder, A.E., Mathews, S.W., Hough, D., Yin, V.P., and Maina, C.V. (1999). The nuclear receptor superfamily has undergone extensive proliferation and diversification in nematodes. Genome Res *9*, 103-120.

Song, B.J., and Rogulja, D. (2017). SnapShot: Circadian Clock. Cell *171*, 1468-1468 e1461.

Sparrow, D.B., Chapman, G., Turnpenny, P.D., and Dunwoodie, S.L. (2007). Disruption of the somitic molecular clock causes abnormal vertebral segmentation. Birth Defects Res C Embryo Today *81*, 93-110.

Sulston, J.E., and Horvitz, H.R. (1977). Post-embryonic cell lineages of the nematode, Caenorhabditis elegans. Dev Biol *56*, 110-156.

Takahashi, J.S. (2017). Transcriptional architecture of the mammalian circadian clock. Nat Rev Genet *18*, 164-179.

Tennessen, J.M., Gardner, H.F., Volk, M.L., and Rougvie, A.E. (2006). Novel heterochronic functions of the Caenorhabditis elegans period-related protein LIN-42. Dev Biol *289*, 30-43.

Tramm, N., Oppenheimer, N., Nagy, S., Efrati, E., and Biron, D. (2014). Why do sleeping nematodes adopt a hockey-stick-like posture? PLoS One *9*, e101162.

Van Wynsberghe, P.M., Finnegan, E.F., Stark, T., Angelus, E.P., Homan, K.E., Yeo, G.W., and Pasquinelli, A.E. (2014). The Period protein homolog LIN-42 negatively regulates microRNA biogenesis in C. elegans. Dev Biol *390*, 126-135.

Van Wynsberghe, P.M., Kai, Z.S., Massirer, K.B., Burton, V.H., Yeo, G.W., and Pasquinelli, A.E. (2011). LIN-28 co-transcriptionally binds primary let-7 to regulate miRNA maturation in Caenorhabditis elegans. Nat Struct Mol Biol *18*, 302-308.

Yochem, J., Tuck, S., Greenwald, I., and Han, M. (1999). A gp330/megalin-related protein is required in the major epidermis of Caenorhabditis elegans for completion of molting. Development *126*, 597-606.

Yoo, S.H., Kojima, S., Shimomura, K., Koike, N., Buhr, E.D., Furukawa, T., Ko, C.H., Gloston, G., Ayoub, C., Nohara, K.*, et al.* (2017). Period2 3'-UTR and microRNA-24 regulate circadian rhythms by repressing PERIOD2 protein accumulation. Proc Natl Acad Sci U S A *114*, E8855-E8864.

CHAPTER II

Feedback among a Retinoid-Related Nuclear Receptor and *let-7* miRNAs Controls the Pace and Number of Molts in *C. elegans*

This chapter was submitted to *eLife* on January 15, 2020, peer-reviewed and is currently under revision.

Feedback among a Retinoid-Related Nuclear Receptor and *let-7* miRNAs Controls the Pace and Number of Molts in *C. elegans*.

Ruhi Patel[1], Himani A. Galagali[2], John K. Kim[2] and Alison R. Frand[1]*

[1]Department of Biological Chemistry

David Geffen School of Medicine

University of California, Los Angeles

Los Angeles, CA 90095

[2] Department of Biology

Johns Hopkins University

Baltimore, MD 21218

*To whom correspondence should be addressed: afrand@mednet.ucla.edu

Keywords: developmental timers, circadian clocks, behavioral quiescence (sleep), genetic oscillators, heterochronic pathway

Abbreviations:

UTR	Untranslated Region
RNA	Ribonucleic Acid
RNAi	RNA interference
ROR	Retinoid-related Orphan Receptor
HRE	Hormone Response Element
NHR	Nuclear Hormone Receptor
PER	PERIOD gene
GFP	Green Fluorescent Protein
iCLIP	Individual-nucleotide resolution Crosslinking Immunoprecipitation
ChIP	Chromatin Immunoprecipitation
PCR	Polymerase Chain Reaction
qPCR	Quantitative Polymerase Chain Reaction
RORE	ROR Response Element
LCS	*let-7* consensus site
NHR	Nuclear Hormone Receptor
Mlt	Molting Cycle Defective
MFE	Minimum Free Energy
pri	Primary
Let	Lethal
CRISPR	Clustered Regularly Interspersed Short Palindromic Repeats
crRNA	CRISPR RNA

tracrRNA	Trans-activating crRNA
nt	Nucleotides
td	Tandem
ssODN	Single Stranded Oligo DNA Nucleotides
VPC	Vulval Precursor Cell

SUMMARY

C. elegans larvae behave as though asleep while molting at regular intervals set by a genetic oscillator with unspecified components. We characterize NHR-23, a retinoid-related nuclear hormone receptor, and *let-7*-family microRNAs as core components of this timer alongside LIN-42/PERIOD. Quiescent phases were advanced in gain-of-function *nhr-23* and loss-of-function *let-7* mutants, delayed in *nhr-23* knockdowns, and scheduled more regularly in *let-7 nhr-23(RNAi)* double mutants. Explicating this, NHR-23 binds response elements in *let-7s* promoters and activates transcription. Conversely, *let-7s* and a 3′UTR site repress expression of *nhr-23*. Moreover, rising *let-7s* levels normally dampen *nhr-23* expression, extinguishing the cycle after four iterations. Forced expression of *nhr-23* reanimates the molting cycle in sexually mature animals. Thus, transcriptional-posttranscriptional feedback among NHR-23 and *let-7s* unites two timekeeping mechanisms that together control the pace and finite number of molts. Conservation of this mechanism has clear implications for human circadian clocks, related sleep and metabolic disorders, and cancers.

INTRODUCTION

Several critical events in development occur multiple times at regular intervals set by genetic oscillators called "developmental clocks" (Keyte and Smith, 2014; Uriu, 2016). The segmentation clocks of vertebrates and insects serve as prominent examples (Pourquie, 2011; Sarrazin et al., 2012). Both the finite number and frequency of related morphogenetic events, relative to rates of continuous processes, substantially influence the animal's physique (Benazeraf and Pourquie, 2013; Woltering, 2012). Further, mutations that affect core components of the segmentation (somitogenesis) clock in humans cause birth defects and neonatal fatalities (Sparrow et al., 2007), highlighting the medical significance of this class of timekeeping mechanisms. Yet, few of the many anticipated developmental clocks have been characterized to date.

Molecular-genetic clocks include feedback, which generates cycles with distinct phases or partitions. This time-keeping mechanism is well-suited for dynamic yet robust systems. A distinct mechanism – called an hourglass – tracks time based on the accretion or depletion of a specific molecule relative to some critical concentration. This mechanism often controls the time elapsed between two distinct and non-recurrent events, rather than sequential iterations of one and the same event. This timekeeping mechanism can operate within a genetic oscillator. In that scenario, the threshold becomes a trigger or checkpoint for a phase transition in the clock-controlled cycle (Johnson and Day, 2000).

Most juvenile animals have external skeletons (cuticles) that are periodically removed and remade as the animal grows and develops—via the molting cycle (Aguinaldo et al., 1997). In the model nematode *Caenorhabditis elegans*, larvae undergo four molts at regular intervals prior to emergence in the adult stage (Figure 1A). As such, L1 larvae simultaneously released from starvation-induced diapause and cultivated with food subsequently complete the molts in concert.

Dramatic but reversible changes in both animal and cellular behavior associated with progression of the nematode molting cycle are comparable to specific biorhythms of mammals. First, *C. elegans* enter and exit a state of behavioral quiescence (lethargus) during each molt. Distinctive, shared features of worm lethargi and mammalian sleep include the following: regulation by specific neuropeptides, sensory depression, and homeostatic drive (Singh et al., 2011; Trojanowski and Raizen, 2016; Van Buskirk and Sternberg, 2007). Second, the reiterative activation of epidermal stem cells coordinated with the molting cycle mirrors the waves of stem cell activation observed in mammalian neuroblasts, intestinal crypts, and hair follicles (Bouchard-Cannon et al., 2013; Janich et al., 2011; Matsu-Ura et al., 2016; Zhao et al., 2013). Third, evolutionarily conserved molecules comprise the mechanical networks and enzymatic cascades that together remodel the epidermis and collagen-based cuticle across the molts (Chisholm and Hsiao, 2012; Frand et al., 2005; Katz et al., 2018; Page and Johnstone, 2007). Related mechanisms effect physiologic and pathologic episodes of tissue remodeling, including wound repair and tumor metastasis (Kessenbrock et al., 2015; Martin and Goldstein, 2014).

We previously reported that LIN-42, the *C. elegans* homolog of the core circadian clock protein and tumor suppressor PERIOD (Jeon et al., 1999), sets or sustains the 8 h intervals between molts (Monsalve et al., 2011). This finding suggested that an evolutionarily ancient but largely uncharacterized timer governs the biorhythm. Other components of the timer – especially regulators of gene expression – were envisioned but not identified. Based on existing and emerging knowledge about developmental and circadian clocks, we assigned priority to the evaluation of specific candidate genes through genetic, biochemical and bioinformatic approaches.

Interconnected positive and negative feedback loops (‘limbs’) with intrinsic delays – related, in part, to unequal rates of RNA versus protein synthesis and degradation – comprise both

developmental and physiologic clocks (Novak and Tyson, 2008). Transcriptional-translational feedback loops (TTFLs) are the mainstay of circadian clocks (Takahashi, 2016). Therein, PER proteins repress the transcription of *CLOCK* and *BMAL* during the night, whereas CLOCK and BMAL1 activate the transcription of *PER* and other genes during the day (Partch et al., 2014; Takahashi, 2017). Retinoid-Related Orphan Receptors (ROR) activate the expression of *BMAL1* in peripheral organs and the central nervous system (Cook et al., 2015; Zhang et al., 2017). A few microRNAs (miRNAs) have been identified in peripheral clocks and auxiliary regulatory loops, but the significance of post-transcriptional, rather than post-translational, repression in physiologic clocks is not yet known (Alvarez-Saavedra et al., 2011; Chen et al., 2013; Du et al., 2014).

The genome of *C. elegans* encodes a single homolog of mammalian RORs – the nuclear hormone receptor NHR-23 (Antebi, 2015) – but does not encode obvious homologs of *CLOCK* or *BMAL*. Several additional attributes of *nhr-23* motivated evaluation of its role in the molting timer: reiterative expression in the larval epidermis; an essential role in all four molts; several relevant target genes; and genetic interaction with *lin-42* (Frand et al., 2005; Kostrouchova et al., 1998, 2001; Kouns et al., 2011; Monsalve, 2013).

We also considered the *let-7* family of miRNAs (*let-7*, *mir-48*, *mir-84*, and *mir-241*; hereafter *"let-7s"*) as logical candidates for components of the molting timer. Historically, *let-7* and its paralogs were identified and characterized as genetic switches that direct chronological cell fates of epidermal stem cells—manifest by stage-specific patterns of cell division, fusion, and differentiation (Ambros and Ruvkun, 2018; Reinhart et al., 2000). As crucial factors in the heterochronic pathway, the *let-7* paralogs bring about the L2 fate, distinguished by asymmetric division of the seam cells (Abbott et al., 2005), whereas *let-7* itself brings about the L4 fate, distinguished by homotypic fusion of the seam cells into lateral syncytia. However, primary *let-7s*

transcripts are cyclically expressed in phase with the molts (Van Wynsberghe et al., 2011), consistent with temporally reiterated, as well as stage-specific, function(s). Moreover, *let-7s* repress the expression of *lin-42* and *vice versa* (McCulloch and Rougvie, 2014; Perales et al., 2014; Van Wynsberghe et al., 2014) – this is a direct mechanistic connection to the molting timer.

All nematodes molt four and only four times – striking and specific uniformity across some 25,000 different species including numerous parasites of humans and inhabitants of virtually all planetary ecosystems. In contrast, intra- and interspecies variation in the number of molts both before and after reproductive maturity occurs in animals of other phyla in the Ecdysozoan clade (Aguinaldo et al., 1997). Therein, the total number of molts varies in response to intrinsic and extrinsic factors including the salinity and temperature of aquatic habits, the availability of blood meals and other food sources, and the photoperiod (Esperk et al., 2007). The fundamental basis of this seemingly invariant limitation among nematodes is not known, despite the long-standing recognition of supernumerary molts associated with loss-of-function mutations in *let-7* and other heterochronic genes.

Here, we provide compelling evidence that both *nhr-23* and *let-7s* are central components of a unified timekeeping mechanism that governs both the frequency and finite number of molts in *C. elegans.* This evidence is based on longitudinal studies of the molting biorhythm in relevant genetic backgrounds, molecular and cell biological analyses, and bioinformatic approaches. Specifically, we show that a transcriptional – post-transcriptional feedback loop between NHR-23/ROR and *let-7s* operates within a genetic oscillator that governs the pace of the cycle, and also operates as an 'hourglass' timer that limits the number of molts. As both the core components and *cis*-regulatory elements composing this feedback loop are conserved from nematodes to mammals, our findings may apply to specific developmental and circadian clocks of

humans and related pathologies including birth defects, malignancies, sleep disorders, and metabolic syndromes (Oyama et al., 2017; Patke et al., 2017; Puram et al., 2016; Roenneberg and Merrow, 2016).

RESULTS

Counterbalancing effects of *nhr-23* and *let-7* on the pace of the molting cycle

As explained, we hypothesized that both *nhr-23* and *let-7s* function in the molting cycle timer—a genetic oscillator with at least three central components (Figure 1B). To test this hypothesis, we compared the biorhythm of molting in stage-specific *nhr*-23 knockdowns, *let-7s* mutants, and wild-type animals through a series of longitudinal studies that together spanned the L2 through young adult stages. By design, each study focused on three metrics: the interval of physical activity in the target stage – defined as the time elapsed between epochs of behavioral quiescence associated with the preceding and ensuing molts; the interval of quiescence associated with the ensuing molt; and the wake-to-wake interval – defined as the time elapsed between two sequential transitions from quiescence to activity. These metrics, sample sizes of each cohort, and statistical analyses are provided in Supplemental Table 1. All P values for related pair-wise comparisons were determined by an ordinary one-way ANOVA with Bonferroni's correction for multiple comparisons.

To knock down *nhr-23* during a particular target stage, wild-type hatchlings were first fed bacteria that expressed dsRNAs complementary to *nhr-23* on an empirically determined schedule (see Methods). This tactic ensured that all test subjects emerged in the target stage superficially normal, but none of the test subjects fully shed the cuticle from the target stage—signifying complete penetrance of the molting-defective (Mlt) phenotype associated with RNAi of *nhr-23*.

Age-matched, wild-type larvae fed the same bacterial strain transformed with an empty vector served as controls.

To evaluate the prospective role of *let-7s*, we tracked cohorts of *let-7(n2853)*, *let-7(mg279)*, and *let-7(mg279) mir-84(tm1304)* double mutants across late larval stages. Both *n2853* and *mg279* are associated with lower levels of mature *let-7*, relative to wild-type animals. However, *n2853* is a substitution in the seed sequence, whereas *mg279* is a 27 bp deletion upstream of the mature miRNA (Bracht et al., 2004; Reinhart et al., 2000). The null allele of *mir-84* enhances relevant phenotypes associated with *let-7(mg279)* (Hayes and Ruvkun, 2006). We also tracked *mir-48(Δ) mir-241(Δ); mir-84(n4037)* triple mutants across L2—when the corresponding miRNAs are expressed but mature *let-7* has not been detected (McCulloch and Rougvie, 2014).

The two rows of actograms in Figure 1C display the results of important longitudinal studies. Each actogram corresponds to an isogenic cohort of animals. Therein, each column represents one animal that emerged in the target stage (L4, top row or L3, bottom row), developed, and underwent the ensuing molt. Each animal was isolated during the preceding molt to achieve stringent synchronization at the outset. After it emerged, the worm was observed for approximately 1 min at regular 1-h intervals. At each timepoint, the worm was "active" if both pharyngeal muscle contractions (pumps) and sinusoidal locomotion were observed. Conversely, the subject was "lethargic" if neither pharyngeal pumps nor sinusoidal locomotion were observed, while its body posture resembled a hockey stick (Iwanir et al., 2013; Raizen et al., 2008). Separation of the preexisting cuticle from the body and detection of the shed cuticle on the culture plate signified the commencement and completion of ecdysis, respectively (Singh and Sulston, 1978).

As expected, the cohort of wild-type (control) animals that first emerged as L4s then entered and exited lethargus, shed the larval cuticle (ecdysed), and emerged as young adults

practically in sync (Figure 1C, top row and Supplemental Table 1). The cohort of *nhr-23(RNAi)* animals that emerged as L4s entered lethargus later and remained lethargic twice as long as the control cohort. All of the *nhr-23(RNAi)* animals began to pump and locomote once again, but oftentimes at lower rates than wild-type adults. In principle, this intermittent sluggishness might result from incomplete arousal or hindrance by unshed parts of the L4-stage cuticle. Regardless, the wake-to-wake interval of the L4-stage *nhr-23(RNAi)* cohort was 13 ± 1.1 h as compared with 10.3 ± 0.4 h for the control cohort (P≤0.0001). Following this trend, the L3-stage cohort of *nhr-23(RNAi)* larvae entered lethargus 1.4 ± 1.3 h later and remained in lethargus 2.2 ± 1.9 h longer than did the age-matched wild-type cohort (Figure 1C, bottom row). Remarkably, a particular *nhr-23(RNAi)* larva was quiescent but responsive to adverse stimuli across 9 consecutive time samples. Moreover, the cohort of *nhr-23(RNAi)* larvae molting from L2 to L3 were quiescent 3-fold longer than were age-matched controls; the respective lethargic intervals were 3.9 ± 1.1 h for *nhr-23* knockdowns versus 1.6 ± 0.4 h for control larvae (P≤0.0001). Thus, delayed and protracted sleep-like phases were associated with knockdown of *nhr-23* across three larval stages.

In contrast, *let-7(n2853)* mutants both entered and exited lethargus more quickly than did wild-type animals. For example, the wake-to-wake interval for the *let-7(n2853)* cohort developing from L4s into adults was only 7.9 ± 0.6 h—an acceleration of 2.9 ± 0.7 h relative to the wild-type cohort (Figure 1C, top row). All of the *let-7(n2853)* animals subsequently ruptured at the vulva—a hallmark of this strong loss-of-function allele (Ecsedi et al., 2015). In complementary studies, L4-stage cohorts of both *let-7(mg279)* single and *let-7(mg279) mir-84(tm1304)* double mutants also entered lethargus ahead of wild-type L4s (Supplemental Table 1). Moreover, the cohort of *let-7(n2853)* mutants observed from emergence in L3 onward passed through two consecutive lethargic phases and emerged as young adults ahead of the entire wild-type cohort (Figure 1C,

bottom row). As such, repetition of the L3 stage – a retarded heterochronic phenotype – cannot explain the acceleration of the L4 stage observed in *let-7(n2853)* mutants, because both the L3 and L4 stages of the mutants were shorter than those of wild-type larvae. Thus, advanced sleep-like phases and accelerated larval development were observed in three distinct *let-7s(-)* strains.

When we combined stage-specific *nhr-23(RNAi)* with *let-7(n2853)*, the altered biorhythms associated with each single mutant were partially co-suppressed. The L4-stage cohort of *nhr-23(RNAi) let-7(n2853)* double mutants entered lethargus later than did *let-7(n2853)* single mutants, but reawakened earlier than did *nhr-23(RNAi)* single mutants. As a result, the wake-to-wake interval of the L4-stage cohort of *nhr-23(RNAi) let-7(n2853)* double mutants was 10.6 ± 0.8 h—similar to the value of the wild-type cohort ($P \geq 0.9$). Partial co-suppression was also apparent during the L3 stage—the wake-to-wake interval of the double mutants was 1.4 ± 1.4 h shorter than *nhr-23(RNAi)* alone ($P = 0.0002$). Moreover, a triple knockout of *let-7* sisters partially suppressed the prolonged lethargy associated with knockdown of *nhr-23* across the L2/L3 molt, shortening the lethargic interval by 0.9 ± 1.0 h ($P=0.002$) (Supplemental Table 1). The metrics of the biorhythm of molting for the triple mutants were not significantly different from that of wild type. However, the relatively fast pace of the L2 stage combined with the resolution of the assay may have prohibited the detection of any acceleration.

Notably, *nhr-23(RNAi) let-7(n2853)* double mutants undergo aberrant ecdysis, indicating that the role of *nhr-23* in the sleep-wake cycles and ecdysis are genetically separable. However, none of the double mutants ruptured, suggesting that *let-7* antagonizes *nhr-23* in both the sleep-wake cycle and morphogenesis of the vulva.

Together, findings from the longitudinal studies suggest that both *nhr-23* and *let-7s* modulate the biorhythm of molting. Furthermore, the partial interdependence of opposing phenotypes of

loss-of-function alleles is consistent with the model that the molecules compose a feedback loop within a genetic oscillator rather than function in parallel genetic pathways to regulate the timing of the molting cycle.

A gain-of-function allele and high-copy *nhr-23* both accelerate the molting cycle.

We theorized that the partial co-suppression was dependent on increased expression of *nhr-23.* To further explore this possibility, we tracked cohorts of larvae that expressed multiple copies of *nhr-23* from an integrated, tandem array across both the L3 and L4 stages (Celniker et al., 2009). The majority of *wgIs43[nhr-23^{++}]* larvae, which overexpress *nhr-23*, entered lethargus and emerged in the next life stage faster than age-matched, wild-type animals (Figure 2). The wake-to-wake interval was 6.9 ± 0.6 h for the *wgIs43* cohort developing from L3 to L4, compared with 7.8 ± 0.6 h for the wild-type cohort (P ≤0.01). Combining *wgIs43[nhr-23^{++}]* with *let-7(n2853)* led to larval lethality and prohibited a similar analysis.

As a complementary approach, we also tracked *nhr-23(aaa20-ΔLCS)* larvae across the late larval stages (Figure 2). As we shall describe, *aaa20* is a precise deletion of the functional *let-7* consensus site (LCS) from the endogenous 3′ UTR of *nhr-23.* The majority of *nhr-23(aaa20-ΔLCS)* L3s entered lethargus and emerged as L4s before most wild-type L3s began to molt. The wake-to-wake interval of the *nhr-23(aaa20-ΔLCS)* L3-stage cohort was abbreviated by 1.5 ± 0.9 h relative to that of wild-type L3s. Thus, both increased dosage and de-repression of *nhr-23* were associated with advanced quiescent intervals and faster cycles—similar to earlier findings with *let-7(-)* mutants.

Taken together, the results from the longitudinal studies strongly suggest that reciprocal interactions between NHR-23 and *let-7s* ultimately impinge on the expression of *nhr-23* to govern

the pace of molting cycle. One molecular model that explains the results from the abovementioned longitudinal studies is that NHR-23 accelerates the cycle, partly by directly activating the expression of *let-7s*, whereas *let-7s* decelerates the cycle, partly by directly repressing the expression of *nhr-23*.

NHR-23 promotes the transient, reiterative expression of *let-7*.

NHR-23 and its mammalian ortholog RORα are two of the few nuclear hormone receptors that bind asymmetric DNA response elements (REs) as monomers, rather than bind repeated DNA REs as homo- or hetero-dimers. Both receptors bind the consensus sequence 5′-(A/G)GGTCA-3′ to activate transcription of target genes (Giguere et al., 1994; Kouns et al., 2011).

The minimal promoter of *let-7* (Johnson et al., 2003) contains three retinoid-related orphan receptor response elements (ROREs) identified by standard search algorithms (Figure 3A). The modENCODE consortium previously found that NHR-23 occupies a ~300 bp region aligned with the cluster of ROREs by chromatin immunoprecipitation paired with genome-wide sequence analysis (ChIP-Seq) (Celniker et al., 2009). To further substantiate and define the interactions among NHR-23 and promoters of *let-7s*, we paired chromatin immunoprecipitation with gene-specific, quantitative polymerase chain reactions (ChIP-qPCR). Toward this goal, we appended the coding sequence for a 3xFLAG affinity tag to the endogenous *nhr-23* gene using the CRISPR-CAS9 system (Paix et al., 2015) and out-crossed the resulting *nhr-23(xk22)* allele. NHR-23::3XFLAG proteins cross-linked to genomic DNA were then isolated from developmentally synchronized larvae. The signal flanking RORE3 was enriched 21-fold in QK159[*nhr-23::3xflag*] samples as compared with wild-type (N2) samples. In contrast, signal from the promoter of *col-19*, which is not targeted by NHR-23, was not detectably enriched in

either strain (Figure 3B). Notably, we captured protein-DNA interactions in mid-L4 larvae while the consortium captured such interactions in mid-L3 larvae. Together, the data show that NHR-23 binds one or more ROREs in the promoter of *let-7* during two sequential larval stages. Using the same combination of bioinformatic and biochemical approaches, we also found that NHR-23 occupies the promoters of three *let-7* sisters (*mir-48*, *mir-241* and *mir-84*) in both mid-L3 and mid-L4 larvae (Supplemental Figure 1).

We next asked whether *nhr-23* promotes temporally reiterated expression from the promoter of *let-7*. To address this question, we measured and compared the abundance of nuclear-localized GFP expressed from the *let-7* promoter (Kai et al., 2013) in stage-specific *nhr-23* knockdowns and age-matched control animals via quantitative fluorescence microscopy. In preliminary studies, we tracked the cycling signal associated with this particular *let-7p::nls-gfp* fusion gene and detected peaks early in the third and fourth molts. Accordingly, nuclei in the lateral epidermis were imaged within the first hour of the L3/L4 and L4/Adult molts (Figure 3C). The signal intensity in hyp7 nuclei was 2.3 ± 1.3-fold (mean ± sd) lower in *nhr-23(RNAi)* than control animals (Figure 3D). Levels of GFP detected in seam nuclei were more variable during the L3-to-L4 molt than the L4-to-Adult molt, possibly due to continuation of the cell cycle. Even so, the mean signal intensity in the seam was consistently lower in *nhr-23* knockdowns than control animals.

As a complementary approach, we used TaqMan qRT-PCR to detect both primary and mature *let-7* in successive samples of *nhr-23* knockdowns and mock-treated, wild-type (control) animals developing from L3s into young adults. Attenuation of the RNAi of *nhr-23* enabled the collection of hundreds of *nhr-23(RNAi)* animals late in larval development, as only 35% of *nhr-23(RNAi)* animals exhibited molting defects by the endpoint. Under these conditions, peak

levels of *nhr-23* transcripts were 4.1-fold lower in *nhr-23(RNAi)* than wild-type animals (data not shown). Levels of pri-*let-7* in control samples peaked in L3 and once again in L4. No such peak was detected in *nhr-23(RNAi)* animals. Specifically, transcript levels of pri-*let-7* detected in *nhr-23* knockdowns at 42 h were 3-fold lower than the peak value detected in age-matched, control larvae (Figure 3E). Levels of mature *let-7* stagnated in attenuated *nhr-23(RNAi)* knockdowns but rose continuously in control samples collected across the larval-to-adult transition (Figure 3F). Molting-defective larvae were first observed as levels of *let-7* plateaued, consistent with the attribution of both phenotypes to knockdown of *nhr-23*. Collectively, these findings strongly suggest that NHR-23 directly and repeatedly activates the transcription of primary *let-7* and might also instigate the pulsatile expression of other primary *let-7s* transcripts.

The 3′ UTR of *nhr-23* contains a repressive element complementary to *let-7s.*

We next asked whether *let-7*-family miRNAs target *nhr-23* transcripts in developing larvae. We identified a single element in the 868-bp 3′ UTR of *nhr-23* (Mangone et al., 2010) that perfectly complements the 5′ seed of *let-7* and partly complements the remainder of the miRNA. Hereafter, this element is called the *let-7* consensus site (LCS). Three other sequences in the 3′ UTR of *nhr-23* partially complement *let-7s* with mismatches to the seed (Figure 4A and Supplemental Table 2).

To assess the significance of the LCS, we designed and utilized a set of bicistronic reporters for post-transcriptional *cis*-regulatory elements, each housed in a distinct extrachromosomal array and unique transgenic strain (Figure 4B). Briefly, the coding sequence of tandem (td) Tomato was fused with the 3′ UTR of *nhr-23*, whereas the coding sequence of GFP was fused with the 3′ UTR of *unc-54*, which is not targeted by *let-7s.* An SL2 trans-splice site bridged the two fusion genes.

The promoter of *dpy-7* drove expression of the operon in the hypodermis. The readout was the ratiometric signal of TdTomato to GFP detected in the lateral epidermis. This approach controlled for potential differences in gene expression associated with particular arrays or mosaic animals rather than the test 3′ UTR.

Figure 4C shows the merged and individual signals detected in transgenic animals in the L4-to-A molt, when both *let-7* and *dpy-7* are highly expressed. The ratiometric signal for the *nhr-23* 3′ UTR reporter was ~6 fold lower than the negative control *unc-54* 3′ UTR reporter (Figure 4D). Any difference in the efficacy of trans-splicing or nonsense-mediated decay of pre-mRNAs could not account for the apparent repression of tdTomato, as no significant difference was detected in the absolute intensity of GFP expressed from either bicistronic reporter (1076 ± 704 A.U. versus 829 ± 392 A.U., respectively). Similarly, the ratiometric signal for the positive control *lin-41* 3′ UTR reporter was 3-fold lower than the negative control.

To identify the specific repressive elements(s), we systematically excised each of the four sites partially complementary to *let-7* from the bicistronic reporter for the 3′ UTR of *nhr-23* and compared the signal detected from each of the four resulting constructs with the signal detected from the full-length reporter for the *nhr-23* 3′ UTR. Excision of the LCS led to a two-fold increase in the ratio of tdTomato/GFP signals, relative to the average ratio (0.40 ± 0.10) associated with the unaltered reporter for the 3′ UTR of *nhr-23* (Figure 4E). Shortening the 3′ UTR could not explain the de-repression of tdTomato, considering that deletion of any other prospective target site led to customary, if not lower, levels of tdTomato, as compared with same-day controls. In theory, deletion of nt. 26-42 or nt. 623-646 from the 3′ UTR of *nhr-23* might relieve intramolecular competition for *let*-7s, potentiating the efficacy of the functional LCS. Alternatively, deletion of those particular residues could destabilize tdTomato transcripts. Regardless, this approach

identified a functional LCS in the 3′ UTR of *nhr-23*. Consistent with this result, a highly-sensitive, high-throughput approach to catalog *bona fide* targets of miRNAs identified the 3′ UTR of *nhr-23* among cellular transcripts associated with the ALG-1, the catalytic component of the worm RISC complex (Broughton et al., 2016; Grishok et al., 2001). Thus, the LCS in the 3′ UTR of *nhr-23* transcripts almost certainly binds *let-7s in vivo* and limits the expression of NHR-23 across multiple life stages.

Both the LCS and *let-7s* contribute to dampening the expression of *nhr-23.*

Going further, we generated a new allele of *nhr-23* – *aaa20* – by precise excision of the endogenous LCS using the CRISPR/CASPR9 system (Paix et al., 2015). The resulting strain was out-crossed to N2 thrice, generating ARF414 [*nhr-23(aaa20-ΔLCS)*]. Next, we detected and compared temporal waves in the abundance of *nhr-23* transcripts among wild-type animals and both *nhr-23(aaa20-ΔLCS)* and *let-7(n2853)* mutants developing from late L2s into young adults by TaqMan qRT-PCR. To skillfully delineate the chronology of alternating active and quiescent phases in each strain, we inspected and scored the behavior of ~100 worms at each timepoint, prior to collection of the sample. Lethargi were then identified *post-hoc* based on these measurements. Wild-type larvae developed more slowly than did gain-of-function *nhr-23(aaa20-ΔLCS)* or loss-of-function *let-7(n2853)* mutants in this particular experiment, consistent with the longitudinal studies. However, we captured oscillatory expression of *nhr-23* across the target stages among the time samples of each strain (Figure 5A and Supplemental Figure 3A).

Peak levels of *nhr-23* were typically detected one-third to one-half of the way through the L2, L3 and L4 stages in wild-type time samples. However, the amplitude of sequential waves dropped by a regular increment of 1.4-fold from one life stage to the next. Also, the steepness of

the curve (slope of ascent from the preceding trough to the stage-specific peak) typically exceeded the decay (slope of descent from the stage-specific peak to the ensuing trough). Both the amplitude and steepness of sequential waves declined in-step—an indication of dampening (Figure 5A′).

The expression curves for *nhr-23* were sharper – with higher peaks and wider troughs – both in *nhr-23(aaa20-ΔLCS)* mutants and *let-7(n2857)* mutants as compared with wild-type animals (Figure 5A). Sequential peaks in *nhr-23* transcript levels detected early in L3 and L4 were ~1.6-fold higher in *nhr-23(aaa20-ΔLCS)* samples than in wild-type samples, despite the dampening. The amplitude of oscillations in *let-7(n2853)* mutants was both elevated and also sustained, so the relative surplus increased steadily from one life stage to the next. The expression curves associated with *nhr-23*(*aaa20-ΔLCS)* and *let-7(n2853)* were ~3-fold and ~5-fold steeper than those detected in wild-type, respectively (Figure 5A′). Moreover, an extra pulse of *nhr-23* expression was detected in both *nhr-23*(*aaa20-ΔLCS)* and *let-7(n2853)* time samples collected after the fourth molt, intimating the potential for a supernumerary molt. The extent of escalation in both the amplitude and steepness of expression curves detected in *nhr-23*(*aaa20-ΔLCS)* and *let-7(n2853)* mutants, relative to the curve detected in wild-type animals, was nearly identical in a second, independent experiment (Supplemental Figure 3A-A′).

We used a similar approach to determine the extent to which *let-7s* repress the expression of *nhr-23* during the L2 stage. We compared the abundance of *nhr-23* transcripts in regular time samples of *nhr-23(aaa20-ΔLCS)* single mutants, *mir-241(Δ) mir-48(Δ) mir-84(n4037)* triple mutants, and wild-type larvae developing from late L1s into early L3s (Supplemental Figure 3B). The L2 stage wavelets detected in both mutants were 3-fold steeper and peaked at 2.2-fold higher levels than the wavelet detected in wild-type larvae.

In complementary studies, we tracked the abundance of NHR-23 in epidermal nuclei as indicated by the signal associated with functional NHR-23::GFP fusion proteins. Protein levels also cycled from the L2 through the L4 stage. For example, the signal peaked 3 h after emergence in the L4 stage but was not detected 2 h later (Supplemental Figure 4). Both the extent and kinetics of protein accretion and attrition corresponded well with the expression curves for *nhr-23* transcripts detected in wild-type larvae.

We went on to ask if *let-7s* regulate the abundance of NHR-23 proteins by comparing the abundance of NHR-23::GFP fusion proteins in *let-7(mg279) mir-84(tm1304)* mutants and transgenic but otherwise wild-type animals (Figure 5B). GFP was detected in the epidermal nuclei of *let-7s(-)* mutants molting from L4s to adults but was not readily detected in wild-type molting animals. The signal from NHR-23::GFP became conspicuous in *let-7(mg279) mir-84(tm1304)* mutants that had emerged as adults but remained dim in wild-type adults. Notably, the corresponding 3.4-fold increase in fluorescence intensity matched the 3.4-fold increase in abundance of *nhr-23* transcripts detected in *let-7(n2853)* versus wild-type samples collected at a comparable timepoint. Notably, the native *nhr-23* 3′ UTR was fused to *nhr-23::gfp* in the corresponding genetic reagent whereas the ectopic 3′ UTR of *unc-54*, which is impervious to *let-7s*, was fused to *nhr-23::gfp* in a similar but distinct reagent used in previous research (Hayes et al., 2006; Kostrouchova et al., 1998). As such, *let-7s* directly targeting *nhr-23::gfp::nhr-23* 3′ UTR transcripts can account for the dearth of GFP seen in wild-type adults and the profusion of GFP seen in *let-7s* mutants in the current study.

Together, these findings show that the endogenous LCS is indeed a *cis*-regulatory repressive element, strongly suggesting that *let-7* and its paralogs bind this functional LCS and

negatively regulate the expression of *nhr-23* transcripts and proteins while larvae transit the molts and emerge in the subsequent life stage.

Derepression and overexpression of *nhr-23* both elicit supernumerary molts.

As described above, there was no detectable dampening of *nhr-23* transcript levels in *let-7(n2853)* mutants, whereas the phenomenon was obvious in wild-type animals. Historically, mutations in *let-7* were isolated as retarded heterochronic mutants that underwent supernumerary molts (Hayes et al., 2006; Reinhart et al., 2000). Considering this, we hypothesized that *let-7*-dependent dampening of the oscillatory expression of *nhr-23* effectively counts down the molts and ultimately extinguishes the molting cycle.

To test this idea, we tracked and compared instances of molting-associated behaviors and fatalities between wild-type adults and age-matched, gain-of-function *nhr-23(aaa20-ΔLCS)* mutants or *wgIs43[nhr-23^{++}]* transgenic animals. At first, we inspected partially synchronized populations at regular timepoints 2–5 days after the emergence of adults. Behavioral quiescence – defined by a lack of detectable pharyngeal pumps or locomotion – was more common among both *nhr-23(aaa20-ΔLCS)* and *wgIs43[nhr-23^{++}]* adults than wild-type animals across this interval. Moreover, the percentage of quiescent *nhr-23(gf)* adults peaked and significantly exceed the percentage of quiescent wild-type adults during 3 to 4 successive time samples (Figure 6A). We next asked whether quiescent *nhr-23(aaa20-ΔLCS)* and *wgIs43[nhr-23^{++}]* adults observed at those particular timepoints were in fact undergoing lethargi associated with supernumerary molts rather than transient, satiety-induced quiescence (You et al., 2008). To distinguish between these two possibilities, we singled quiescent adults into 3 respective cohorts per genotype and tracked the animals within each cohort for an additional 12 h (Figure 6B). In parallel, we singled and tracked

quiescent wild-type adults. The overwhelming majority of singled *nhr-23(gf)* adults were quiescent for several hours and then attempted to ecdyse—a sequence of events indicative of a supernumerary molt. Most animals perished in the attempt to ecdyse but several nonetheless shed entire cuticles or parts thereof. By the abovementioned criteria, 97% (n = 34) of singled *nhr-23(aaa20-ΔLCS)* adults and 91% (n = 33) of singled *wgIs43[nhr-23^{++}]* adults underwent supernumerary molts whereas none (n = 11) of the wild-type adults did so ($P < 0.0001$, chi-square test). This phenotype co-segregated with both *nhr-23(aaa20-ΔLCS)* and *wgIs43[nhr-23^{++}]* through multiple out-crosses, indicative of genetic linkage (data not shown).

Figure 6C shows one example each of an *nhr-23(aaa20-ΔLCS)* and a *wgIs43[nhr-23^{++}]* adult that underwent aberrant molts and became trapped in partly shed cuticles. Both animals had eggs in the uterus. However, the *nhr-23(aaa20-ΔLCS)* animal had an old cuticle attached to its tail. Also, alae were visible on both the lateral surface of the extant cuticle and the partly shed cuticle, implying that the epidermis had terminally differentiated prior to the attempted molt. In this regard, the supernumerary molts associated with *nhr-23(aaa20-ΔLCS)* differ from the supernumerary larval-to-larval (L4/L5) molt associated with particular heterochronic mutations including *lin-29(n333)* (Ambros and Horvitz, 1984).

These results show that forced expression of *nhr-23* is sufficient to reanimate many of the behavioral and cell biological subroutines that comprise the molting cycle, but not sufficient to coordinate or orchestrate those events. Furthermore, *let-7(-)* mutants undergo extra molts (Hayes et al., 2006; Reinhart et al., 2000). Taken together, these data strongly suggest that the balance between the activity of NHR-23 and *let-7s* affects the total number of molts. Tipping the balance toward higher levels of NHR-23 triggers additional molts whereas tipping the balance toward

higher levels of *let-7s*, which occurs as normally over the course of development, causes cessation of the molting cycle.

NHR-23 and *let-7s* regulate most downstream effectors of the molting timer.

Biological clocks generate and sustain orderly waves in the expression of both core clock components and groups of "clock-controlled genes (CCGs)" that encode coordinated effectors of the resulting biorhythm. From this perspective, we considered how the negative feedback loop between *nhr-23* and *let-7s* might affect the timing of events that happen during specific phases and transitions between phases of the molting cycle.

To investigate this potential phenomenon, we selected a set of high-confidence output genes of the molting timer based on two criteria: first, expression of the gene oscillates with a period of 8–10 h across larval development (Hendriks et al., 2014; Kim et al., 2013), and second, activity of the gene affects one of the many distinct but interdependent steps within the molting cycle. Collectively, the 67 selected CCGs encode transcription factors and signaling molecules that control various subroutines, enzymes and matrix proteins that are involved in the synthesis and removal of cuticles, and neuropeptides that regulate quiescence and arousal (Supplemental Table 3). Next, we systematically and independently evaluated each CCG as a probable target of NHR-23 or *let-7s* through meta-analyses of published datasets and original bioinformatic approaches. A CCG classified as a direct target of NHR-23 met two or three of the following criteria: 1) NHR-23 occupied the 5′ regulatory region of the gene *in vivo*–as annotated in a ChIP-Seq dataset (Celniker et al., 2009); 2) the same regulatory region contained more ROREs than explicable by chance alone; and 3) knock down of *nhr-23* resulted in lower transcript levels (Kouns et al., 2011). A CCG classified as a target of *let-7s* met two criteria: 1) ALG-1 bound the

3′ UTR of the respective mRNA *in vivo*–as recorded in an iCLIP dataset (Broughton et al., 2016); and 2) the 3′ UTR contained more LCSs than explicable by chance. By these rubrics, 57% of CCGs were classified as shared targets of both NHR-23 and *let-7s*; 24% as targets of only NHR-23; 10% as targets of only *let-7s*; and 13% as targets of neither factor (Figure 7A, Supplemental Table 3). Notably, multiple response elements for the seemingly absent regulatory factor were identified within the regulatory regions of almost all CCGs classified as individual rather than shared targets. Therefore, 57% may be an underestimate and more outputs of the molting timer may ultimately be recognized as dual targets of both NHR-23 and *let-7s*. For comparison with non-CCGs, we randomly selected two dozen genes, culled particular genes that qualified as CCGs, and evaluated the remainder as described. Only 10% (2/20) of non-CCGs were classified as shared targets of both NHR-23 and *let-7s,* suggesting that NHR-23 and *let-7* together may regulate the expression of CCGs.

To determine the extent to which *nhr-23* and *let-7s* independently affect the oscillatory expression of an exemplary shared target, we detected and compared the levels of *mlt-10* transcripts in wild-type animals, *nhr-23(aaa20-ΔLCS)* mutants, and *let-7(n2853)* mutants collected at regular intervals from late L2 through young adulthood (Figure 7B). The amplitude of successive waves was practically constant in all three strains (Figure 7B)—despite the fact that expression of MLT-10 ceases in adults. However, the amplitude and steepness of expression waves for *mlt-10* were, respectively, ~1.8-fold and ~4-fold higher in both *nhr-23(aaa20-ΔLCS)* and *let-7(n2853)* mutants as compared with wild-type animals. These findings indicate that co-regulation by NHR-23 and *let-7s* alone is not sufficient to cause an incremental diminution of successive waves of gene expression—as observed in the specific case of *nhr-23*. Nonetheless, the sharper curves of *mlt-10* expression observed in both mutants imply that partly interdependent

waves in the abundance of NHR-23 and *let-7s* sculpt the temporal expression profiles of *mlt-10* and possibly many additional effectors of the molting timer.

The bioinformatics analysis refined and better substantiated our model for the regulatory interactions among core components of the oscillator. First and foremost, we gained direct evidence that NHR-23 promotes the expression of both *lin-42/PER* and *let-7s* transcripts, whereas *let-7s* repress the expression of both *lin-42/PER* and *nhr-23* transcripts—as depicted in Figure 1B. As described, three major isoforms of *lin-42* are recognized regulators of the molting cycle and components of the heterochronic pathway (Edelman et al., 2016; Jeon et al., 1999; Monsalve et al., 2011). We identified three ROREs in the unique promoter of *lin-42a* and three additional ROREs in the shared promoter of *lin-42b* and *c*. The ROREs in both promoters correspond with sites of NHR-23 enrichment detected by ChIP-Seq and annotated by the modENCODE consortium. To determine the extent to which NHR-23 activates the pulsatile expression of *lin-42*, we measured and compared the levels of *lin-42* transcripts across the L4 stage in attenuated *nhr-23* knockdowns and controls animals (Supplemental Figure 5B). As expected, levels of *lin-42* in control samples peaked in L3 and once again in L4. No such peak was detected in *nhr-23(RNAi)* L4s. The transcript levels of *lin-42* detected in *nhr-23* knockdowns at 42 h were 2.6-fold lower than the peak value detected in age-matched, control larvae. Moreover, we identified a single RORE 827-833 bp upstream of the start codon of human *PER2*.

We also identified four LCSs – one with perfect complementarity to the *let-7* seed region – in the shared 3′ UTR of *lin-42a* and *b*, suggesting that *let-7s* directly repress both *lin-42* isoforms (Supplemental Figure 5C). Although *lin-42* was previously described as containing sites complementary to *let-7s*, the specific *cis*-regulatory elements were not well defined(Reinhart et al., 2000). No LCSs were detected in the 3′ UTR of *lin-42c*, which is modelled as a dominant

negative. Yet again, we identified two LCSs perfectly complementary to the *let-7* seed in the 3′ UTR of human *Per2* transcripts, suggesting that the regulatory interactions among LIN-42 and *let-7s* are also conserved.

The bioinformatics analysis also provided evidence of both positive and negative autoregulation of *nhr-23*. We found eight ROREs within the upstream regulatory region of *nhr-23*; two of these ROREs were occupied by NHR-23 *in vivo*, as indicated by ChIP-Seq data from the modENCODE consortium. These data imply that NHR-23 activates the expression of itself—positive autoregulation by NHR-23 may regulate both the rate at which *nhr-23* transcripts rise and the amplitude of *nhr-23* expression during each larval stage. Negative autoregulation is likely caused by an isoform of NHR-23 that only has the ligand-binding domain (LBD)—in theory, this dominant negative would compete for the ligand with other isoforms of NHR-23 that have both the DNA-binding domain (DBD) and the LBD. Strikingly, the 3′ UTR of the LBD-only variant of NHR-23 lacks detectable LCSs and could therefore outcompete other NHR-23 isoforms, which have 3′ UTRs containing LCSs, more effectively late in larval development when the levels of *let-7s* increase.

Thus, we have found that dual regulation by NHR-23 and *let-7s* is a signature of clock-controlled genes. Because the number of *cis*-regulatory elements for both NHR-23 and *let-7s* varies among shared targets, it is reasonable to theorize that the predictable fluctuations in the ratio of NHR-23 versus *let-7s* produces orderly waves of expression of downstream effectors.

Broad conservation of reciprocal regulatory sites among *let-7* and *ROR* genes.

Is the feedback loop between NHR-23/ROR and *let-7s* conserved between nematodes and vertebrates? Using bioinformatic approaches, we searched for ROREs upstream of the homologs

of *let-7* in the fully sequenced and annotated genomes of humans, mice, and zebrafish (Figure 8A). We inspected the genomic region 3000 bp upstream of the precursor miRNA and identified 1 to 5 distinct ROREs upstream of the precursor miRNAs of all 11 homologs. Figure 8A depicts the ROREs found upstream of selected homologs of *let-7.* In each example, as many, if not more, ROREs were found than predicted by chance.

Next, we searched for LCSs in the 3′ UTRs of all 13 homologs of *nhr-23/ROR* annotated in the reference genomes of flies, frogs, zebrafish, chickens, mice and humans (Figure 8B). Before executing any particular search, we aligned and compared the nucleotide sequence of the query 3′ UTR with the sequences of corresponding ESTs. In two cases – zebrafish RORβ and RORγ – multiple ESTs supported longer 3′ UTRs than those presently annotated on the respective server (see Key Resources Table). We found one, two, or three LCSs perfectly complementary to the seed sequence of *let-7* within 3′ UTRs of 10 homologous genes. We found one or two more LCSs with a single mismatch to the seed sequence of *let-7* in six of the corresponding 3′ UTRs. For example, we identified one perfectly complementary LCS in the center of the validated 3′ UTR of human RORβ, flanked by two more sites with respective single nucleotide mismatches to the seed of *let-7* (Figure 8B). Similar LCSs with at most a single mismatch to the seed sequences of *let-7s* were found in the 3′ UTRs for each of the remaining four homologs (Supplemental Table 2 and data not shown). The apparent conservation of these particular cis-regulatory elements suggests that similar feedback loops among ROR and *let-7s* may control the cyclical expression of target genes in human tissues.

DISCUSSION

The principal findings of this report unite two distinct time keeping mechanisms mutually dependent on a transcriptional – post-transcriptional feedback loop between NHR-23 and *let-7s*: namely, the genetic pathway that controls the singular switch from larval to adult fates, and the genetic oscillator that controls the biorhythm of the molting cycle (Figure 9A).

The negative feedback between NHR-23 and *let-7s* sets the pace of the oscillator.

Core components of the molting cycle timer, including NHR-23 and the *let-7* family miRNAs, together govern the period of the molting cycle. The feedback loop between NHR-23 and *let-7s* functions in an oscillator-based mechanism to regulate the duration of the molting cycle. Therein, NHR-23/ROR transcriptionally activates *let-7,* the *let-7* sisters and *lin-42/per*, which represses the expression of pri-*let-7* (McCulloch and Rougvie, 2014; Perales et al., 2014; Van Wynsberghe et al., 2014). The *let-7* family post-transcriptionally represses both *nhr-23* and *lin-42*. These interconnected positive and negative feedback loops generate waves in expression of both core clock components, as well as output/target genes. (Figure 9A)

In theory, intrinsic rates of accumulation of core components and small differences in the threshold concentrations of core components needed to regulate specific downstream targets could enable a single timer to illicit orderly waves in the expression of distinct sets of proteins to mediate sequential transitions or events in the molting cycle (Figure 9C-D). We propose that the levels of NHR-23 are rate-limiting. Thus, early in each larval stage, as animals commit to a forthcoming molt, NHR-23 first reaches a functional concentration at the promoters of genes with relatively higher numbers of ROREs, such as *fbn-1* and *noah-1*, and initiates biogenesis of the sheath. At the same time, NHR-23 also promotes accumulation of the repressor *let-7*. As NHR-23 continues to

accumulate, the protein activates the expression of genes with relatively fewer ROREs such as *mlt-10* and *osm-11*, which respectively encode components of the cuticle and sleep-promoting peptides (Meli et al., 2010; Singh et al., 2011). In this manner, NHR-23 schedules the start of cuticle biogenesis and onset of lethargus. Then, *let-7*-mediated repression of the same CCGs and *nhr-23* schedules both the end of cuticle remodeling and lethargus. Repression of *nhr-23* delays accumulation of the protein in the next life stage and the onset of any subsequent molt. Thus, negative feedback between NHR-23 and *let-7s* regulates the pace of the molting cycle in part by controlling the rate at which *nhr-23* transcripts accumulate and the amplitude of *nhr-23* expression. The relatively slow ascent and rapid descent of *nhr-23* transcript levels, the evidently short half-life of NHR-23 proteins made in the epidermis and the ~1.6 h time difference between the accumulation of NHR-23 and accumulation of *let-7s* together likely impact the expression curves of multiple CCGs and, by extension, the temporal organization of critical subroutines within progressive phases of the molting cycle.

Consistent with this model, earlier onset of lethargus and accelerated development are observed in both *nhr-23(aaa20-ΔLCS)* and *let-7(n2853)* mutants—both mutants have steeper curves and higher amplitude of *nhr-23* expression. In contrast, delayed and protracted lethargi are observed in *nhr-23(RNAi)* animals, which have shallower curves and lower amplitude of *nhr-23* expression.

The concept that levels of NHR-23 must reach target-specific thresholds to effectively regulate gene expression is supported by particular findings in this report and also by current knowledge in the fields of gene regulation and chronobiology (Antebi, 2015; Takahashi, 2017). Indeed, the capacity of NHR-23 to activate any specific target might depend on its concentration relative to the number of functional ROREs in the target promoter; the abundance of co-activators,

co-repressors, and competitive NHRs; and the availability of as-yet unidentified ligand(s) derived from dietary steroids or exogenous cholesterol (Galles et al., 2018; Santori et al., 2015). Based on conservation of several key residues that are necessary for ligand-binding between the mammalian and worm homologs, the ligand for NHR-23 is likely either cholesterol itself, a precursor for cholesterol or a derivative of cholesterol (Kallen et al., 2002; Santori et al., 2015).

Intrinsic differences between the rates of both protein and miRNA biogenesis and decay influence the time intervals needed for levels of core clock components to rise from troughs to effective/functional concentrations—thereby dictating the period of the rhythm. Intrinsic factors such as nutritional status and body size and extrinsic factors such as temperature and biophysical aspects of the microenvironment likely entrain the rhythm by impinging on the rise or fall in abundance of core clock components.

let-7 **mediated dampening of** ***nhr-23*** **levels sets the number of oscillations.**

We invoke an hourglass-like mechanism to describe the effect of *let-7* on the total number of molts in *C. elegans* (Figure 9B). We propose that the balance between the activity of NHR-23 versus activity of *let-7*s controls the finite number of molts. In our model, NHR-23 is a positive effector and *let-7s* are negative regulators of molting—consistent with this model, both *nhr-23(gf)* and *let-7(lf)* mutants undergo extra molts. As larvae develop from one stage to the next, the amplitude of NHR-23 expression gradually declines whilst the levels of *let-7s* gradually increase, culminating in the extinction of the cycle in adulthood. We have shown that *let-7*-mediated repression is at least partially responsible for the dampening of *nhr-23* expression.

The precipitous increase in the levels of *let-7s* during the L3 and L4 stages is in part due to the action of the heterochronic pathway—for example, the induction of transcriptional activators

of *let-7s* such as DAF-12 and down-regulation of post-transcriptional repressors such as LIN-28 (Bethke et al., 2009; Hammell et al., 2009; Rougvie, 2001). The capacity of *let-7s* to silence any specific target might depend on the number of LCSs within the 3′UTR; the abundance of cooperative miRNAs, and the availability of processing factors or RISC components such as Dicer and ALG-1, respectively. Many of these factors change in predictable ways over time, adding layers of complexity to the timing machinery.

Gradual reduction of positive autoregulation by NHR-23 and increase in negative autoregulation of NHR-23 through successive larval stages are two more factors that could contribute to the dampening of *nhr-23* expression. Thus, NHR-23 and *let-7s* are both points of integration between the molting cycle timer and the heterochronic pathway.

NHR-23 and *let-7* act together with other feedback loops, by a possibly conserved mechanism, to regulate developmental timing.

This study recognizes and integrates miRNA-mediated feedback loops within developmental timers. Our findings are consistent with the emerging concept that miRNA-mediated feedback loops increase the robustness of numerous gene regulatory networks and related outcomes, including cell fate decisions, stress responses, and developmental trajectories. In this context, our work shows that feedback loops among NHR-23/RORα, LIN-42/PER, and *let-7* family miRNAs appear to preserve the capacity of cells and developing animals to switch between bi-stable states at regular intervals. *let-7* then functions to shut down the “pro-molt” cue NHR-23 when animals become adults and start laying eggs.

ROR and mammalian *let-7* both regulate the expression of core clock components in the hepatic circadian clock. Specifically, RORs promote the expression of the clock components

Bmal1 and *Cry1*, as well as clock-controlled genes *Elovl3* and *Cyp8b1*, in both the livers of mice and cultured human liver cell lines (Takeda et al., 2012; Zhang et al., 2017). Liver-specific genetic disruption of only RORγ, or in combination with RORα, alters the levels of serum cholesterol, HDL and LDL, and liver triglycerides relative to wild-type mice (Takeda et al., 2014; Zhang et al., 2017). Additionally, the 3′UTR of *Cry2* represses expression of a *firefly luciferase* reporter gene in the liver – the repression is dependent on an LCS in the 3′UTR (Du et al., 2014). Both the core components and cis-regulatory sites comprising the molting timer are conserved between nematodes and mammals. Thus, our work on the molting timer has implications for mammalian clocks and related disorders of sleep and metabolism. Our findings provide a different and authentic perspective of related gene regulatory networks that complements and extends current models and applies to human health and disease.

ACKNOWLEDGEMENTS

The American Cancer Society (RSG-12-149-01-DDC to ARF), the National Science Foundation (IOS1258218 to ARF), and the National Institutes of Health (R01 GM118875-04 awarded to JKK) supported this research. Some strains were provided by the *Caenorhabditis* Genetics Center (CGC), which is funded by the NIH Office of Research Infrastructure Programs (P40 OD010440). We thank Amy Pasquinelli (University of California, San Diego) for helpful discussions and sharing reagents. We also thank Ann Rougvie (University of Minnesota) for helpful discussions and critiques of this manuscript.

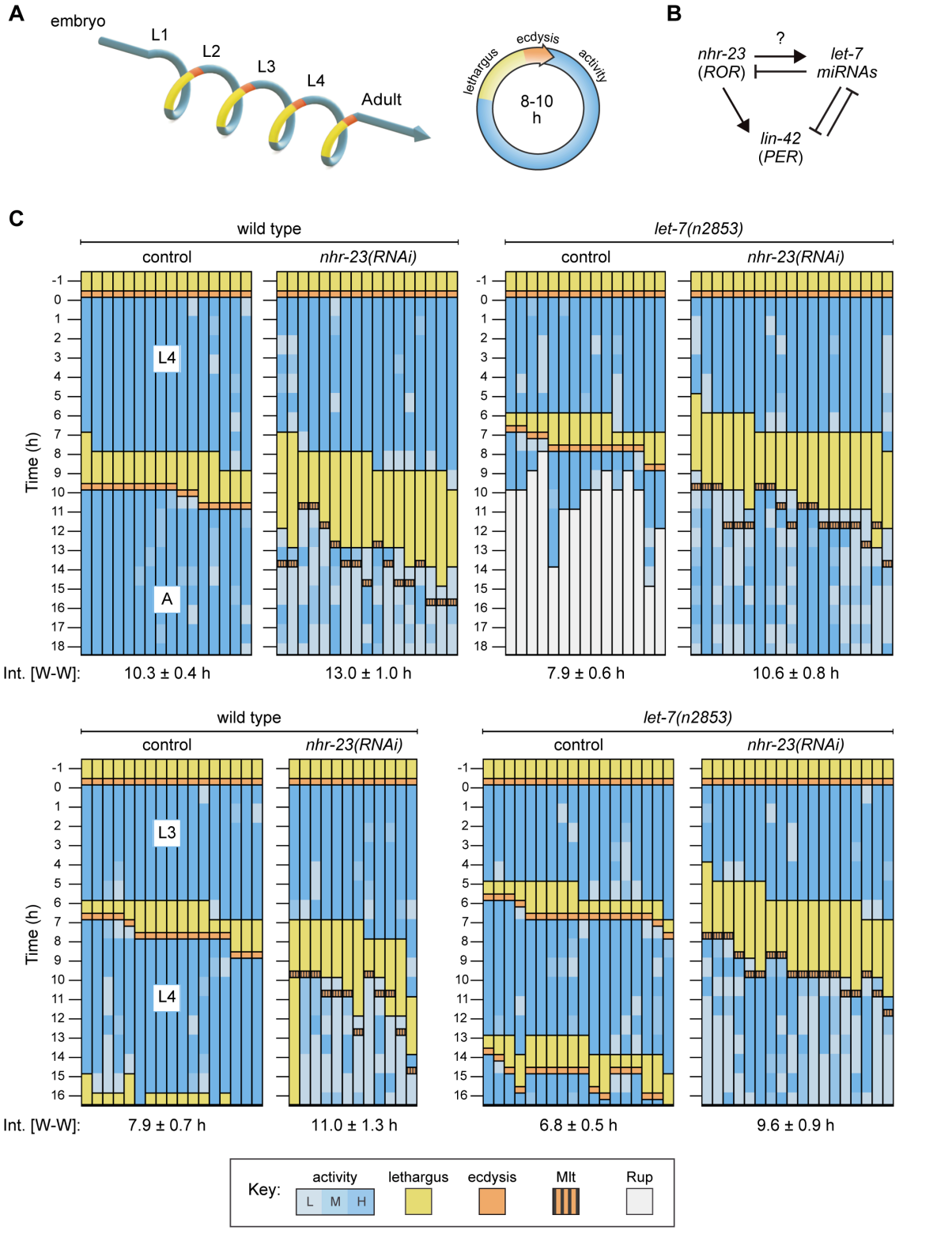
A
embryo
L1
L2
L3
L4
Adult
lethargus
ecdysis
activity
8-10 h
B
?
nhr-23 (ROR)
let-7 miRNAs
lin-42 (PER)
C
wild type
let-7(n2853)
control
nhr-23(RNAi)
Time (h)
L4
A
Int. [W-W]:
10.3 ± 0.4 h
13.0 ± 1.0 h
7.9 ± 0.6 h
10.6 ± 0.8 h
L3
7.9 ± 0.7 h
11.0 ± 1.3 h
6.8 ± 0.5 h
9.6 ± 0.9 h
Key:
activity
L M H
lethargus
ecdysis
Mlt
Rup

Figure 1. Opposite and codependent effects of *nhr-23* and *let-7* on molting biorhythms. **A)** Stages of the life cycle (left) and the molting cycle (right) of *C. elegans*—emphasizing the regular intervals of sleep-like lethargi and physical activity. The same color-code applies to the following actograms. **B)** Diagram of the predicted molecular-genetic oscillator underlying this biorhythm. Arrowheads signify positive regulation; bars, negative regulation. Question marks distinguish regulatory events evaluated in this study from those previously established. **C)** Actograms depict the behavior, life stage and phenotype of worms observed at 1 h intervals from emergence in L4 (top) or L3 (bottom) forwards. Each chart combines records from two independent trials. The chronological records within each column correspond to a single worm. For aesthetic purposes, columns were arranged (left to right) by the start and end of lethargi. In addition, the molting-defective phenotype is labelled only when first detected. Relevant scoring rubrics are fully defined in the results and methods. Herein, tiers of activity were assigned *post-hoc* using a one-way, standard scale defined by standard deviations from the mean pumping rate of age-matched, wild-type animals. The wake-to-wake (w-w) interval of each cohort is indicated. Supplemental Table 1 includes the active, lethargic, and w-w intervals of these eight cohorts and additional cohorts of both *let-7s(-)* mutants and *nhr-23* knockdowns. Strains N2 [wild-type] and QK059 [*let-7(n2853)*] were tested in this study.

Supplemental Table 1 – Relates to Figures 1 and 2

Metrics of the Molting Biorhythm Associated with Specific Genotypes														
			Interval (h)											
L4 stage cohort			Active				Lethargic				Wake-to-Wake			
Strain	RNAi	N	mean	sd	cv	p	mean	sd	cv	p	mean	sd	cv	p
wild type (N2)	–	16	8.1	0.5	0.06	–	2.2	0.4	0.18	–	10.3	0.4	0.05	–
wild type	*nhr-23*	17	8.4	0.8	0.09	n.s.	4.6	0.7	0.16	****	13.0	1.1	0.08	****
let-7(n2853)	–	15	6.3	0.4	0.08	****	1.5	0.5	0.33	*	7.9	0.6	0.08	****
let-7(n2853)	*nhr-23*	19	6.7	0.6	0.10	****	3.9	0.6	0.16	****	10.6	0.8	0.07	n.s.
let-7(n2853) †	–	17	6.7	0.6	0.09	****	1.6	0.5	0.30	**	8.4	0.6	0.07	****
wild type (GR1395)	–	20	7.8	0.5	0.07	–	2.2	0.6	0.18	–	10.0	0.5	0.05	–
let-7(mg279)	–	20	7.2	0.6	0.08	**	2.2	0.4	0.17	n.s.	9.3	0.6	0.06	**
let-7(mg279) mir-84(tm1304)	–	18	6.1	0.9	0.15	****	2.4	0.6	0.25	n.s.	8.5	0.9	0.15	****
wild type (N2)	–	12	8.1	0.7	0.08	–	2.0	0.0	0.0	–	10.0	0.7	0.07	–
wgIs43[nhr-23++]	–	17	7.2	0.5	0.07	***	2.2	0.6	0.29	n.s.	9.4	0.5	0.05	**
nhr-23(*aaa20-ΔLCS*)	–	25	6.8	0.7	0.1	****	2.1	0.3	0.16	n.s.	8.9	0.6	0.07	****
L3 stage cohort			Active				Lethargic				Wake-to-Wake			
Strain	RNAi	N	mean	sd	cv	p	mean	sd	cv	p	mean	sd	cv	p
wild type (N2)	–	17	6.3	0.4	0.07	–	1.6	0.5	0.31	–	7.9	0.7	0.08	–
wild type	*nhr-23*	12	7.7	1.2	0.15	****	3.8	1.9	0.49	****	11.0‡	1.3	0.12	****
let-7(n2853)	–	18	5.6	0.6	0.11	*	1.3	0.4	0.36	n.s.	6.8	0.5	0.07	*
let-7(n2853)	*nhr-23*	18	5.8	0.8	0.13	n.s.	3.8	0.6	0.17	****	9.6	0.9	0.09	****
wild type (N2)	–	13	6.4	0.7	0.11	–	1.4	0.5	0.37	–	7.8	0.6	0.08	–
wgIs43[nhr-23++]	–	15	5.2	0.9	0.18	***	1.7	0.6	0.34	n.s.	6.9	0.6	0.09	**
nhr-23(*aaa20-ΔLCS*)	–	19	5.1	0.7	0.14	***	1.2	0.5	0.44	n.s.	6.3	0.7	0.11	****
L2 stage cohort			Active				Lethargic				Wake-to-Wake			
Strain	RNAi	N	mean	sd	cv	p	mean	sd	cv	p	mean	sd	cv	p
wild type (N2)	–	18	5.9	0.3	0.05	–	1.3	0.5	0.36	–	7.2	0.4	0.06	–
wild type	*nhr-23*	19	6.1	0.6	0.10	n.s.	3.9	1.1	0.28	****	9.9	1.0	0.10	****
mir-48(Δ) mir-241(Δ); mir-84(n4037)	–	17	6.3	0.7	0.11	n.s.	1.3	0.5	0.36	n.s.	7.6	0.7	0.10	n.s.
mir-48(Δ) mir-241(Δ); mir-84(n4037)	*nhr-23*	15	6.4	0.8	0.13	n.s.	3.0	0.4	0.13	****	9.4	0.8	0.09	****

†Entry for the L3 cohort fortuitously observed throughout L4 and depicted by the penultimate actogram in Figure 1C.

‡Value excludes the one and only *nhr-23(RNAi)* larvae that remained lethargic at the final time-sample.

Supplemental Table 1. Metrics of the molting biorhythm associated with specific genotypes. The active, lethargic, and wake-to-wake intervals are defined in the text. The values derived from longitudinal studies of stage-specific cohorts of singled, isogenic worms. The top row of each section corresponds to the same-day cohort of singled, wild-type worms. Dashes (–) beneath 'RNAi' indicate continuous cultivation of the worms on *E. coli* HT115(DE3). "N" is the cumulative sample size from two independent trials. All *p* values were generated by pairwise comparisons between individual metrics tabulated for a specific cohort of test subjects and also for the same-day, age-matched cohort of control subjects: ****$p \leq 0.0001$, ***$p \leq 0.001$, *$p \leq 0.05$; Ordinary One-Way ANOVA with Bonferroni's correction for multiple comparisons. Entries in the top row of each subsection correspond to six distinct cohorts of control subjects. By order of first appearance in the table, the other strains tested were QK509 [*let-7(n2853)*], GR1395, GR1436, ARF249, OP43, ARF414 and VT1066. Notably, both QK509 [*let-7(n2853)*] and the ancestral strain MT7626 [*let-7(n2853)*] developed at an accelerated pace: 71% of QK059 hatchlings and 79% of MT7626 hatchlings transited the larval stages and emerged as young adults within 42 h of cultivation with food, as compared with 12% of N2 hatchlings (N=100, $p \leq 0.0001$, chi-square test).

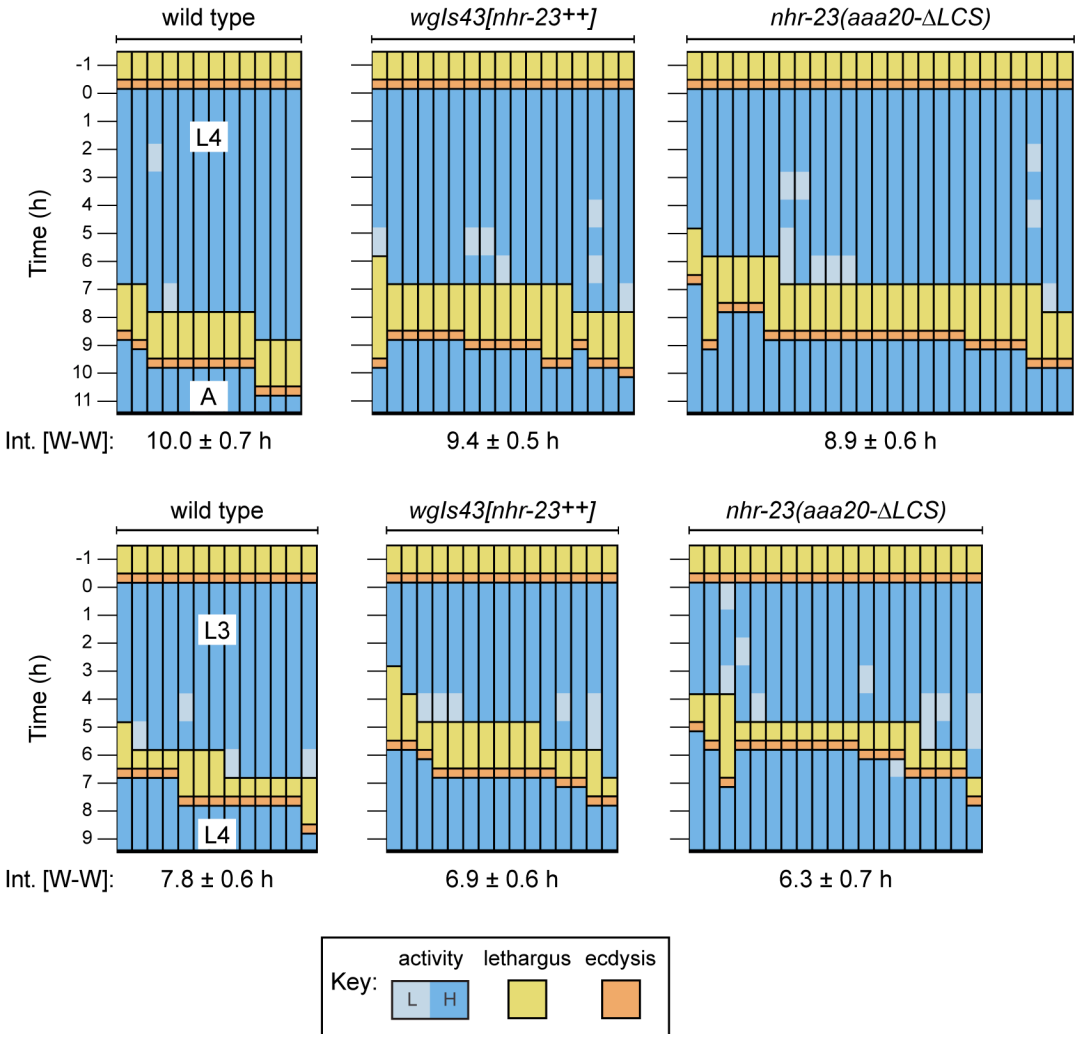
wild type
wgIs43[nhr-23++]
nhr-23(aaa20-ΔLCS)
Time (h)
-1
0
1
2
3
4
5
6
7
8
9
10
11
L4
A
Int. [W-W]: 10.0 ± 0.7 h
9.4 ± 0.5 h
8.9 ± 0.6 h
wild type
wgIs43[nhr-23++]
nhr-23(aaa20-ΔLCS)
Time (h)
-1
0
1
2
3
4
5
6
7
8
9
L3
L4
Int. [W-W]: 7.8 ± 0.6 h
6.9 ± 0.6 h
6.3 ± 0.7 h
Key:
activity
lethargus
ecdysis
L
H

Figure 2. High copy-number and derepression of *nhr-23* both lead to advanced lethargi and rapid development. Actograms depict the behavior and life stage of single animals observed at regular 1 h intervals, as described in Figure 1C. In this case, high or low activity refers to continuous or sporadic pharyngeal pumping observed during the time sample. Strains tested were: N2, OP43[*wgIs43*], and ARF414[*nhr-23(aaa20-ΔLCS)*].

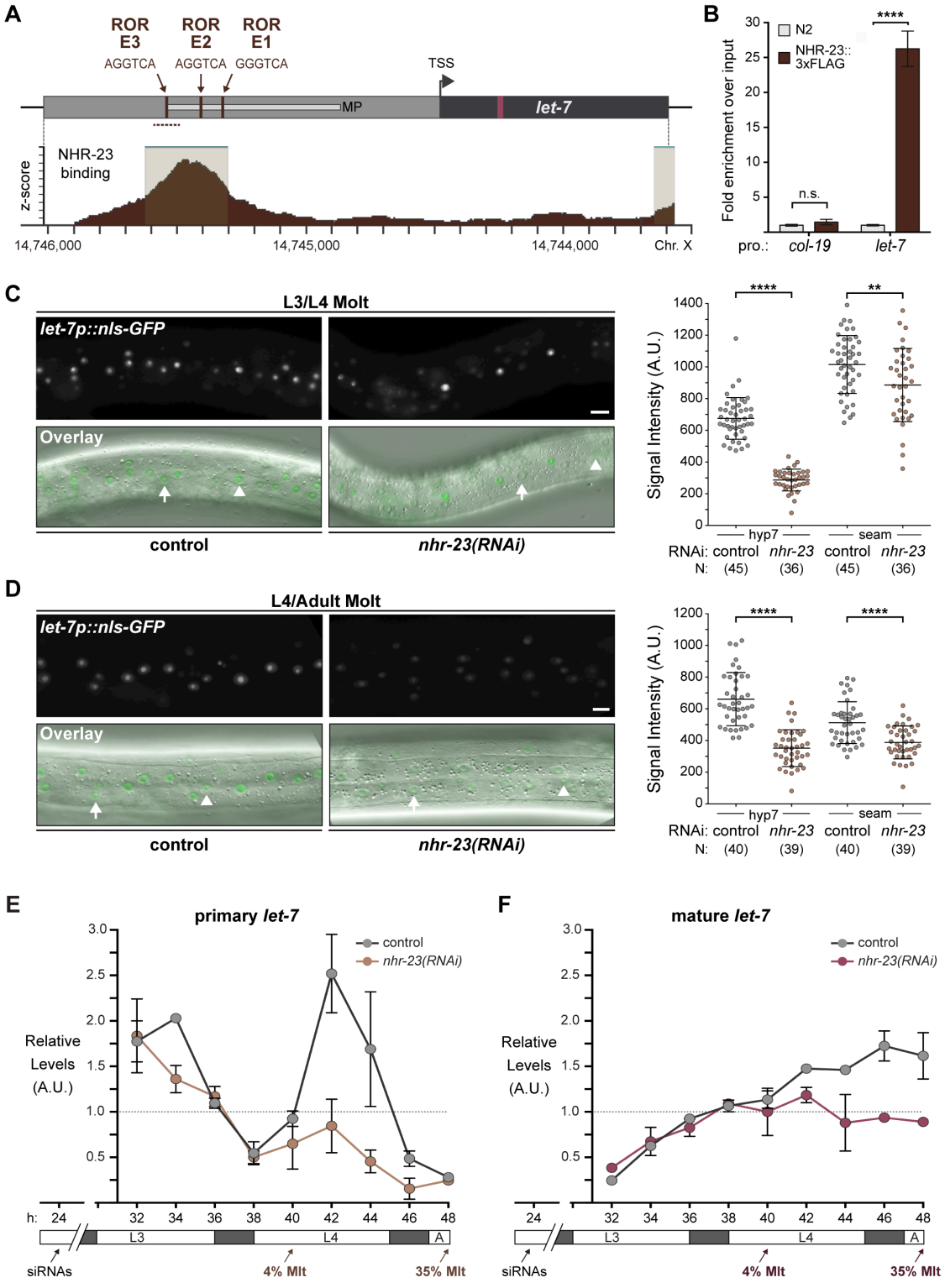
A
ROR E3
ROR E2
ROR E1
AGGTCA
AGGTCA
GGGTCA
TSS
MP
let-7
NHR-23 binding
z-score
14,746,000
14,745,000
14,744,000
Chr. X
B
N2
NHR-23:: 3xFLAG
****
n.s.
Fold enrichment over input
pro.:
col-19
let-7
C
L3/L4 Molt
let-7p::nls-GFP
Overlay
control
nhr-23(RNAi)
****
**
Signal Intensity (A.U.)
hyp7
seam
RNAi: control nhr-23 control nhr-23
N: (45) (36) (45) (36)
D
L4/Adult Molt
let-7p::nls-GFP
Overlay
control
nhr-23(RNAi)
****
****
Signal Intensity (A.U.)
hyp7
seam
RNAi: control nhr-23 control nhr-23
N: (40) (39) (40) (39)
E
primary let-7
control
nhr-23(RNAi)
Relative Levels (A.U.)
h:
L3
L4
A
siRNAs
4% Mlt
35% Mlt
F
mature let-7
control
nhr-23(RNAi)
Relative Levels (A.U.)
L3
L4
A
siRNAs
4% Mlt
35% Mlt

Figure 3. NHR-23 activates the pulsatile transcription of *let-7*. **A)** Schematic of the *let-7 locus* aligned with ChIP-Seq data for NHR-23 contributed by the modENCODE consortium. This schematic shows the correspondence between ROREs; the minimal promoter (MP) of *let-7*; and the chromosomal region bound to NHR-23 *in vivo*. In the gene model, gray shading denotes upstream regulatory sequences; arrow, the major transcriptional start site (TSS); black shading, transcribed sequences; and red shading, the sequence of mature *let-7*. Dotted line represents the amplicon quantified by ChIP-qPCR. **B)** Enrichment of the *let-7* promoter in chromatin crosslinked to NHR-23, as determined by ChIP-qPCR. Samples of mid-L4 stage larvae that expressed either NHR-23::3xFLAG or untagged NHR-23 from the endogenous *nhr-23* locus were collected and processed in parallel. Values represent the mean ± sd of two independent trials, each of which included two technical replicates. Values for the amplicon of interest in QK159 [*nhr-23::3xflag*] were normalized to the average value of the amplicon in N2 within each trial. ****p≤0.0001; Two-way ANOVA with Bonferroni's correction for multiple comparisons. A third independent trial showed that NHR-23::3XFLAG was enriched at the promoter of *let-7* by 11.4 ± 2.7-fold (mean ± sd) in QK159 samples relative to wild type, consistent with the trend observed in the two trials depicted here. **C-D)** Representative pairs of fluorescence images and respective overlays (GFP/DIC) show nuclear-localized GFP expressed from the promoter of *let-7* in the lateral epidermis. Arrows point to nuclei in hyp7 syncytia; arrowheads, seam nuclei. Scale bars = 20 μm. Adjacent scatter plots show aggregated values from two independent trials. Bars signify the mean and sd. ****p≤0.0001, **p≤0.01, Ordinary One-Way ANOVA with Bonferroni's correction for multiple comparisons. **E)** Levels of pri-*let-7* determined by TaqMan qRT-PCR. Each value was normalized to *ama-1* transcript levels in the same sample. Values were then normalized to the average of all control time samples. Symbols represent the mean and range from two biological

replicates. The x-axis indicates time elapsed (h) on food. The underlying bar depicts developmental stages; gray boxes therein signify observed intervals of behavioral quiescence. The times of initial exposure to *nhr-23* siRNAs and the appearance of molting-defective *nhr-23(RNAi)* larvae are indicated. **F)** As above for levels of mature *let-7*, except that values were first normalized to levels of the snoRNA U18 in the same sample. The strains used were N2, PQ462, and QK159.

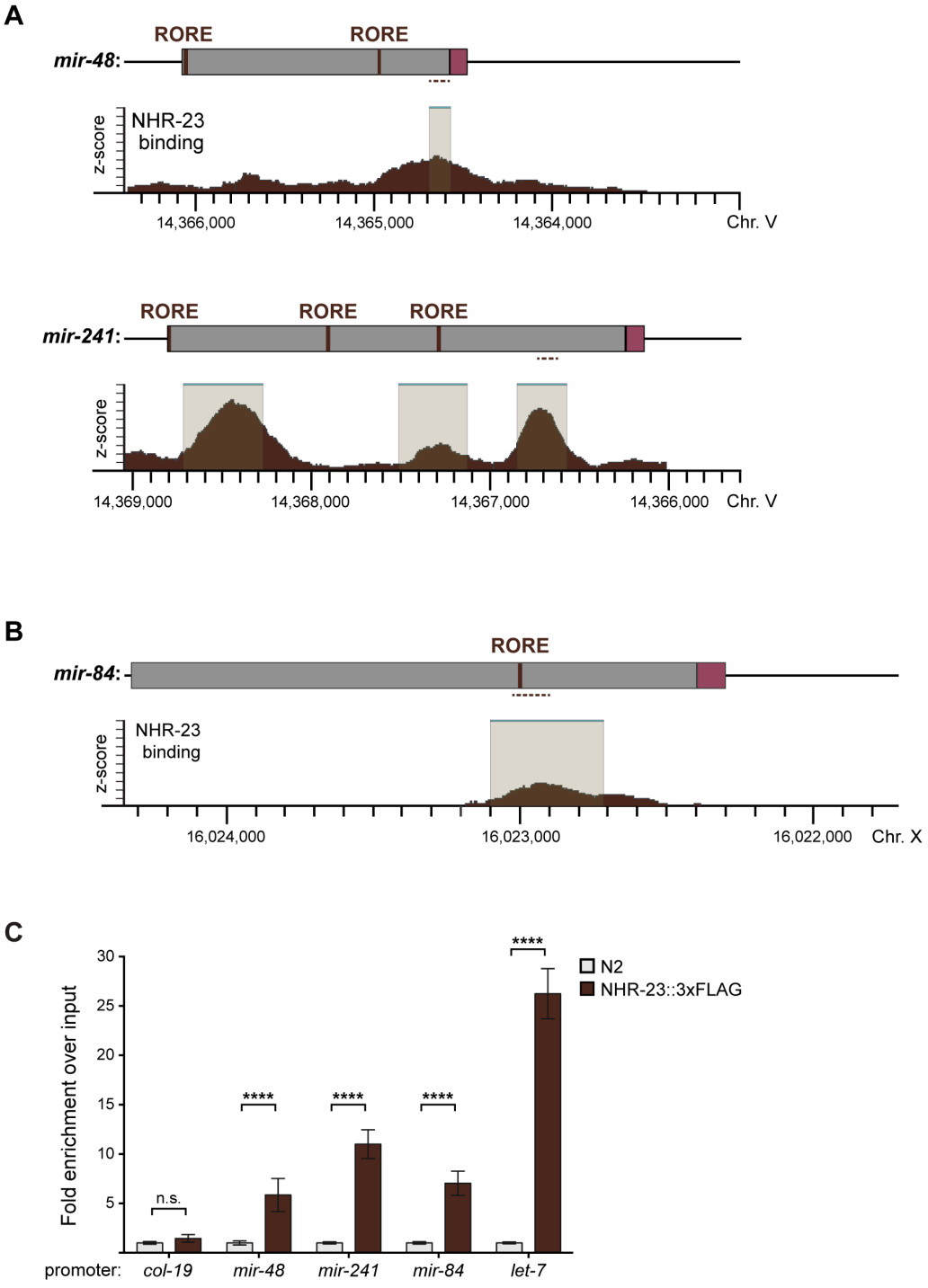
A
RORE
RORE
mir-48:
NHR-23
binding
z-score
14,366,000
14,365,000
14,364,000
Chr. V
RORE
RORE
RORE
mir-241:
z-score
14,369,000
14,368,000
14,367,000
14,366,000
Chr. V
B
RORE
mir-84:
NHR-23
binding
z-score
16,024,000
16,023,000
16,022,000
Chr. X
C
Fold enrichment over input
30
25
20
15
10
5
n.s.
****
****
****
****
N2
NHR-23::3xFLAG
promoter:
col-19
mir-48
mir-241
mir-84
let-7

Supplemental Figure 1. NHR-23 interacts with ROREs upstream of *let-7* paralogs**. A)** Three analogous schematics show the alignment of ROREs identified in verified or predicted upstream regulatory regions (gray shading) of *mir-48*, *mir-241* and *mir-84* with NHR-23 occupancy of the respective chromosomal regions (brown shading) as captured in mid-L3s by ChIP-Seq, analyzed and contributed by the modENCODE consortium (Celniker et al., 2009). Beige shading with a teal liner indicates regions of significant enrichment. Coordinates refer to *C. elegans* Chr. X (NC_003284.9) and Chr. V (NC_003283.11) as indicated. **B)** Detection and quantitation of the indicated 100 bp fragments upstream of *mir-48*, *mir-241* and *mir-84* by ChIP-qPCR, as described in Figure 3B. Arrows mark the location of qPCR primers. Plungers and bars represent the mean ± sd from four distinct samples: two technical replicates per two biological replicates. ****$p \leq 0.0001$, Two-way ANOVA with Bonferroni's correction for multiple comparisons. For a particular gene-specific amplicon, the value for each QK159 or N2 sample was first normalized to the respective input. The average fold-enrichment in QK159 samples was then normalized to the average fold-enrichment in N2 samples. Following the same trend, normalized values for the fold-enrichment of promoter fragments for *mir-48*, *mir-241,* and *mir-84* detected in a third biological replicate were 2.9 ± 0.3, 4.7 ± 0.6, and 1.5 ± 0.3, respectively.

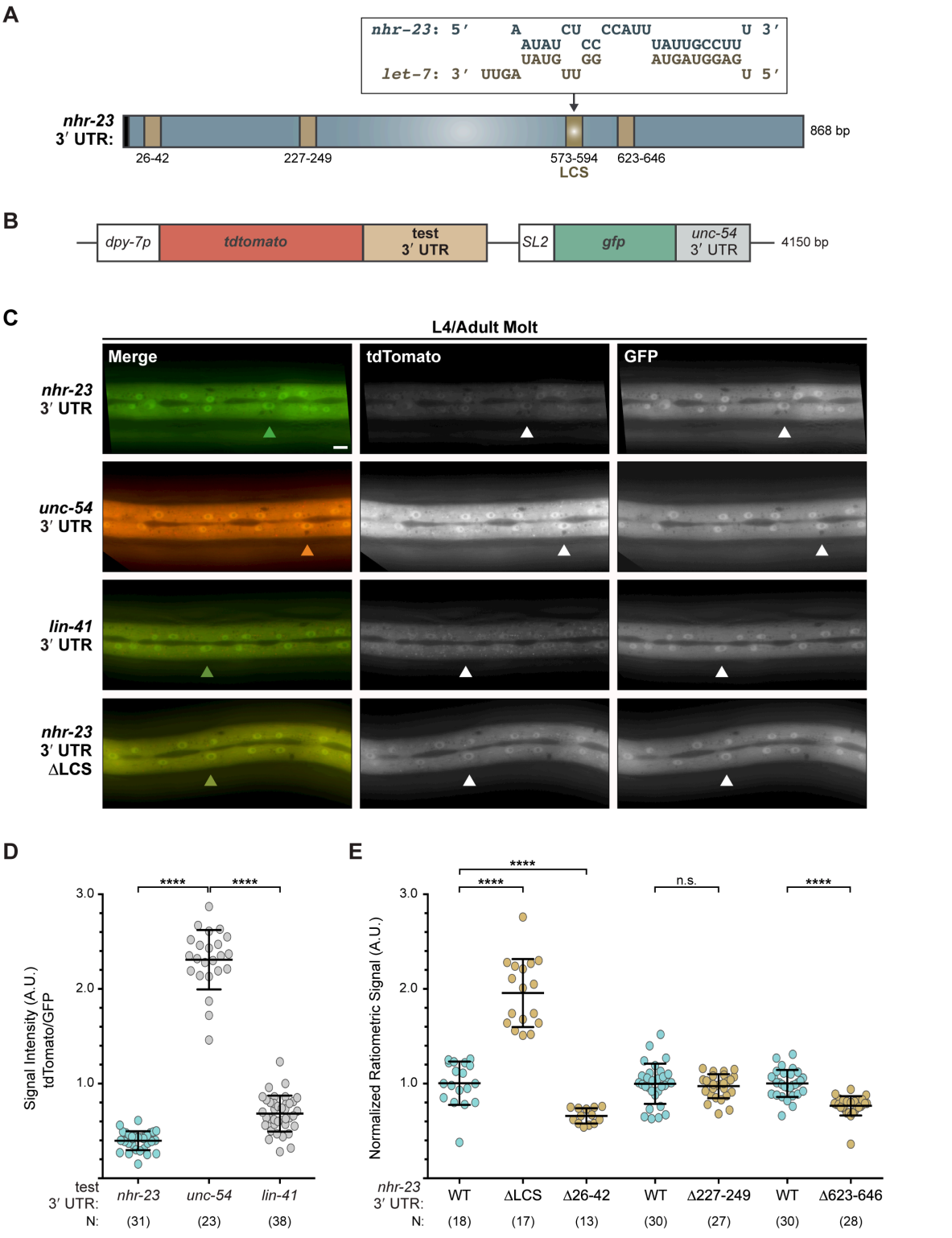
A
nhr-23: 5′ A CU CCAUU U 3′
AUAU CC UAUUGCCUU
UAUG GG AUGAUGGAG
let-7: 3′ UUGA UU U 5′
nhr-23 3′ UTR:
868 bp
26-42
227-249
573-594
623-646
LCS
B
dpy-7p
tdtomato
test 3′ UTR
SL2
gfp
unc-54 3′ UTR
4150 bp
C
L4/Adult Molt
Merge
tdTomato
GFP
nhr-23 3′ UTR
unc-54 3′ UTR
lin-41 3′ UTR
nhr-23 3′ UTR ΔLCS
D
Signal Intensity (A.U.) tdTomato/GFP
3.0
2.0
1.0
****
****
test 3′ UTR:
nhr-23
unc-54
lin-41
N:
(31)
(23)
(38)
E
Normalized Ratiometric Signal (A.U.)
3.0
2.0
1.0
****
****
n.s.
****
nhr-23 3′ UTR:
WT
ΔLCS
Δ26-42
WT
Δ227-249
WT
Δ623-646
N:
(18)
(17)
(13)
(30)
(27)
(30)
(28)

Figure 4. The 3′ UTR of *nhr-23* contains a functional LCS. **A)** Predicted base-pairing between the transcribed LCS and mature *let-7.* Schematic shows the LCS and three similar sites identified in the 3′ UTR of *nhr*-23. Numbers refer to nt. from the stop codon – shown as a black box. **B)** Design of bicistronic reporters for 3′ UTR-mediated gene regulation. **C)** Rows of representative fluorescence images show merged and individual signals from tdTomato and GFP co-expressed in the lateral epidermis of the same worm. Labels indicate the 3′ UTR fused to tdTomato in the corresponding reporter. Arrowheads point to hyp-7 nuclei. Scale bar = 10 μm. All images were captured with an exposure time of 10 milliseconds. **D)** Quantitation of the ratiometric signal (tdTomato/GFP) associated with each 3′ UTR reporter detected. Each symbol represents the average value of three ROIs per worm. N indicates the cumulative sample size from two independent experiments. Bars signify the mean ± sd for the cumulative sample. ****p≤0.0001, ***p≤0.001, Ordinary One-Way ANOVA with Tukey's correction for multiple comparisons. **E)** As above, except that ratiometric values were normalized to same-day controls. The full-length *nhr-23* construct is depicted in blue; deletion constructs, in brown. The strains used were ARF370, ARF372, ARF373, ARF374, ARF399, ARF400 and ARF401.

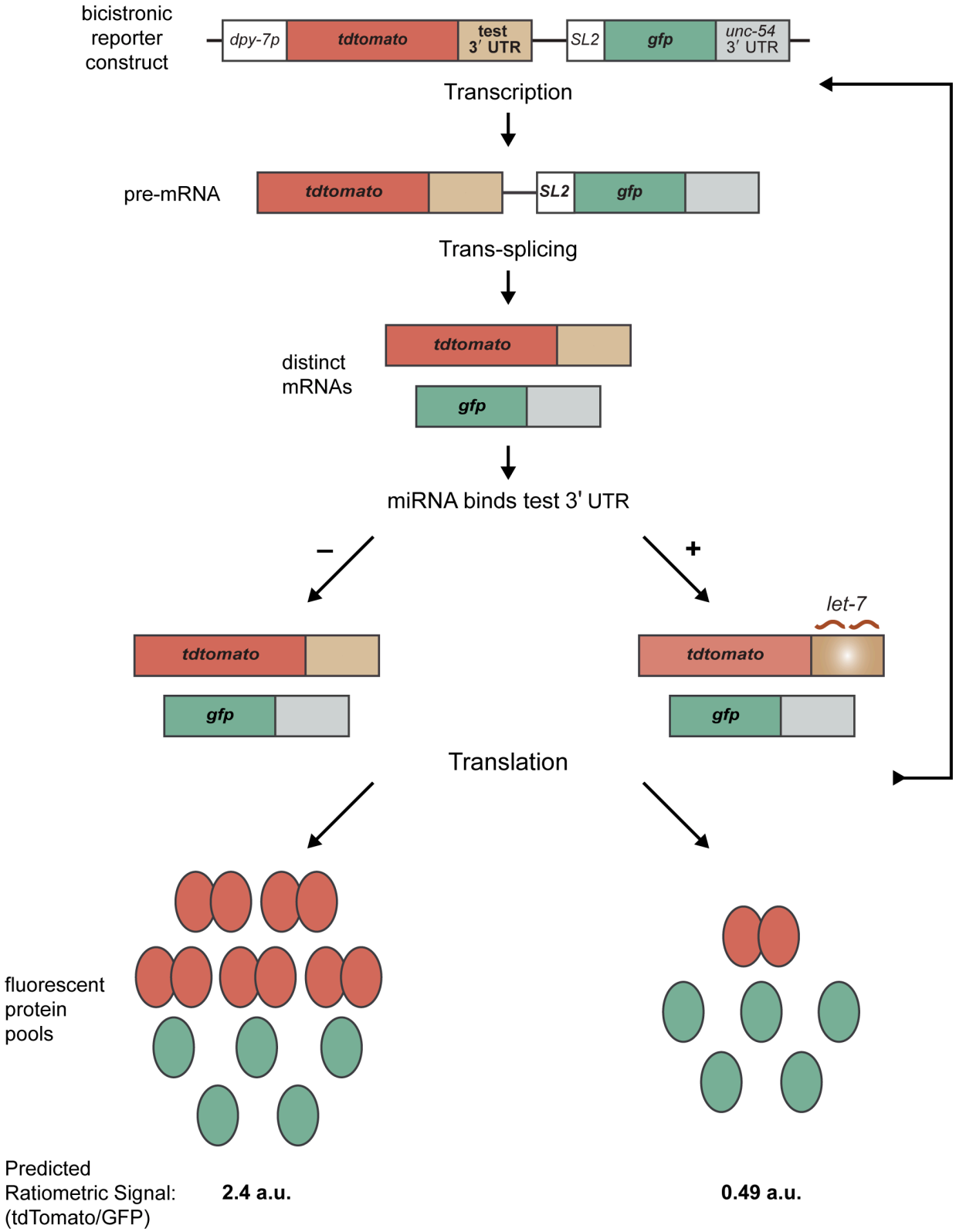
bicistronic reporter construct
dpy-7p
tdtomato
test 3′ UTR
SL2
gfp
unc-54 3′ UTR
Transcription
pre-mRNA
tdtomato
SL2
gfp
Trans-splicing
distinct mRNAs
tdtomato
gfp
miRNA binds test 3' UTR
–
+
let-7
tdtomato
gfp
tdtomato
gfp
Translation
fluorescent protein pools
Predicted Ratiometric Signal: (tdTomato/GFP)
2.4 a.u.
0.49 a.u.

Supplemental Figure 2. Molecular mechanisms relevant to the design and performance of bicistronic reporters for *cis*-regulatory elements in 3′ UTRs of interest. Schematic depicts the following series of anticipated events: 1) transcription of the bicistronic reporter under control of the *dpy-7* promoter; 2) trans-splicing of the resulting pre-mRNA, which generates distinct *tdTomato::test 3′ UTR* and *gfp::unc54 3′ UTR* mRNAs; and 3) standalone translation of the latter messages into fluorescent proteins. (Left) In theory, multiple iterations of these events give rise to equimolar pools of tdTomato and GFP if neither *let-7* nor any other repressor binds the test 3′ UTR. In this scenario, a ratiometric (tdTomato/GFP) signal of 2.4 A.U. is predicted based on the difference in brightness of tdTomato versus GFP—95 $(mM•cm)^{-1}$ versus 39 $(mM•cm)^{-1}$ respectively (Shaner et al., 2005). The nearly equivalent value of 2.3 A.U. observed and tabulated for the *unc-54* 3′ UTR reporter, which was used as a negative control, corroborated three suppositions about this experimental system: 1) that efficient trans-splicing generates both messages in equal number, 2) that both proteins are synthesized at equal rates, and 3) that tdTomato and GFP have similar half-lives *in* vivo. (Right) Anticipated outcome when *let-7* miRNAs bind LCSs in the test 3′ UTR, or some other repressor(s) bind distinct regulatory elements. The ratiometric signal for the depicted protein pools matches the observed value for the full-length *nhr-23* 3′ UTR reporter.

Supplemental Table 2 – Relates to Figures 4 and 8

let-7 Consensus Sites (LCSs) Identified in 3' UTRs of Selected Nematode and Vertebrate Homologs of *ROR*						
Species	Gene	Identifier	3' UTR Length (nt.)	LCS Position (3' nt.)	TS (kcal/mol)	Alignment of LCS (5' to 3') with *let-7* (3' to 5')
C. elegans	*nhr-23*	NM_001025806	868	42	-21.8	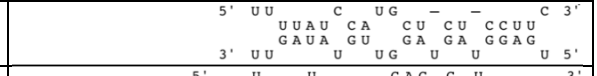
				249	-15.2	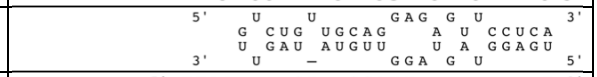
				594	-17.0	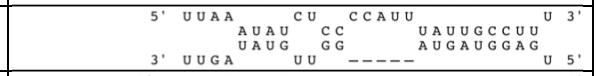
				646	-17.6	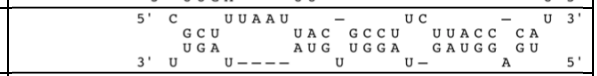
C. briggsae	*nhr-23*	WBGene 00040598	866	629	-20.7	
				835	-21.8	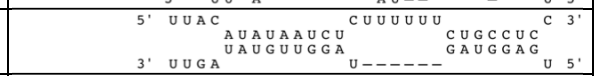
H. sapiens	*RORβ*	NM_006914	7559	3576	-25.9	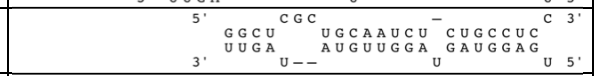
				4055	-23.1	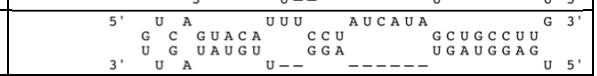
				4961	-23.1	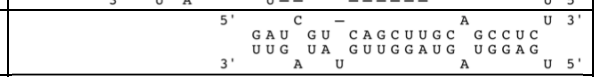
M. musculus	*RORβ*	NM_146095	7271	**3817**	-23.8	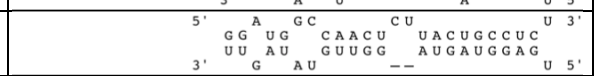
				5242	-22.7	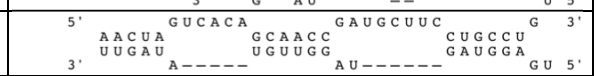
				6675	-26.7	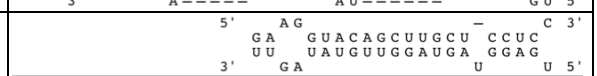
D. rerio	*RORβ*	NM_001082856	5431	**949**	-21.8	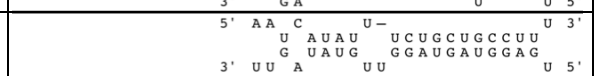
				4318	-23.8	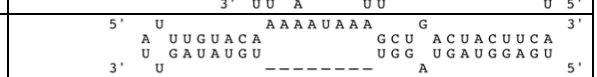
				4421	-23.3	
H. sapiens	*RORα*	NM_134261	9171	3079	-23.7	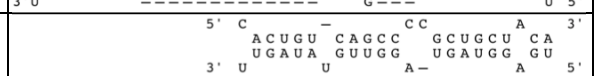
				3142	-22.8	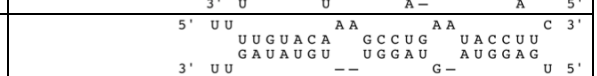
				6480	-24.0	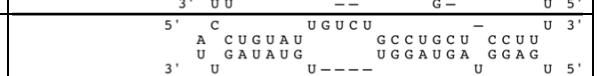
				8321	-22.2	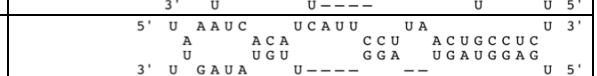
M. musculus	*RORα*	NM_013646	9285	**2055**	-23.9	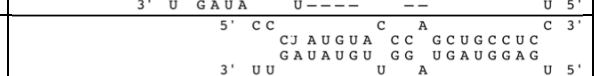
				2184	-23.7	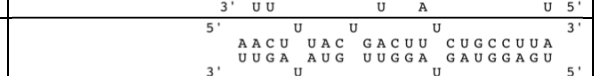
				4913	-22.6	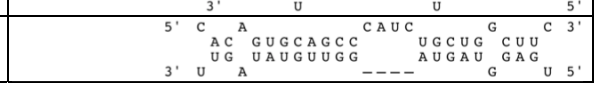

Supplemental Table 2. LCSs found in selected nematode and vertebrate homologs of *ROR*. Entries correspond to sites shown in Figure 8B. The number of nt. between the 3′ end of each LCS and the stop codon is specified. The thermostability of each and every RNA duplex between a prospective LCS and mature *let-7*, as predicted by RNAhybrid, was lower than the predicted thermostability (-29 kcal/mol) of duplexes between the functional LCS in the 3′ UTR of *lin-41* and *let-7* (Rehmsmeier et al., 2004). The 3' UTRs were supported by ESTs archived in WBcel235/ce11, WBPS9, GRCh38/hg38, GRCm38/mm10, and GRCz10/danRer10.

A

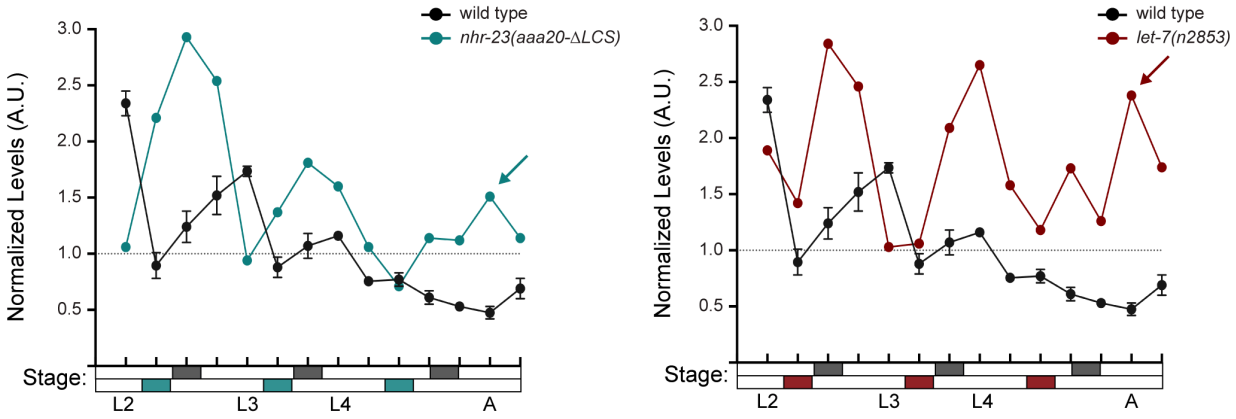

A′

	L2		L3		L4		Young Adult	
	Amplitude	Rising Slope	Amplitude	Rising Slope	Amplitude	Rising Slope	Amplitude	Rising Slope
wild type	2.2	0.38	1.7	0.14	1.2	0.07	0.7	0.01
nhr-23(aaa20)	5.1	1.64	2.9	0.33	1.8	0.22	1.5	0.13
let-7(n2853)	-	-	2.8	0.71	2.7	0.40	2.4	0.56

B

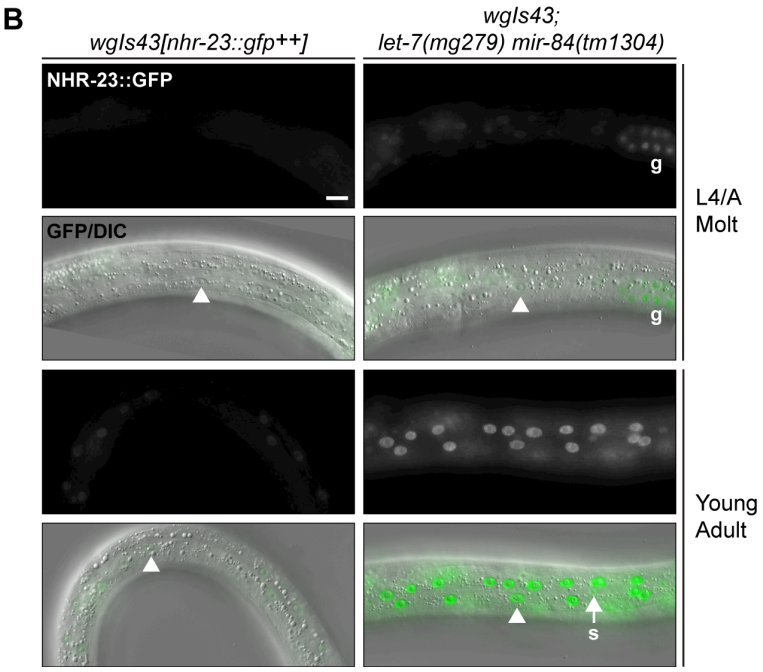

Figure 5. Waves of *nhr-23* expression dampen as wild-type larvae develop, but sharpen in gain-of-function *nhr-23* mutants and further intensify in loss-of-function *let-7* mutants.

A) Levels of *nhr-23* transcripts detected by TaqMan qRT-PCR in regular time samples of wild-type, *nhr-23*(*aaa20-ΔLCS)* and *let-7(n2853)* animals collected from late L2 through early adulthood. Rectangles beneath the x-axis signify observed intervals of molting-associated quiescence–shaded by genotype, as per the legend; white rectangles signify intervals of physical activity. Values for *nhr-23* were first normalized to *ama-1* transcripts within each same time sample. The resulting values were further normalized to the mean of all wild-type time samples—represented by the dashed y-axis gridline. Dots and error bars represent the mean and range from two technical replicates. For aesthetic purposes, the curves associated with *nhr-23(aaa20-ΔLCS)* and *let-7(n2853)* are displayed in separate charts—alongside one and the same wild-type time samples. Supplemental Figure 3 shows the results of an independent biological replicate. Arrows point to the supernumerary peaks in *nhr-23* transcript levels detected in both *nhr-23(aaa20-ΔLCS)* and *let-7(n2853)* animals. Wild-type animals were sampled 24-50 h after release from L1 diapause followed by cultivation with food; both mutant animals, 22-48 h. The respective strains were N2, ARF414 and QK059. **A′)** Metrics used to compare the sequential waves of *nhr-23* expression associated with each of the indicated genotypes. Amplitude refers to the highest (peak) normalized transcript level detected within the life stage. The rising slope (steepness) refers to the rate at which transcript levels ascend from the trough detected before or during the preceding molt to the peak detected within the specified stage. The values that are listed for the L2 stage are derived from an additional experiment shown in Supplemental Figure 3B and were included to emphasize the incremental dampening in the amplitude of *nhr-23* expression. **B**) Pairs of fluorescence and merged GFP/DIC micrographs show NHR-23::GFP fusion proteins detected in the lateral

epidermis of *wgIs43[nhr-23::gfp^{++}]* and *wgIs43; let-7(mg279) mir-84(tm1304)* animals at the indicated stages. Arrowheads point to nuclei in the syncytial hypodermis. The arrow points to a seam (s) nucleus. The letter g underscores signal detected in several germline nuclei. Scale bar = 10 µm. The respective strains were OP43 and ARF422.

A

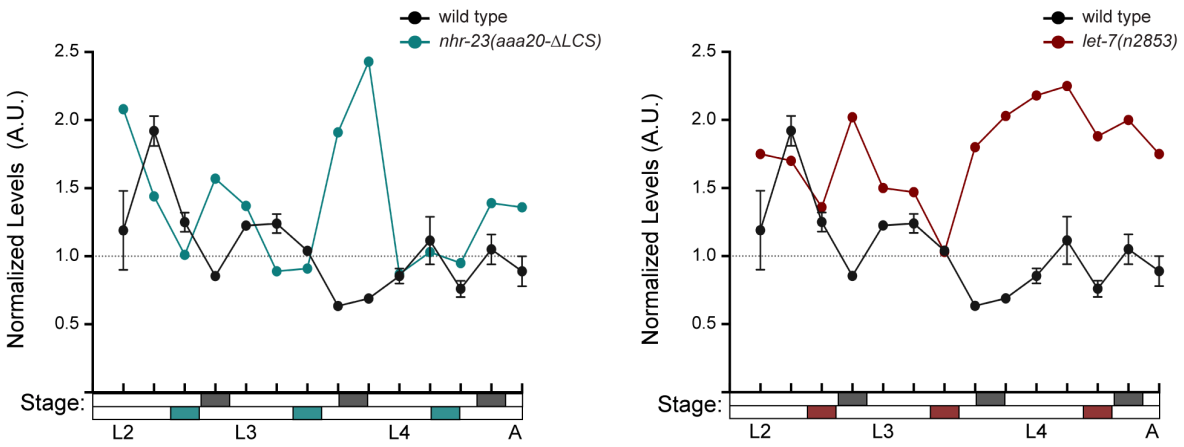

A′

	L3		L4	
	Amplitude	Rising Slope	Amplitude	Rising Slope
wild type	1.2	0.10	1.1	0.08
nhr-23(aaa20)	1.6	0.28	2.4	0.38
let-7(n2853)	2.0	0.33	1.8	0.40

B

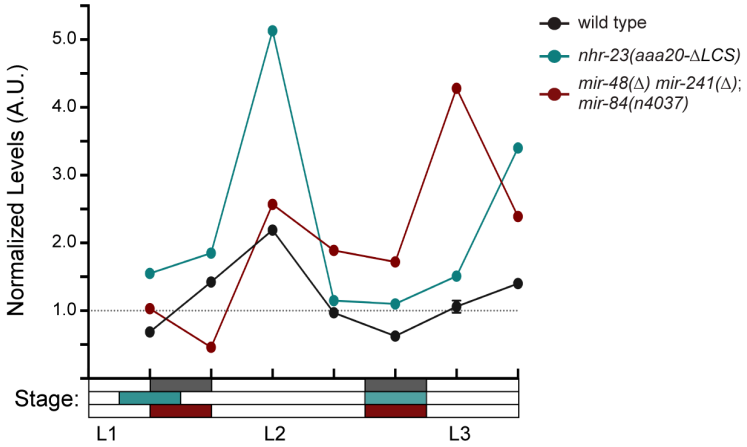

B′

	L2	
	Amplitude	Rising Slope
wild type	2.2	0.38
nhr-23(aaa20)	5.1	1.64
mir-48(Δ) mir-241(Δ); mir-84(n4037)	2.6	1.10

Supplemental Figure 3. Both the functional LCS in the 3′ UTR of *nhr*-23 and *let-7*-family miRNAs limit the abundance of *nhr-23* transcripts across larval development. **A)** Charts show data from an independent replicate of the experiment described in Figure 5A. Briefly, the values represent normalized levels of *nhr-23* transcripts detected in regular 2 h time samples of wild-type, *nhr-23(aaa20-ΔLCS)* and *let-7(n2853)* larvae and newly emerged adults. These particular samples were collected after hatchlings were cultivated on food for 24-50 h. **A′)** Metrics used to compare sequential waves of *nhr-23* expression, also as described in Figure 5. **B)** Normalized *nhr-23* transcript levels detected in wild-type larvae, *nhr-23(aaa20-ΔLCS)* single mutants, and *mir-48(Δ) mir-241(Δ); mir-84(n4037)* triple mutants sampled across the L2 stage. Both wild-type and *let-7s* triple mutant larvae were collected after cultivation with food for 14–26 h; *nhr-23(aaa20-ΔLCS)* larvae, after 16–28 h. By order of appearance, the strains tested were N2, ARF414, QK059 and VT1066.

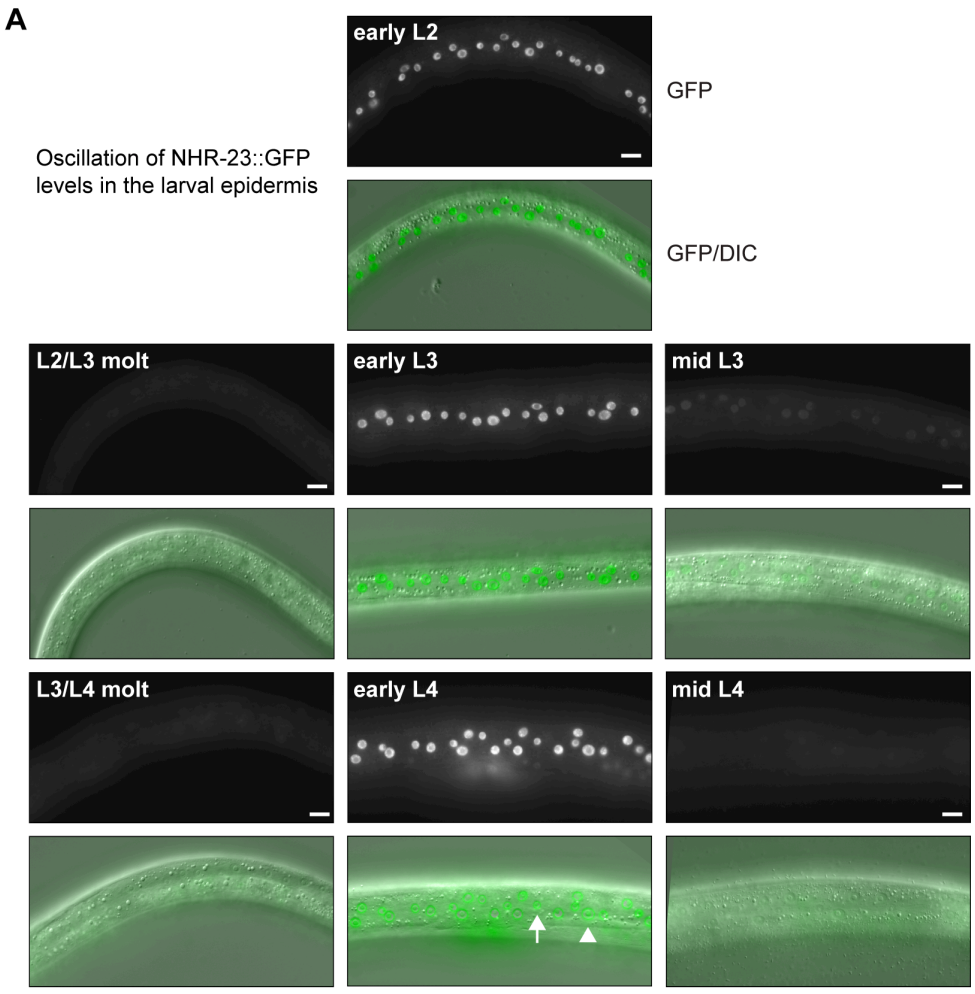
A
Oscillation of NHR-23::GFP levels in the larval epidermis
early L2
GFP
GFP/DIC
L2/L3 molt
early L3
mid L3
L3/L4 molt
early L4
mid L4
B
Signal Intensity (A.U.)
2000
1800
1600
1400
1200
1000
800
600
400
200
-2
-1
0
1
2
3
4
5
6
7
8
9
10
Time (h) – Relative to Emergence in L4

Supplemental Figure 4. The abundance of NHR-23 cycles across larval development. Representative images show NHR-23::GFP fusion proteins detected in the lateral epidermis of OP43 [*wgIs43[nhr-23::gfp]*] larvae at the indicated stages. Pairs of fluorescence and fluorescence merged with DIC micrographs. Fluorescence images were all captured with an exposure time of 300 milliseconds. In the image of an early L4, the arrowhead points to a nucleus in the seam; the arrow, to a nucleus in hyp7. Scale bars = 10 μm. B) Quantification of the NHR-23::GFP signal detected in cohorts of larvae collected at regular 1 h intervals across the entirety of the L4 stage. Gray and white rectangles drawn above the x-axis approximate phases of quiescence and activity, respectively. Values represent the mean ± sd derived from samples of 6-10 worms per timepoint. Within each worm, signals detected in 3 hyp7 nuclei and 3 seam nuclei were measured and the average value applied to further analysis.

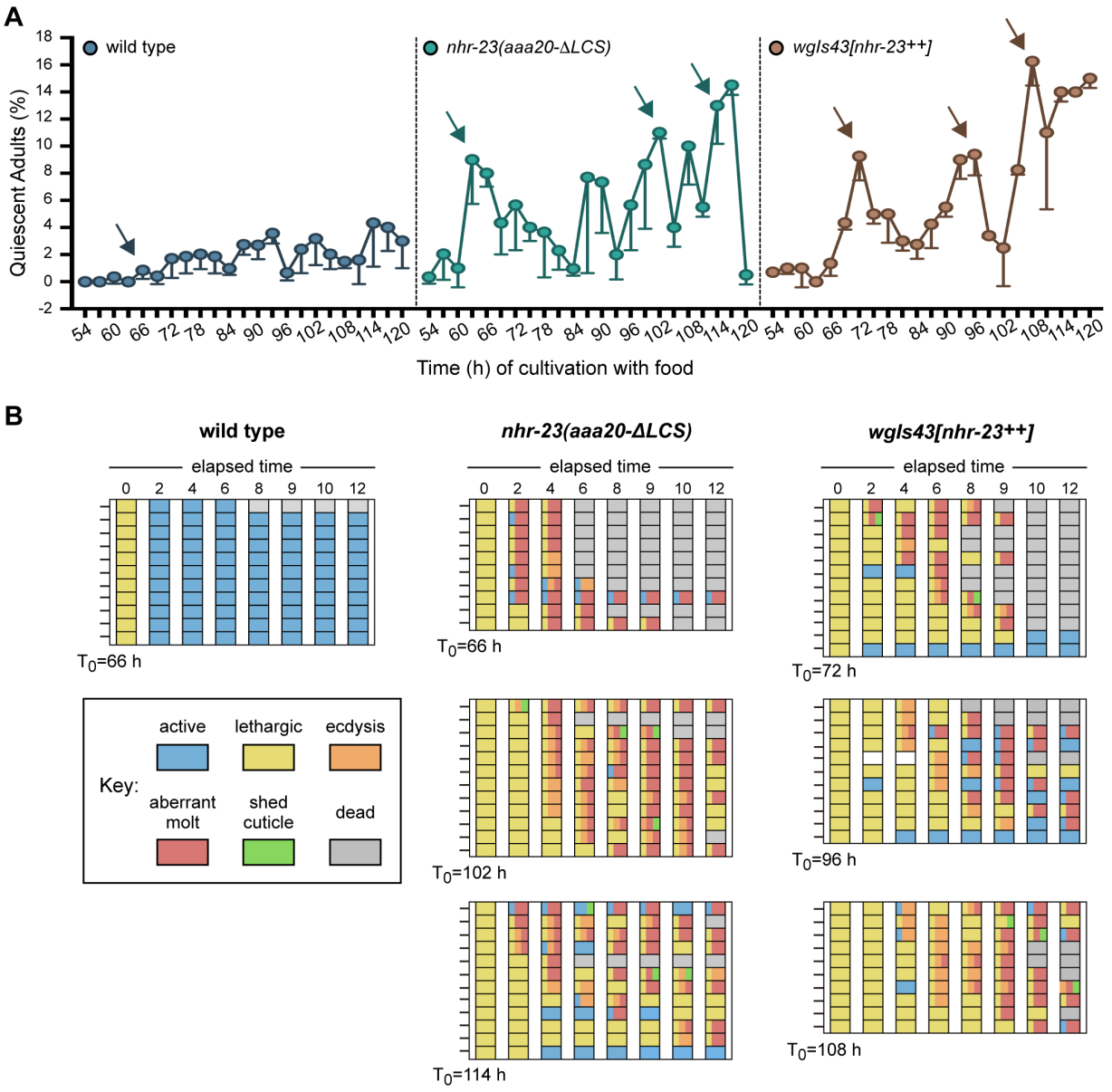
A
wild type
nhr-23(aaa20-ΔLCS)
wgIs43[nhr-23++]
Quiescent Adults (%)
Time (h) of cultivation with food
B
wild type
nhr-23(aaa20-ΔLCS)
wgIs43[nhr-23++]
elapsed time
T0=66 h
T0=66 h
T0=72 h
T0=102 h
T0=96 h
T0=114 h
T0=108 h
Key:
active
lethargic
ecdysis
aberrant molt
shed cuticle
dead
C
nhr-23(aaa20-ΔLCS)
wgIs43[nhr-23++]
tail
prior cuticle
shed cuticle
e
vulva
lateral surface
e
vulva

Figure 6. Both derepression and overexpression of *nhr-23* trigger additional molts in reproductively mature animals. **A)** Analogous charts show the percentage of wild-type, *nhr-23*(*aaa20-ΔLCS)*, and *wgIs43[nhr-23^{++}]* adults that appeared quiescent at regular timepoints 54 to 120 h after release from diapause and cultivation with food. Values represent the mean minus sd from 2 independent trials, with cumulative sample sizes of 300 to 400 animals per timepoint. Sequential peaks in the prevalence of quiescent animals are marked by arrows. The corresponding values significantly exceeded the values for age-matched, wild-type animals ($p<0.0001$, chi-square test, χ^2 ranged from 39 to 223). **B)** Actograms depict the behavior and fate of quiescent adults singled at each timepoint marked by an arrow and then observed at regular 2 h intervals. Chronological records within each row correspond to a single worm. For aesthetic purposes, columns were arranged (top to bottom) by the first detection of an attempted ecdysis. The behavior of a worm at a particular timepoint was scored as active or lethargic, as described. In addition, behavior was scored as "ecdysis" if the subject performed one or more of the idiosyncratic movements typically used to escape an outmoded cuticle. "Aberrant molts" were recorded either when a dislodged cuticle encased part of the body or repeated attempts to ecdyse wrecked the body. Detection of a shed cuticle, or parts thereof, on the culture plate was recorded separately. The latter categories were not mutually exclusive. An inactive or decrepit worm unresponsive to adverse stimuli was pronounced dead. Absence of a supernumerary molt was inferred if the animal was active and superficially normal at the endpoint. **C)** DIC micrographs show examples of adults that attempted to molt. Arrows point to former cuticles dislodged from the tail or head; arrowheads, to alae on both the passing and emergent cuticles. The letter "e" denotes fertilized embryos within the uterus. Scale bars = 10 μm. The strains tested were N2[wild-type], OP43[*wgIs43*] and ARF414[*nhr-23 (aaa20-ΔLCS)*].

A

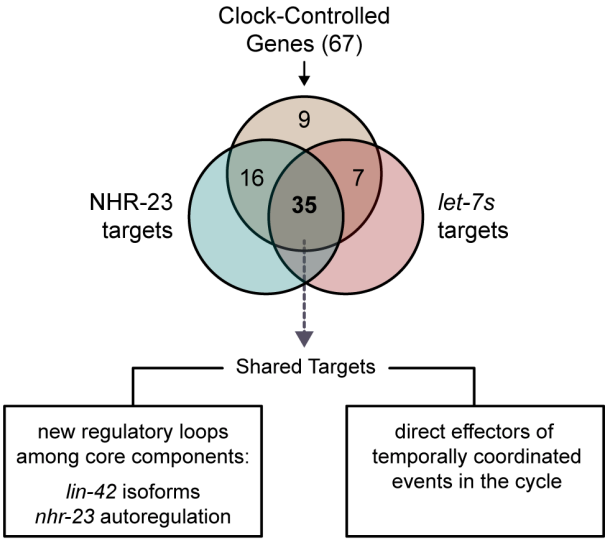

B

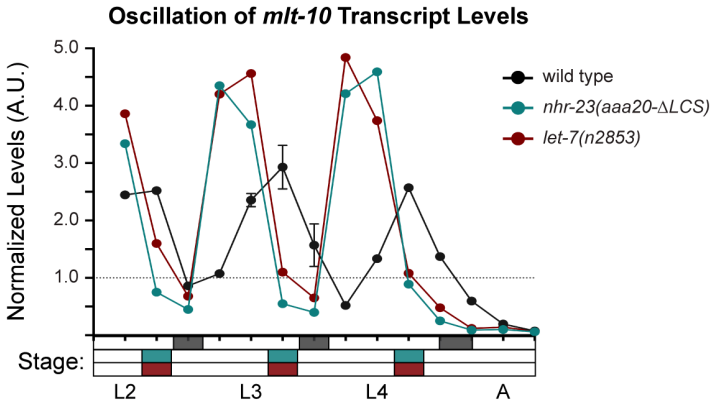

B′

	L2		L3		L4	
	Amplitude	Rising Slope	Amplitude	Rising Slope	Amplitude	Rising Slope
wild type	2.5	-	2.9	0.35	2.6	0.51
nhr-23(aaa20)	3.9	-	4.2	1.76	4.8	2.10
let-7(n2853)	3.3	-	4.4	1.95	4.6	1.91

Figure 7. Most genes regulated by the molting clock are shared targets of both NHR-23 and *let-7s.* **A)** Venn diagram summarizes the classification of 67 clock-controlled genes (CCGs) as direct targets of NHR-23, *let-7s*, both or neither based on original bioinformatic approaches and meta-analyses of published ChIP-Seq, comparative microarray, and ALG-1-iCLIP data sets (Broughton et al., 2016). Supplemental Table 3 provides the detailed information used to classify each gene of interest. Relevant scoring rubrics are fully described in the results and methods. The flowchart beneath the Venn diagram shows examples of prospective components of the molting timer and effectors of specific subroutines of the molting cycle that emerged as dual targets from the meta-analysis. **B)** Levels of *mlt-10* transcripts detected by TaqMan qRT-PCR in regular time samples of wild-type, *nhr-23*(*aaa20-ΔLCS)* and *let-7(n2853)* animals collected from late L2 through early adulthood. As previously described, rectangles beneath the x-axis signify observed intervals of molting-associated quiescence–shaded by genotype, as per the legend; white rectangles signify intervals of physical activity. Values for *mlt-10* were first normalized to *ama-1* transcripts within each same time sample. The resulting values were further normalized to the mean of all wild-type time samples—represented by the dashed y-axis gridline. Dots and error bars represent the mean and range from two technical replicates. Wild-type animals were sampled 24-50 h after release from L1 diapause followed by cultivation with food; both mutant animals, 22-48 h. The respective strains were N2, ARF414 and QK059.

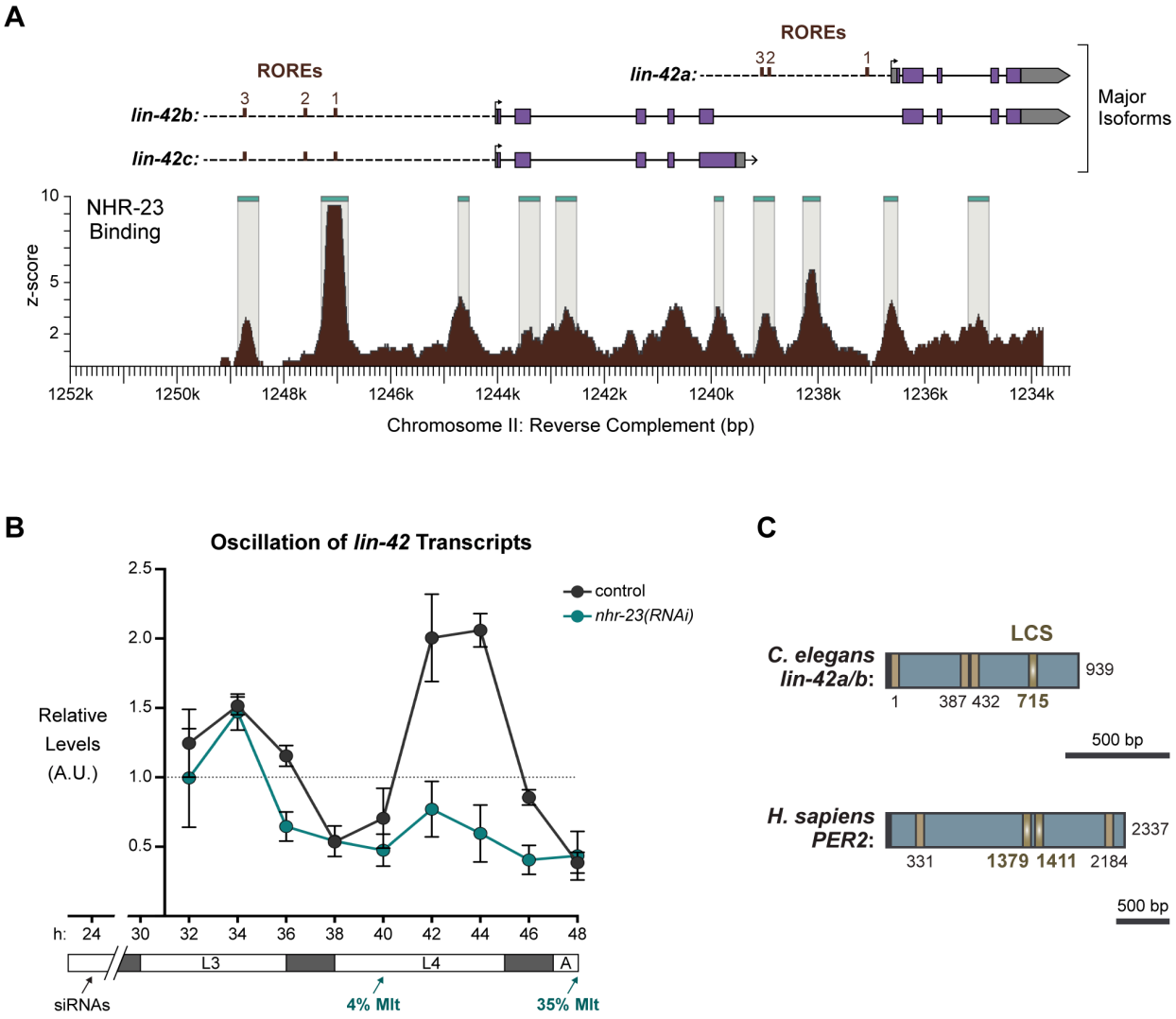
A
RORE s
RORE s
lin-42a:
lin-42b:
lin-42c:
Major Isoforms
NHR-23 Binding
z-score
Chromosome II: Reverse Complement (bp)
B
Oscillation of lin-42 Transcripts
control
nhr-23(RNAi)
Relative Levels (A.U.)
h:
L3
L4
A
siRNAs
4% Mlt
35% Mlt
C
LCS
C. elegans lin-42a/b:
H. sapiens PER2:
500 bp

Supplemental Figure 5. The *lin-42* gene is a shared target of NHR-23 and *let-7s*. **A)** Schematic shows the correspondence among annotated regulatory regions of the three major isoforms of *lin-42* (WS264) and chromosomal regions occupied by NHR-23 in mid-stage larvae. Dashed lines demarcate defined promoters; arrows label transcriptional start sites. Coordinates refer to *C. elegans* Chr. II (NC_003280). Four additional isoforms of *lin-42* were recently annotated in the reference genome but otherwise remain uncharacterized. **B)** Quantitation of *lin-42* transcripts in successive time samples of attenuated *nhr-23(RNAi)* animals and control animals by TaqMan qRT-PCR. Each value was first normalized to *ama-1* transcript levels in the same time sample. Values were then normalized to the mean of all time samples from the wild-type control. Symbols represent the mean and range from two biological replicates. The x-axis indicates time elapsed (h) on food. Bars beneath the x-axis depict progression of the life cycle; gray boxes therein signify observed intervals of quiescence. The time of initial exposure to *nhr-23* siRNAs and the subsequent appearance of molting-defective *nhr-23(RNAi)* larvae are indicated. **C)** Comparison of LCSs identified in the 3' UTR of *C. elegans lin-42a/b* and human *PER2.* Schematic shows the LCSs (gold), 3′ UTR (blue), and stop codons (black). Gradients and bold labels distinguish sites perfectly complementary to the seed of *let-7s*. Each 3′ UTR was retrieved from the UCSC genome browser; verified by comparison with curated ESTs; and LCSs identified using RNAhybrid. Accession numbers for the related ESTs and genomic sequences are included in the Key Resources Table.

Supplemental Table 3 – Relates to Figure 7.

Classification of Clock-Controlled Genes (CCGs) as Direct Targets of NHR-23, *let-7s*, neither or both.

Gene Name	Sequence	Criteria for targets of NHR-23: Size of upstream regulatory region & first intron (kb)	RORE #	RORE # Obs. / # Exp.	mRNA levels after *nhr-23* RNAi	NHR-23 ChIP-Seq Peaks (#)	NHR-23 target (Y/N)	Criteria for targets of *let-7s*: Size of 3' UTR (nt.)	LCS #	LCS # Obs. / # Exp.	ALG-1 iCLIP Peaks (+/-)	*let-7s* target (Y/N)	Target class	Cyclic mRNA levels (≈)
Potential Core Clock Components														
let-7	C05G5.6	1.5	3	5.8	↓	1	Y	N/A	–	–	–	N/A	NHR-23	≈
lin-42a	F47F6.1	3.7	3	2.3	↓	4	Y	939	4	3.2	+	Y	Shared	≈
lin-42b	F47F6.1	5.5	3	1.6	↓	3	Y	939	4	3.2	+	Y	Shared	≈
lin-42c	F47F6.1	5.5	3	1.6	↓	3	Y	156	0	0.0	–	N	NHR-23	≈
mir-48	F56A12.3	1.7	2	3.4	–	1	Y	N/A	–	–	–	N/A	NHR-23	≈
mir-241	F56A12.4	2.0	2	2.9	–	2	Y	N/A	–	–	–	N/A	NHR-23	≈
mir-84	B0395.4	2.8	1	1.1	–	2	Y	N/A	–	–	–	N/A	NHR-23	≈
nhr-23	C01H6.5	6.1	8	3.8	↓	3	Y	868	4	2.6	+	Y	Shared	≈
nhr-25	F11C1.6	6.9	3	1.3	–	3	Y	749	1	1.0	+	Y	Shared	≈
Other Gene Regulatory Factors														
alg-1	F48F7.1	9.9	11	3.2	–	3	Y	400	1	1.9	+	Y	Shared	≈
bed-3	F25H8.6	1.7	2	3.4	–	1	Y	459	1	1.6	+	Y	Shared	≈
blmp-1	F25D7.3	6.7	7	3.0	–	4	Y	861	3	2.6	+	Y	Shared	≈
bro-1	F56A3.5	1.2	0	0.0	–	1	N	379	1	2.0	–	N	–	≈
dre-1	K04A8.6	7.5	8	3.1	–	4	Y	376	2	4.0	+	Y	Shared	≈
mab-10	R166.1	6.0	8	3.9	–	2	Y	374	1	2.0	–	N	NHR-23	≈
nhr-41	Y104H12A.1	11.1	23	6.0	–	2	Y	332	1	2.3	–	N	NHR-23	≈
pqn-47	F59B10.1	5.9	7	3.4	–	5	Y	804	2	1.9	+	Y	Shared	≈
rnt-1	B0414.2	9.2	4	1.3	–	0	N	221	0	0.0	–	N	–	≈
Signaling Pathway Components														
acn-1	C42D8.5	4.0	4	2.9	↓	3	Y	384	1	2.0	+	Y	Shared	≈
apl-1	C42D8.8	4.9	4	2.4	–	5	Y	678	1	1.1	+	Y	Shared	≈
calu-1	M03F4.7	1.7	3	5.1	–	3	Y	256	1	3.0	+	Y	Shared	≈
cki-1	T05A6.1	1.9	2	3.1	–	1	Y	235	2	6.5	+	Y	Shared	≈
glf-1	H04M03.4	2.4	1	1.2	↓	1	Y	247	2	6.2	–	N	NHR-23	≈
lon-1	F48E8.1	4.8	3	1.8	–	5	Y	185	2	8.3	+	Y	Shared	≈
lrp-1	F29D11.1	7.9	3	1.1	–	6	Y	346	2	4.4	+	Y	Shared	≈
mlt-8	W08F4.6	3.5	2	1.7	↓	1	Y	270	2	5.6	+	Y	Shared	≈
nekl-2	ZC581.1	1.1	1	2.6	–	0	N	73	0	0.0	–	N	–	≈
nlp-22	T24D8.3	0.8	0	0.0	–	0	N	1000	2	1.5	–	N	–	≈
osm-7	T05D4.4	3.5	1	0.8	–	0	N	121	1	6.5	+	Y	*let-7s*	≈
osm-11	F11C7.5	2.8	1	1.1	–	3	Y	545	4	5.5	+	Y	Shared	≈
phi-59	T19B10.2	1.5	0	0.0	↓	1	Y	121	1	6.5	+	Y	Shared	≈
pod-2a	W09B6.1	3.0	4	3.9	–	2	Y	324	1	2.3	–	N	NHR-23	≈
ptr-4	C45B2.7	4.5	4	2.6	↓	2	Y	221	2	6.9	–	N	NHR-23	≈
ptr-23	ZK270.1	2.0	0	0.0	–	2	N	311	3	7.3	+	Y	*let-7s*	≈
qua-1	T05C12.10	5.7	3	1.5	↓	4	Y	340	1	2.2	+	Y	Shared	≈
	E03H4.8	3.4	1	0.9	–	0	N	307	1	2.5	–	N	–	≈
	T19A5.3	4.9	2	1.2	↓	2	Y	347	1	2.2	+	Y	Shared	≈
	Y47D3B.1	4.9	3	1.8	–	1	Y	98	1	8.1	–	N	NHR-23	≈
Extracellular Matrix Proteins and Receptors														
adt-2	F08C6.1	7.6	7	2.7	–	6	Y	621	1	1.2	+	Y	Shared	≈
bli-5	F45G2.5	1.4	0	0.0	–	0	N	300	1	2.5	+	Y	*let-7s*	≈
bus-8	T23F2.1	3.6	0	0.0	↓	0	N	453	2	3.3	–	N	–	≈
clc-1	C09F12.1	5.4	0	0.0	–	0	N	101	1	7.8	–	N	–	≈
col-12	F15H10.1	0.7	0	0.0	–	0	N	101	1	7.8	+	Y	*let-7s*	≈
dpy-13	F30B5.1	3.8	5	3.8	–	4	Y	63	2	26.1	+	Y	Shared	≈
dpy-17	F54D8.1	0.4	1	7.3	–	0	N	54	1	15.5	–	N	–	≈
dpy-4	Y41E3.2	2.4	0	0.0	–	1	N	102	1	7.8	+	Y	*let-7s*	≈
dpy-5	F27C1.8	0.8	1	3.6	↓	1	Y	39	0	0.0	–	N	NHR-23	≈
dpy-7	F46C8.6	0.7	2	8.3	↓	1	Y	236	1	3.2	–	N	NHR-23	≈
fbn-1	ZK783.1	8.3	12	4.2	↓	6	Y	457	1	1.7	+	Y	Shared	≈
ina-1	Y116A8A.9	8.0	8	2.9	–	2	Y	261	1	2.9	+	Y	Shared	≈
mam-1	ZC13.3	3.8	3	2.3	–	0	N	243	0	0.0	–	N	–	≈
mlt-10	C09E8.3	8.6	4	1.3	↓	1	Y	139	2	11.2	+	Y	Shared	≈
mlt-11	W01F3.3	5.2	11	6.1	↓	4	Y	353	1	2.1	+	Y	Shared	≈
mlt-7	ZK430.8	11.5	15	3.8	–	1	Y	317	2	4.8	+	Y	Shared	≈
mlt-9	F09B12.1	3.5	1	0.8	↓	5	Y	313	1	2.4	–	N	NHR-23	≈
mup-4	K07D8.1	5.8	5	2.5	–	2	Y	394	0	0.0	–	N	NHR-23	≈
nas-36	C26C6.3	1.1	1	2.6	↓	0	Y	327	5	11.6	+	Y	Shared	≈

Classification of Clock-Controlled Genes (CCGs) as Direct Targets of NHR-23, *let-7s*, neither or both.															
		Criteria for targets of NHR-23:						Criteria for targets of *let-7s*:							
			RORE						LCS						
Gene Name	Sequence	Size of upstream regulatory region & first intron (kb)	#	# Obs. / # Exp.	mRNA levels after *nhr-23* RNAi	NHR-23 ChIP-Seq Peaks (#)	NHR-23 target (Y/N)	Size of 3' UTR (nt.)	#	# Obs. / # Exp.	ALG-1 iCLIP Peaks (+/-)	*let-7s* target (Y/N)	Target class	Cyclic mRNA levels (≈)
nas-37	C17G1.6	3.6	7	5.6	↓	2	Y	240	4	12.7	–	N	NHR-23	≈
noah-1	C34G6.6	7.9	9	3.3	↓	5	Y	550	1	1.4	+	Y	Shared	≈
noah-2	F52B11.3	8.9	3	1.0	↓	6	Y	316	2	4.8	+	Y	Shared	≈
pan-1	M88.6	2.5	2	2.3	–	2	Y	393	2	3.8	+	Y	Shared	≈
pat-2	F54F2.1	4.0	4	2.9	–	2	Y	292	2	5.2	+	Y	Shared	≈
rol-6	T01B7.7	3.4	2	1.7	↓	4	Y	117	1	6.7	+	Y	Shared	≈
pat-3	ZK1058.2	5.0	0	0.0	–	2	N	400	1	1.9	+	Y	*let-7s*	≈
Cytoskeletal Components														
ifa-2	W10G6.3	1.7	1	1.7	–	1	Y	186	2	8.3	–	N	Shared	≈
ifc-2	M6.1	3.0	0	0.0	–	0	N	536	2	2.8	+	Y	*let-7s*	≈
nmy-2	F20G4.3	1.8	6	9.7	–	1	Y	448	2	3.4	+	Y	Shared	≈
Genes linked to the molting cycle whose expression is not known to oscillate														
daf-9	T13C5.1	1.1	0	0.0	↓	1	Y	214	2	7.2	+	Y	Shared	–
daf-12	F11A1.3	17.0	12	2.0	–	7	Y	1393	5	2.7	+	Y	Shared	–
gei-8	C14B9.6	1.8	1	1.6	–	3	Y	449	4	6.7	+	Y	Shared	–
let-767	C56G2.6	0.6	1	4.8	–	1	Y	87	1	9.2	+	Y	Shared	–
lin-3	F36H1.4	5.5	5	1.9	–	0	N	442	5	8.5	+	Y	*let-7s*	–
nhr-67	C08F8.8	5.5	5	2.6	–	0	N	241	3	9.5	–	N	–	–
skn-1	T19E7.2	5.1	2	1.1	–	2	Y	677	1	1.1	+	Y	Shared	–
Non-CCGs (Randomly Selected)														
acs-13	Y65B4BL.5	4.9	3	1.8	–	2	Y	424	1	1.8	+	Y	Shared	–
ced-8	F08F1.5	0.7	0	0.0	–	0	N	85	0	0.0	–	N	–	–
cyp-33C12	Y5H2B.6	1.5	0	0.0	–	0	N	148	0	0.0	–	N	–	–
ech-5	F56B3.5	0.5	0	0.0	–	1	N	602	1	1.2	–	N	–	–
map-2	Y116A8A.9	1.5	1	1.9	–	0	N	274	2	5.6	–	N	–	–
mpst-7	R186.6	1.0	0	0.0	–	1	N	84	0	0.0	+	N	–	–
nhr-176	F14H3.11	0.2	0	0.0	–	0	N	54	1	15.5	–	N	–	–
nlp-37	F48B9.4	2.9	3	3.0	–	0	N	302	2	5.0	–	N	–	–
nuo-2	T10E9.7	0.2	0	0.0	–	1	N	109	1	14.5	–	N	–	–
srz-10	ZK1037.11	1.1	1	2.6	–	0	N	16	0	0.0	–	N	–	–
ttll-12	D2013.9	0.1	0	0.0	–	0	N	175	1	4.4	+	Y	*let-7s*	–
unc-112	C47E8.7	2.8	1	1.1	–	1	Y	295	1	2.6	+	Y	Shared	–
viln-1	C10H11.1	7.0	3	1.1	–	0	N	119	2	13.2	–	N	–	–
	C01G6.9	0.1	0	0.0	–	0	N	76	1	10.6	–	N	–	–
	F44E5.5	0.4	0	0.0	–	1	N	39	0	0.0	–	N	–	–
	R10E8.6	1.3	0	0.0	–	0	N	31	0	0.0	–	N	–	–
	R12B2.2	0.5	0	0.0	–	0	N	115	0	0.0	–	N	–	–
	T06D4.1	2.3	3	3.8	–	0	N	234	0	0.0	–	N	–	–
	W02D7.3	2.0	1	1.3	–	0	N	78	0	0.0	–	N	–	–
	Y53C10A.6	6.3	0	0.0	–	0	N	201	2	7.6	–	N	–	–

Supplemental Table 3. Evaluation and classification of clock-controlled genes as direct targets of NHR-23, *let*-7s, neither or both. The bioinformatic approaches and criteria for assignment of queries to categories are described in the Method Details. The name and WormBase accession number of each gene is listed. The shorthand "# Obs./# Exp." stands for the number of observed DNA or RNA response elements divided by the number of elements predicted by chance alone. The "↓" symbol denotes down-regulation of the query transcript in *nhr-23(RNAi)* animals as compared with wild-type controls. The "+" symbol in column 12 denotes association of the 3′ UTR with ALG-1 *in vivo*. The symbol "≈" indicates that expression of the gene oscillates

across larval development. Relevant datasets are identified in the text, Method Details and Key Resources Table.

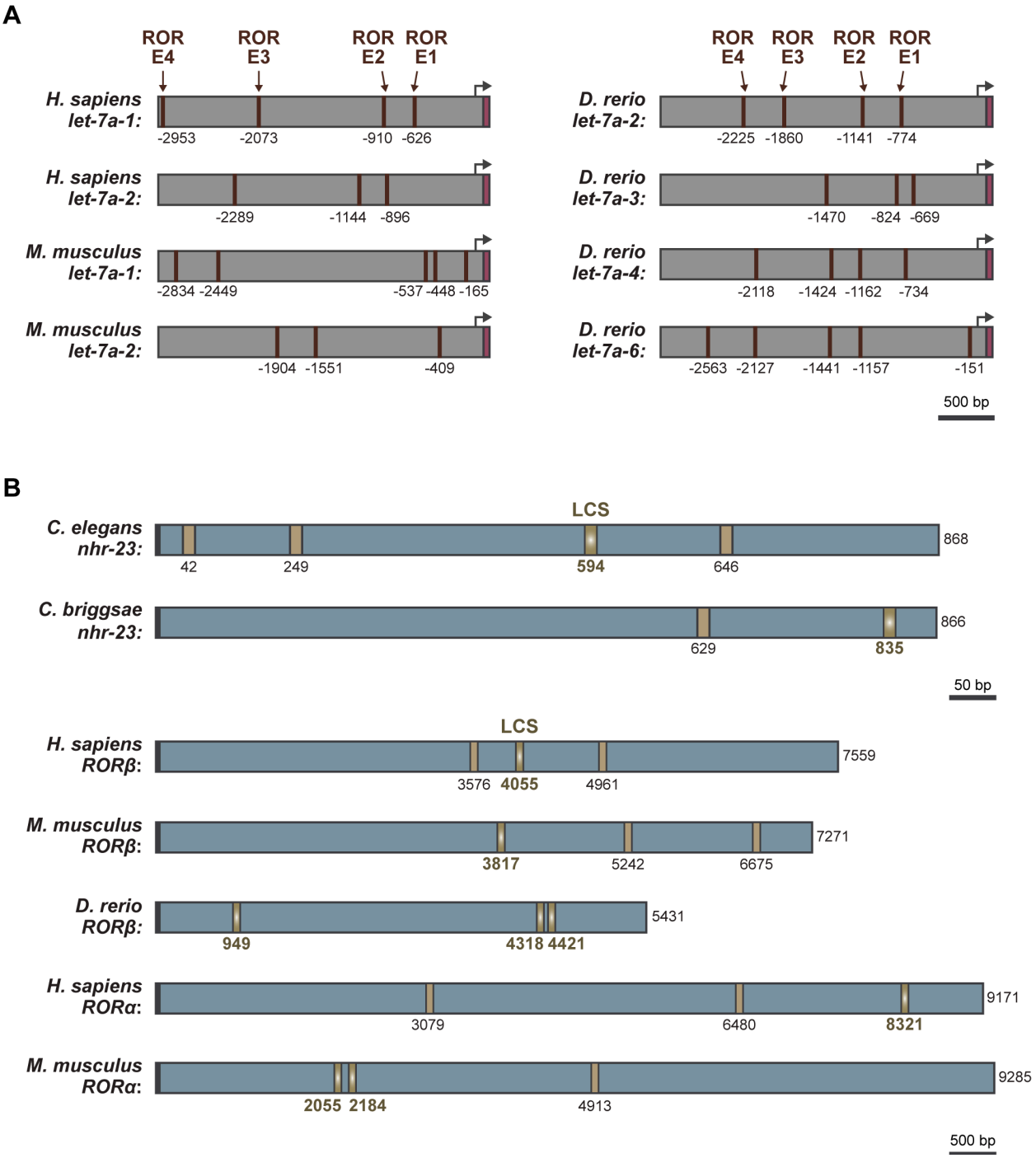
A
ROR E4
ROR E3
ROR E2
ROR E1
H. sapiens let-7a-1:
-2953 -2073 -910 -626
H. sapiens let-7a-2:
-2289 -1144 -896
M. musculus let-7a-1:
-2834 -2449 -537 -448 -165
M. musculus let-7a-2:
-1904 -1551 -409
D. rerio let-7a-2:
-2225 -1860 -1141 -774
D. rerio let-7a-3:
-1470 -824 -669
D. rerio let-7a-4:
-2118 -1424 -1162 -734
D. rerio let-7a-6:
-2563 -2127 -1441 -1157 -151
500 bp
B
LCS
C. elegans nhr-23:
42 249 594 646 868
C. briggsae nhr-23:
629 835 866
50 bp
LCS
H. sapiens RORβ:
3576 4055 4961 7559
M. musculus RORβ:
3817 5242 6675 7271
D. rerio RORβ:
949 4318 4421 5431
H. sapiens RORα:
3079 6480 8321 9171
M. musculus RORα:
2055 2184 4913 9285
500 bp

Figure 8. Conservation of both the transcriptional and post-transcriptional *cis*-regulatory elements underlying the negative feedback loop between NHR-23/ROR and *let-7* miRNAs. **A)** Each schematic depicts the 3 kb region upstream of selected homologs of *let-7*. Brown boxes show the multiple ROREs identified upstream of mature *let-7* (red) in the annotated genomes of the indicated species. Black arrows are aesthetic landmarks for probable, but not experimentally verified, transcriptional start sites. **B)** Schematic shows the LCSs (gold), 3′ UTR (blue), and stop codons (black) of six annotated homologs of *nhr-23/ROR*. Gradients and bold labels distinguish sites perfectly complementary to the seed of *let-7s*. Each 3′ UTR was retrieved from the UCSC genome browser; verified by comparison with curated ESTs; and LCSs identified using RNAhybrid. Supplemental Table 2 provides additional information about the prospective duplexes between each of these LCSs and *let-7.* Accession numbers for the related ESTs and genomic sequences are included in the Key Resources Table.

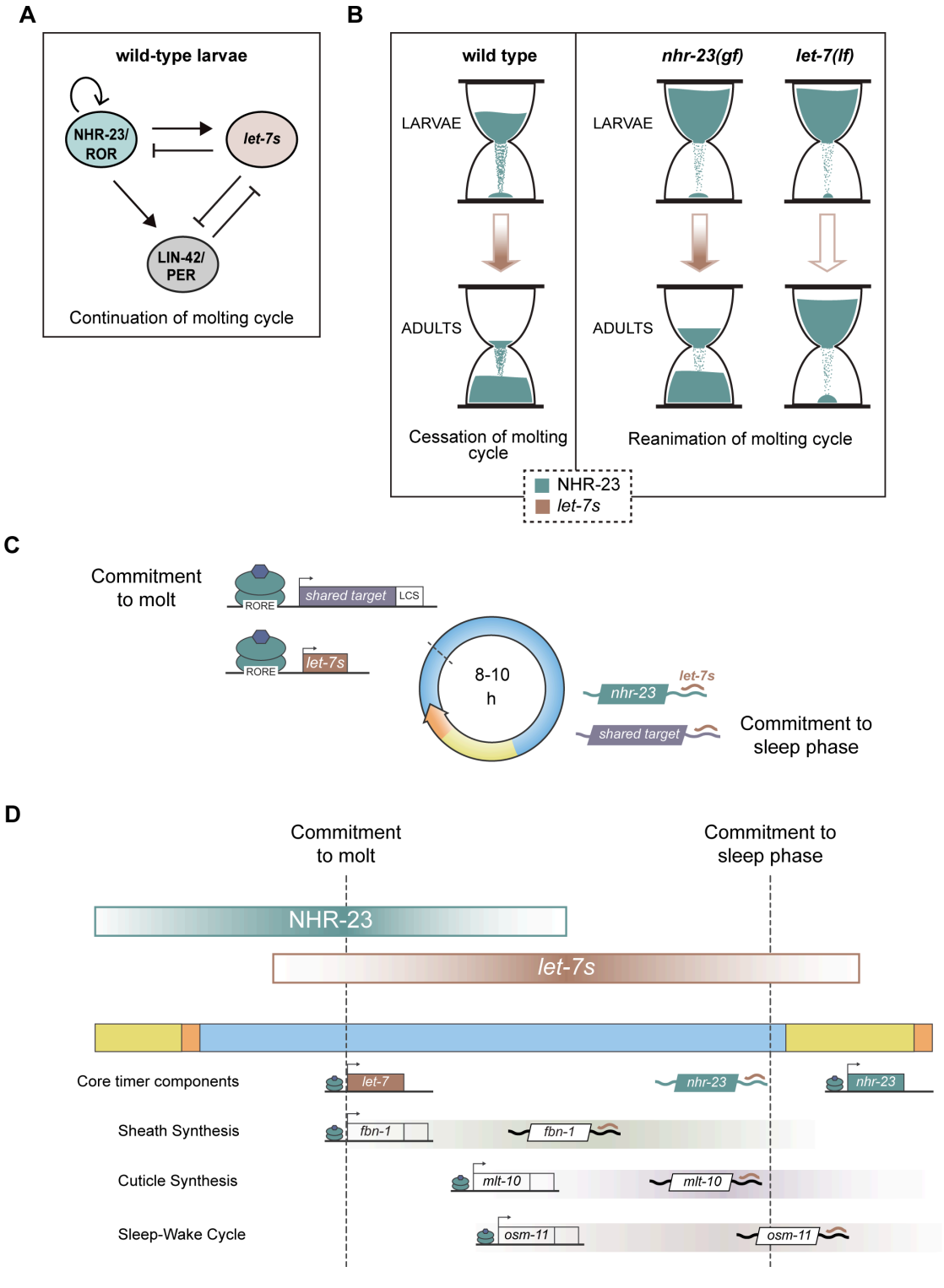
A
wild-type larvae
NHR-23/ ROR
let-7s
LIN-42/ PER
Continuation of molting cycle
B
wild type
nhr-23(gf)
let-7(lf)
LARVAE
LARVAE
ADULTS
ADULTS
Cessation of molting cycle
Reanimation of molting cycle
NHR-23
let-7s
C
Commitment to molt
RORE
shared target
LCS
RORE
let-7s
8-10 h
let-7s
nhr-23
shared target
Commitment to sleep phase
D
Commitment to molt
Commitment to sleep phase
NHR-23
let-7s
Core timer components
let-7
nhr-23
nhr-23
Sheath Synthesis
fbn-1
fbn-1
Cuticle Synthesis
mlt-10
mlt-10
Sleep-Wake Cycle
osm-11
osm-11

Figure 9. Negative feedback between NHR-23 and *let-7s* unites biorhythms generated by the molting timer with major transitions in the life cycle. **A)** Model of the molting cycle timer as a genetic oscillator that includes a transcriptional-post-transcriptional negative feedback loop between NHR-23 and *let-7*-family miRNAs. This diagram depicts regulatory events mediated by interactions between proteins and nucleic acids; the diagram excludes events mediated by interactions between NHR-23 and its predicted ligand. **B)** Complementary model of an hourglass timer that relies on the same negative feedback loop to schedule the larval-to-adult transition. In both cases, the timekeeping mechanism senses and responds to the relative levels of NHR-23 and *let-7s*. In wild-type animals, dampening of *nhr-23* expression by *let-7s* ultimately causes the oscillator to stop or blocks manifestation of the oscillator in the form of additional molts. In contrast, tilting the balance toward higher levels of NHR-23 triggers supernumerary molts in both *nhr-23*(*gf)* and *let-7(lf)* mutants. **C)** Proposed correspondence between the levels of NHR-23 and *let-7s*, the expression and repression of critical CCGs, and recurrent transitions between active and quiescent states during larval development (middle). **D)** Proposed mechanism by which cycles in the relative abundance of NHR-23 and *let-7s* sculpt the expression profiles of CCGs and orchestrate related aspects of the molting cycle. Gradient shading in teal depicts the rise and fall of NHR-23 protein levels during each larval stage. A similar gradient shaded brown depicts the rise and fall of primary *let-7* levels. The underlying bar depicts progression of the molting cycle, as color-coded in Figure 1. The approximate times at which transcript levels for core clock components and selected CCGs start to rise and fall due to transcriptional activation by NHR-23 and post-transcriptional repression by *let-7s*, respectively, are depicted. The respective phases were estimated based on key findings of this report and other experimental evidence (Hendriks et al., 2014; Kim et al., 2013).

METHODS

Detailed methods are provided in the online version of this paper and include the following:

- KEY RESOURCES TABLE
- CONTACT FOR REAGENT AND RESOURCE SHARING
- EXPERIMENTAL MODEL AND SUBJECT DETAILS
- METHOD DETAILS
    - Working with *C. elegans*
    - Bacterial-mediated RNA-interference (RNAi)
    - Longitudinal Studies of Molting-Associated Biorhythms
    - Detection and Characterization of Supernumerary Molts
    - Construction of Fusion Genes and Transgenic Strains
    - Editing the *C. elegans* Genome
    - Quantitative Fluorescence Microscopy
    - Chromatin Immunoprecipitation with Quantitative PCR
    - Isolation of RNA
    - Quantitative RT-PCR
    - Bioinformatic Analyses
- QUANTIFICATION AND STATISTICAL ANALYSIS

SUPPLEMENTAL INFORMATION

The supplemental information for this article includes five figures and four tables.

CONTACT FOR REAGENT AND RESOURCE SHARING

Further information and requests for resources and reagents should be directed to and will be fulfilled by the Lead Contact, Alison R. Frand (afrand@mednet.ucla.edu).

METHOD DETAILS

Working with *C. elegans*

Unique strains of the model nematode *Caenorhabditis elegans* generated by and applied to this research are described in the Key Resources Table. *C. elegans* were cultivated, preserved, observed, and transformed using standard methods (Stiernagle, 2006). Strains were cultivated at 25°C unless otherwise specified. Newly-hatched worms were developmentally synchronized by passage through starvation-induced, L1-stage diapause. Briefly, eggs were isolated by lysis of gravid hermaphrodites in sodium hypochlorite, suspended in M9 buffer supplemented with 5 µg/mL cholesterol, and incubated for 16 to 24 h with rotational aeration. Hatchlings were then plated on solid nematode growth medium (NGM) seeded with *Escherichia coli* strain OP50-1, HT115(DE3) or HB101, as indicated. One to two hundred hatchlings were routinely plated on 6 cm NGM plates; ten to fifteen thousand hatchlings, on 10 cm NGM plates seeded with 10-fold concentrated bacteria.

Bacterial-mediated RNA-interference (RNAi)

Relevant clones of *E. coli* HT115(DE3) were cultured, plated on solid NGM supplemented with 8 mM isopropyl β-D-1-thiogalactopyranoside (IPTG, Laguna Scientific), and incubated for 16 to 24 h at 25° C, allowing for IPTG-induced expression of dsRNAs. Worms used as controls were fed bacteria transformed with the empty vector pPD129.36 (a gift from Andy Fire). Alternatively, worms were fed bacteria transformed with a derivative of the same vector with an

inserted *nhr-23* sequence. The latter clone matched I-3F11 (Source BioScience) but was isolated directly from the Ahringer library (Kamath and Ahringer, 2003). Because the insert corresponds to three constitutive exons at the 3' end of the *nhr-23*, the dsRNA made by this clone targets all 6 isoforms of *nhr-23* annotated in WS273.

To knockdown *nhr-23* during a specific larval stage and circumvent predominant arrest during a preceding molt, hatchlings were fed control bacteria for an empirically determined interval, harvested, washed thrice in M9 buffer, and then divided into two samples. Next, larvae in the test sample were fed bacteria that expressed *nhr-23* dsRNAs; larvae in the control sample were once again fed bacteria that expressed only short, dsRNAs dissimilar from any worm gene (Kamath and Ahringer, 2003). Hatchlings destined to become test subjects in longitudinal studies of newly-emerged L2s, L3s, and L4s were initially fed control bacteria for 0, 6, and 14 h, respectively. To further attenuate the efficacy of RNAi – as needed to collect large time samples of practically synchronized L3s, L4s and young adults – hatchlings were initially fed control bacteria for 24 h and then split into test and control samples, as above.

Longitudinal Studies of Molting-Associated Biorhythms

This section provides additional information about the collection, analysis, and presentation of data in Figure 1, Figure 2 and Supplemental Table 1. Cohorts of larvae molting to the stage of interest were isolated from synchronized populations; singled in 12-well NGM-RNAi plates; and observed for 5 to 60 s at regular 1 h intervals, using a Zeiss M^2BioDiscovery microscope. L4s and older worms were observed at 300-fold magnification; L3s and younger worms, at 600-fold magnification. At each time sample, each subject was classified as active or lethargic based on the observation of defined target behaviors. Molting-defective (Mlt) and ruptured through the vulva

(Rup) worms were identified by conventional criteria (Reinhart et al., 2000).

The longitudinal studies represented in Figure 1 included videotaping the head of the worm using a Sony HDR-XR500V or Nikon D500 camera attached to the microscope. Later, the number of pharyngeal contractions (pumps) in a 15 s recorded interval was counted while the film was viewed at 4-fold reduced speed using iMovie version 10.11.2. Pumping rates (Hz) determined by three independent counts of selected films fell within 95% of the mean, validating this method. High, medium and low levels of activity were then graded *post-hoc* on a one-way standard scale defined by the standard deviations and mean pumping rate of all age-matched, wild-type time samples. As an example, wild-type young adults pumped at 3.9 ± 1.1 Hz (mean ± sd). The activity levels of nearly all worms that reawakened from lethargi associated with the L4/A molt were therefore graded as high, medium, or low if the worm pumped at greater than, or equal to, 2.8 Hz; between 2.8 and 1.7 Hz; or less than 1.7 Hz, respectively. A reasonable exception to this system was made if sinusoidal locomotion was obvious but no pharyngeal pumps were captured on video. In this scenario, the worm was scored as active at a low level. This exception applied to only 8 out of 56 time samples of *nhr-23* single knockdowns and 14 out of 84 time samples of *nhr-23(RNAi) let-7(n2853)* double mutants. Among animals that reawakened from lethargi associated with the L3/L4 molt, the same exception applied to 20 out of 120 time samples of *nhr-23* single knockdowns and 20 out of 180 time samples of *nhr-23(RNAi) let-7(n2853)* double mutants. The longitudinal studies represented in Figure 2 did not involve video-recordings. Instead, high versus low levels of activity were assigned based on the direct observation of continuous versus sporadic pharyngeal pumps during the time sample.

Detection and Characterization of Supernumerary Lethargi and Molts

To score quiescence among populations of young adults, synchronized hatchlings were released from starvation-induced diapause by plating on 10-fold concentrated lawns of *E. coli* OP50-1 at a density of 200-400 worms per 10 cm NGM plate. For each strain of interest, six distinct clutches were plated at 12 h intervals, facilitating the later evaluation of time samples covering a 72-h interval. As described, worms were observed by light microscopy and scored as quiescent or active at regular 3 h intervals, 54 to 120 h post-release from diapause. For related longitudinal studies, quiescent adults were selected and singled in 12-well NGM plates seeded with thin lawns of bacteria. Each cohort of animals was then observed at regular 2 h intervals. All of the previously described scoring rubrics were applied. In addition, ecdysis was recognized by the execution of one or more of the following idiosyncratic movements: rotation on the long axis (flipping), bilateral contraction and relaxation on the long axis, and elevation plus semi-circular rotation of the head. Aberrant molts were scored based on the observation of puckered sections of cuticle along the body, or the adherence of partly shed cuticle fragments to the body. If a particular animal had passed through lethargus, then the following behaviors were also considered evidence of an aberrant molt: pharyngeal spasms, incomplete pumps wherein the grinder failed to close, and incomplete flips that resulted in twists or kinks along the body.

Construction of Fusion Genes and Transgenic Strains

The sequences of all oligonucleotides used in this study are specified in Supplemental Table 4. All DNA nucleotides were synthesized by and purchased from Integrated DNA Technologies (IDT). The bicistronic reporters used to detect regulatory elements within 3′ UTRs were constructed by Gibson Assembly (NEB) and standard methods. Phusion High-Fidelity DNA

Polymerase (NEB) was used to amplify DNA molecules. The resulting plasmids contained the pBR322 backbone of Fire Lab vectors; the *dpy-7* promoter, which corresponds to nucleotides 7,537,914-7,538,219 of *C. elegans* Chr. X (NC_003284); the synthetic intron embedded in primer HM01; the coding sequence for *tandem (td) tomato*, which was isolated from Addgene plasmid #30530 (a gift from Gerhart Ryffel); one of the test 3′ UTRs described below; and an *SL2::gfp::unc-54* 3′ UTR cassette (a gift from John Kim. The gene-specific 3′ UTRs comprised nucleotides amplified from Chr. I (NC_003279) as follows: *nhr-23*, 7,220,953-7,221,820; *unc-54*, 14,855,909-14,856,180; and *lin-41*, 9,334,850-9,335,964. Deletions within the *nhr-23* 3′ UTR reporter (cloned in pHR017) were created using a Q5 Site-Directed Mutagenesis Kit (NEB) and verified by Sanger Sequencing (Genewiz Inc.). To generate distinct extrachromosomal arrays harboring each bicistronic reporter, mixtures of the corresponding plasmid (1 ng/µl), the co-transformation marker *ttx-3::gfp* (40 ng/µl), and filler DNA pRS316 (59 ng/µl) were microinjected into the gonads of wild-type hermaphrodites. Transgenic progeny and unique descendent strains were isolated by standard methods.

The strain ARF422 was made by first crossing *wgIs43* hermaphrodites with *let-7(mg279) mir-84(tm1304)* males. After singling F2s from the crosses, we screened for *wgIs43* homozygotes among the F3 generation. Only the strains that were homozygous for *wgIs43* were selected and screened for *let-7(mg279) mir-84(tm1304)* homozygotes. The transgene *wgIs43* was obtained from OP43 and *let-7(mg279) mir-84(tm1304)* was obtained from ARF249.

Editing the *C. elegans* Genome

The CRISPR/Cas9 system was used essentially as described (Paix et al., 2015) to delete the endogenous LCS from the 3′ UTR of *nhr-23*, generating the allele *nhr-23(aaa20)*. Briefly,

wild-type hermaphrodites were microinjected with a mixture containing the following: *nhr-23* crRNA (400ng/µL), tracrRNA (1µg/µL), *dpy-10* crRNA (160 ng/µL, GE Dharmacon), *dpy-10* ssODN (13.75 ng/µL, IDT), and CAS9 protein (500 ng/µL, PNA Bio) in HEPES buffer pH 7.5 (Sigma-Aldrich) supplemented with 0.025 µM KCL (Sigma-Aldrich). Injected hermaphrodites (P0s) were singled and screened for Dumpy (Dpy) or Roller (Rol) offspring (F1s), both phenotypes associated with mutations in *dpy-10*. One hundred F1s were singled from a selected P0. Genotyping the F1s and their descendants (F2s) identified two strains homozygous for identical chromosomal deletions of precisely the 21 nucleotides comprising the LCS. One *nhr-23(aaa20-*Δ*LCS)* strain was backcrossed to N2 thrice prior to phenotypic analysis. No edits in the *dpy-10* gene were found in the backcrossed strain (ARF414).

To construct *xk22*, wild-type hermaphrodites were injected with *nhr-23* crRNA oHG202 (40µM, IDT Alt-R CRISPR crRNA), *nhr-23::3xflag* repair template (120ng/µL, IDT Ultramer DNA oligo), *dpy-10* crRNA (5.6 µM, IDT Alt-R CRISPR crRNA), *dpy-10* repair template (12 ng/µL, IDT Ultramer DNA oligo), tracrRNA (40 µM, IDT Alt-R CRISPR-Cas9 tracrRNA) and Cas9 (15.5 µM, stock at 40 µM in 20 mM HEPES-KOH pH 7.5, 150 mM KCl, 10% glycerol, 1 mM DTT from Berkeley QB3 MacroLab). All reagents were diluted in IDT duplex buffer. The crRNA and repair template both target the C-terminus of NHR-23, which is common to all predicted isoforms. Injected hermaphrodites were singled and F1 offspring were screened for the same phenotypes described above. One hundred and twenty F1s were singled from plates that had a high penetrance of Dpy and Rol phenotypes. Genotyping the F1s identified 3 lines that had *3xflag* inserted precisely before the stop codon of the *nhr-23* gene. One *nhr-23(xk22)* line was backcrossed to N2 five times to generate QK159. No edits in the *dpy-10* gene were found in QK159.

Quantitative Fluorescence Microscopy

C. elegans were anesthetized with 2.5% NaN_3 (v/v) in M9 buffer, mounted on 2% agarose pads, and observed using a Zeiss Axioplan compound microscope with an attached Hamamatsu Orca ER CCD camera. The image acquisition and analysis software package Volocity 6.3 (Perkin Elmer) was used to control the microscope and digital camera and also to measure average fluorescence intensities within selected regions of interest (ROIs). In particular experiments, transgenic animals were staged partly by DIC microscopy and imaged during the L3/L4 or L4/Adult molts. Molting animals were identified by occlusion of the buccal cavity (Monsalve et al., 2011). Stereotypical rearrangements of vulva precursor cells (VPCs) demarcated early versus late sub-stages of the L3-to-L4 molt. The presence of a lumen in the incipient vulva demarcated early versus late sub-stages of the L4/Adult molt (Gupta et al., 2012; Van Buskirk and Sternberg, 2007).

To measure GFP signals associated with the *let-7p::nls-gfp* transcriptional reporter (Kai et al., 2013), worms were imaged at 400X total magnification. Both DIC and fluorescence images of the lateral epidermis were acquired – the latter with an exposure time of 25 ms. Three nuclei in hyp7 and three in the seam were traced from the DIC image of each worm. The average fluorescence intensity within each nucleus was then measured and corrected for background signal. The average values for both hyp7 and seam nuclei (per worm) were used in further statistical analysis.

Signals associated with tdTomato and GFP expressed from bicistronic reporters for regulatory elements within 3′ UTRs were measured using similar approaches. In this case, three distinct ROIs with areas of 40–70 μm^2 were manually selected per worm; each ROI included approximately equal areas of the nucleus and cytoplasm. In addition, multiple images of tdTomato

and GFP were automatically captured over a range of exposure times. The average fluorescence intensity of each ROI was measured and plotted versus the exposure time. Values within the linear range of the assay were then used to determine the ratiometric signal (tdTomato/GFP) for each ROI. The average ratiometric value of all three ROIs per worm was used for subsequent statistical analysis. Notably, the morphology of the vulva was abnormal in a subset (≤ 10%) of animals that expressed any bicistronic reporter. Because the phenotype precluded staging by the abovementioned criteria, this subset of animals was excluded from the analysis.

Chromatin Immunoprecipitation Coupled with Quantitative PCR

Synchronized QK159[*nhr-23::3xflag*] and N2 larvae were cultivated on lawns of *E. coli* HB101 for 34 h at 25° C. L4s were then collected, washed thrice in M9, and condensed in a ~500 µL worm pellet. To crosslink NHR-23::3XFLAG with DNA molecules that were in direct or indirect contact, the worm pellet was re-suspended in 12 mL of sterilized, distilled water with 2.6% (v/v) formaldehyde and gently rocked on a nutator (Thermo Scientific) for 30 min at room temperature. To quench the reaction, 600 µL of 2.5 M glycine was added and the worms incubated on the nutator for another 5 min. The samples were then washed thrice in water and flash-frozen. Frozen pellets were ground twice, for 1 min each, in a Retsch MM400 CryoMill at 30 Hz in liquid nitrogen-chilled stainless steel cryomill chambers, producing a frozen powder of partially lysed worms. The powder was resuspended and further lysed in 2 mL of RIPA buffer (1x PBS, 1% (v/v) NP40, 0.5% sodium deoxycholate, and 0.1% SDS), supplemented with the HALT Protease and Phosphatase Inhibitor Cocktail (ThermoFisher Scientific), for 10 min at 4° C. To shear the chromatin, samples were sonicated in a Bioruptor Pico (Diagenode) for 3 min (30 s ON/30 s OFF cycles), three times, at 4° C. A 20 µL aliquot of the sample was treated with Proteinase K for 10

min and then cleaned by phenol chloroform extraction, as described below. The concentration of the aliquot was determined using a Qubit Fluorometer 3.0 (Invitrogen). Based on the initial concentration of the aliquot, the chromatin sample was diluted to 20-30 ng/µL. To check the extent of shearing, the same aliquot was run on an agarose gel. The sample was processed and analyzed further provided the DNA smear centered at 200 bp. Of the total amount of chromatin that remained, 10% was used as the input sample – i.e. stored at 4° C – and 90% was subject to immunoprecipitation. Every 10 µg of chromatin was incubated with 2 µg of mouse M2 anti-FLAG monoclonal antibodies (Sigma-Aldrich) overnight at 4° C on a nutator. Next, samples were incubated with 1.5 mg of affinity-purified sheep anti-mouse IgG antibodies covalently attached to superparamagnetic Dynabeads M-280 (Invitrogen) for 2 h, at 4° C. Thereafter, complexes bound to the beads were separated thrice from the supernatant and washed in 800 µL LiCl buffer (100 mM Tris-HCL pH 7.5, 500 mM LiCl, 1% (v/v) NP40, and 1% sodium deoxycholate). The resulting immunoprecipitates were de-crosslinked by incubation with 80 µg of Proteinase K in 400 µL of worm lysis buffer (100 mM Tris-HCL pH 7.5, 100 mM NaCl, 50 mM EDTA, and 1% SDS) at 65° C for 4 h—the input samples also underwent the same treatment in parallel. Residual proteins were removed from both IP and Input samples by phenol-chloroform extraction. Briefly, 400 µL of phenol-chloroform-isoamyl alcohol pH 8.0 (Sigma-Aldrich) was added to each sample. The sample was vortexed vigorously and centrifuged at 15,000 x g for 5 min at 4° C. The top layer was transferred to a new tube and DNA was precipitated by incubating with 1 mL of 0.3 M ammonium acetate (Sigma-Aldrich) in ethanol for 1 h at 30° C. The resulting DNA pellet was washed twice in 100% ethanol and re-suspended in Tris-EDTA, pH 8.0. Prior to use as a template for qPCR, the entire DNA sample was treated with RNase A for 1 h at 37° C.

Quantitative PCR for promoter regions of interest was performed with Absolute Blue SYBR

Green (Thermo Scientific) using a CFX96 Real Time System Thermocycler (BioRad) as per the manufacturers' instructions, with custom primers described in the Key Resources Table. The Ct value for each IP sample was first normalized to the Ct value for the respective input sample. The log 2 transformed fold-change values for samples derived from QK159[*nhr-23::3xflag*] were then normalized to the respective N2 sample. Three biological replicates, each with the same number of technical replicates, were completed for each amplicon of interest, as specified in corresponding figure legends. Pairwise statistical comparisons of the fold enrichment of a given amplicon in samples from QK159[*nhr-23::3xflag*] versus N2 were made by Two-way ANOVA with Bonferroni's correction for multiple comparisons.

Isolation of RNA

RNA was extracted from developmentally synchronized *C. elegans* as described (McCulloch and Rougvie, 2014). Samples of ~1,500 worms were collected at regular 2 h intervals. Because the strains seemed to develop at different rates, light microscopy was used to count the fraction of pumping (active) versus non-pumping (lethargic) animals in each sample prior to collection (n = 50-100). Lethargic phases were empirically identified *post hoc* by troughs in the proportion of pumping animals. Related graphs in Figure 5A, Figure 7B and Supplemental Figure 4 include 14 time samples encompassing three lethargic and two active phases per strain. Pellets containing worms (~100 µl) were re-suspended in 4 volumes of TRIzol (ThermoFisher Scientific) and 1 volume of glass beads 400-625 µm in diameter (Sigma). The suspensions were vortexed, flash frozen, and thawed thrice. Samples were then mixed with 0.17 volumes of 24:1 chloroform: isoamyl alcohol (OmniPur) and centrifuged. The aqueous layer was collected, mixed with an equal volume of 5:1 acid phenol: chloroform (ThermoFisher Scientific), and centrifuged again. After

collection of the top layer, RNA was extracted by precipitation with ice-cold isopropanol (Sigma) and GlycoBlue (ThermoFisher Scientific). The concentration of RNA in each time sample was measured using a NanoDrop 2000 (ThermoFisher Scientific). Thereafter, 5 µg of total RNA per sample was treated with 2U of TURBO DNase (ThermoFisher Scientific) for 1 h. Notably, RNA samples used to quantify mature *let-7* were not pre-treated with DNAse.

Quantitative RT-PCR

The sequences of gene-specific RT primers and identifiers for TaqMan assays used in this research are provided in Supplemental Table 4. To quantify levels of primary *let-7* and *ama-1* transcripts in the abovementioned extracts, we processed 50ng of RNA using a High-Capacity cDNA Reverse Transcription Kit (ThermoFisher Scientific). Reaction mixtures of 15 µL included random primers, dNTPs, RNaseOUT, and reverse transcriptase, per the manufacturer's guidelines. To quantify levels of mature *let-7* and the U18 small nucleolar (sno) RNA, we processed RNA with the same kit but used gene-specific rather than random primers. Three volumes of nuclease-free water were added to completed RT reactions. Next, we set-up TaqMan assays (ThermoFisher Scientific) in 96-well plates, in triplicate. Per the manufacturer's instructions, each reaction included TaqMan Universal PCR Master Mix, no AmpErase UNG, gene-specific primers, and 1.3 µL of the preceding RT product in a volume of 20 µL. Reactions ran on a Stratagene MX3000P (Agilent Genomics). To measure levels of protein-coding transcripts, 1µg of RNA was reverse transcribed using the enzyme Transcriptor (Roche). Each reaction mixture (20 µL) also included hexadeoxynucleotide primers (Promega), dNTPs and RNasin (Promega). Four volumes of nuclease-free water were added to completed RT reactions. TaqMan assays were performed as described using 2 µL of the RT product as template in a volume of 10 µL.

The amount of template used in each TaqMan assay gave Ct values in the linear range of 21 to 36. In nearly all cases, technical replicates gave Ct values within 95% of the mean and the mean Ct value was used in subsequent analyses. Separate TaqMan reactions using templates made in the absence of reverse transcriptase produced no detectable PCR products, confirming the amplification of RNA rather than genomic DNA. As described, the levels of transcripts of interest were normalized to the levels of *ama-1* mRNAs or U18 snoRNAs within each sample, which were quantified in parallel TaqMan assays. For studies of gene expression over several developmental stages, the normalized values for each time sample were further standardized to the mean of all time samples derived from mock-treated or wild-type animals.

Identification of conserved *cis*-regulatory elements in homologous genes

DNA sequences corresponding to the upstream regulatory region, first intron and 3′ UTR for each nematode gene of interest were retrieved from WormBase (WS) v.264 and saved as SnapGene v.4 (GSL Biotech) files. The upstream sequences extracted from WS included all nucleotides between the transcriptional start site of the gene of interest and the nearest protein-coding gene. Particular sequences were extended or shortened based on gene models, ESTs and transcriptional start sites archived in WS264. If the gene of interest lacked an annotated 3′ UTR, then we initially retrieved 1 kb of sequence downstream of the stop codon. Particular 3′ UTR sequences were revised based on ESTs and poly-AAA sites that are archived in WS264 but not yet incorporated in current gene models.

Both the upstream regulatory regions of vertebrate homologs of *let-7* and the 3′ UTRs of vertebrate homologs of *nhr-23*/*RORs* were retrieved from the UCSC genome browser. Three human genes, two mouse genes, and six zebrafish genes encode mature miRNAs identical in

sequence to *C. elegans let-7*. We extracted 3 kb of sequence upstream of each *let-7* homolog, except in the case of *H. sapiens let-7a-3*, wherein the core promoter has been experimentally delimited to 1 kb of upstream sequence (Wang et al., 2012). For a given gene, the longest 3′ UTR was selected if multiple 3′ UTRs existed. The 3′ UTR sequences were individually and systematically validated by comparison with EST; only those genes with annotated 3′ UTRs supported by ESTs were included in further analyses.

Finding clock-controlled genes regulated by NHR-23 and *let-7s*

Genes were determined to be "involved in molting" based on the literature. For example, if mutations in a particular gene caused a molting defective phenotype, the gene was considered to be involved in molting (Frand et al., 2005). Similarly, if inactivation of the gene had an effect on lethargus, the gene was also considered to be involved in the molting cycle. Genes were annotated as "oscillatory" based on published RNA-Seq studies (Hendriks et al., 2014; Kim et al., 2013); therein, genes whose expression at 8-10 h intervals was significantly correlated ($P<0.05$) were considered to be cycling in expression.

To identify ROR response elements that might function as transcriptional enhancers of miRNAs or protein-coding genes of interest, we searched the upstream regulatory sequences and/or first introns for instances of the consensus response element 5′-(A/G)GGTCA-3′ on both the coding and anti-coding strands of DNA. Figures 1A, 8A and Supplemental Figure 1A depict the results of these computational searches. To accurately calculate the probability of an RORE occurring by chance, we first used the k-mer counting software program DSK (Rizk G. et al, 2013) to determine that the reference genome of *C. elegans*, which comprises 100.2 mega bases, includes 41,203 distinct instances of the consensus RORE. For non-nematodes, the expected frequency was

the chance of either six-nucleotide sequence appearing in a longer oligonucleotide; this frequency is approximately one per 1 kb.

Regions of *C. elegans* chromosomal DNA occupied by NHR-23 *in vivo* were identified on the modEncode *C. elegans* Genome Browser (v. 2.48). The two relevant datasets archived therein were ChIP-Seq of strain OP43 cultivated at 20° C and harvested during the L2 or L3 stage. Most genomic regions where NHR-23 was significantly enriched were detected in the dataset collected from L3 stage larvae, however, we do not discriminate between the two stages in our analysis. The upstream regulatory sequences and/or first intron for each gene of interest were viewed in this browser. Regions of significant enrichment ("peaks") were identified by Z-scores ≥ 2 (Celniker et al., 2009). Sequences extracted and aligned with the upstream regulatory regions and/or first intron as above, adjusting for differences in the related chromosomal coordinates between WS220 and WS264.

Evidence of direct or indirect regulation of transcript levels by NHR-23 – i.e. expression of the gene was at least 1.2-fold reduced in *nhr-23(RNAi)* versus control larvae – was either detected by Affymetrix microarrays (Kouns et al., 2011), or shown in prior publications (*lin-42a/b, nas-36*).

Targets of NHR-23 followed 2 out of the 3 following criteria: 1) The upstream regulatory region and/or first intron contained Chip-Seq NHR-23 peaks (Celniker et al., 2009); 2) the same region contained more ROREs than predicted by chance alone; and 3) Expression was 1.2-fold lower in *nhr-23* knockdowns than mock-treated larvae.

The software RNAhybrid (Rehmsmeier et al., 2004) was used to detect sequences partially complementary to the 21-nt. mature *let-7* in the 3′ UTRs of annotated homologs of *nhr-23* in the genomes of *H. sapiens*, *M. musculus*, *D. rerio* and *C. briggsae*. Mature *C. elegans let-7*, which is

identical to human *let-7*a, was used as the query sequence. No more than 1 mismatched nucleotide within the *let-7* seed sequence was tolerated for the prediction of LCSs in this report.

Targets of *let-7* fulfilled both of the following criteria: 1) LCSs, with up to one mismatch in the seed region, were detected in the 3′ UTR more often than, or equal to, the number predicted by chance alone (Rehmsmeier et al., 2004); and 2) ALG-1 co-IP the 3′ UTR, on the coding strand of the gene by iCLIP-Seq (Broughton et al., 2016).

QUANTIFICATION AND STATISTICAL ANALYSIS

The software package Volocity 6.3 (Perkin Elmer) was used to both acquire fluorescence micrographs and measure the signal intensity of selected ROIs. The software package GraphPad Prism v6.0h was used for all statistical tests except for those done on data from ChIP-qPCR experiments. Statistical tests for the ChIP-qPCR experiments were done using R Studio version 1.1.463 and R version 3.5.2. Samples sizes for all experiments, statistical analysis, and outcomes thereof are specified in each figure and/or corresponding legend.

Key Resources Table

Reagent type (species) or resource	Designation	Source or reference	Identifiers	Additional information
gene (*Caenorhabditis elegans*)	*nhr-23*	WormBaseWS272	*nhr-23* ; C01H6.5	
gene (*C. elegans*)	*let-7*	WormBaseWS272	*let-7* ; C05G5.6	
gene (*C. elegans*)	*lin-42*	WormBaseWS272	*lin-42* ; F47F6.1	
gene (*C. elegans*)	*mir-84*	WormBaseWS272	*mir-84* ; B0395.4	
gene (*C. elegans*)	*mir-48*	WormBaseWS272	*mir-48* ; F56A12.3	
gene (*C. elegans*)	*mir-241*	WormBaseWS272	*mir-241* ; F56A12.4	
gene (*C. elegans*)	*col-19*	WormBaseWS272	*col-19* ; ZK1193.1	
gene (*C. elegans*)	*unc-54*	WormBaseWS272	*unc-54* ; F11C3.3	
gene (*C. elegans*)	*lin-41*	WormBaseWS272	*lin-41* ; C12C8.3	
gene (*C. elegans*)	*mlt-10*	WormBaseWS272	*mlt-10* ; C09E8.3	
gene (*C. briggsae*)	*nhr-23*	WormBase ParaSite WBPS9	*nhr-23;* WBGene00040598	
gene (*D. melongaster)*	*HR3*	Aug. 2014 (BDGP Release 6 + ISO1 MT/dm6)	NM_001259307.3	Coordinates - chr2: 10,203,995-10,227,957 GenBank Accession EC058128, C0278043, EC080062, AY094723
gene (*X. tropicalis)*	*RORA*	Jul. 2016 (Xenopus_tropicalis_v9.1/xenTro9)	NM_001079195.1	Coordinates - chr3: 83,889,614-83,948,330 GenBank mRNAs BC123953
gene (*D. rerio*)	*mirlet7a-1*	Sep. 2014 (GRCz10/danRer10)	NR_029976.1	
gene (*D. rerio*)	*mirlet7a-2*	Sep. 2014 (GRCz10/danRer10)	NR_029977.1	
gene (*D. rerio*)	*mirlet7a-3*	Sep. 2014 (GRCz10/danRer10)	NR_029978.1	
gene (*D. rerio*)	*mirlet7a-4*	Sep. 2014 (GRCz10/danRer10)	NR_029979.1	
gene (*D. rerio*)	*mirlet7a-5*	Sep. 2014 (GRCz10/danRer10)	NR_039088.1	
gene (*D. rerio*)	*mirlet7a-6*	Sep. 2014 (GRCz10/danRer10)	NR_029981.1	
gene (*D. rerio*)	*RORAB*	Sep. 2014 (GRCz10/danRer10)	NM_201067.1	Coordinates - chr7: 29,267,488-29,300,423 GenBank Accession BC051158
gene (*D. rerio*)	*RORB*	Sep. 2014 (GRCz10/danRer10)	NM_001082856.1	Coordinates - chr5: 24,761,303-24,776,994 GenBank Accession CK396220, CK679114, EB861010, B092168, EF107093
gene (*D. rerio*)	*RORC*	Sep. 2014 (GRCz10/danRer10)	NM_001082819.1	Coordinates - chr8: 18,851,532-18,862,800 GenBank Accession EB954643, CA472317, CN51179, CN511196, EB893435, EF107094
gene (*G. gallus*)	*RORA*	Nov. 2011(ICGSC Gallus_gallus-4.0/galGal4)	NM_001289887.1	Coordinates - chr10: 4,187,635-4,536,712 GenBank Accession BU453250, BU298761
gene (*G. gallu* s)	*RORB*	Nov. 2011(ICGSC Gallus_gallus-4.0/galGal4)	NM_205093.1	Coordinates - chrZ: 36,402,033-36,535,271 GenBank Accession Y08638
gene (*M. musculus*)	*Mirlet7a-1*	Dec. 2011(GRCm38/mm10)	NR_029725.1	
gene (*M. musculus*)	*Mirlet7a-2*	Dec. 2011(GRCm38/mm10)	NR_029726.1	
gene (*M. musculus*)	*RORA*	Dec. 2011(GRCm38/mm10)	NM_013646	Coordinates - chr9: 68,653,786- 69,388,246 GenBank Accession AK043990, AK035351, AK087905, AK163917
gene (*M. musculus*)	*RORB*	Dec. 2011(GRCm38/mm10)	NM_146095	Coordinates - chr19: 18,930,605-19,111,196 GenBank Accession AK159011, BC058269
gene (*M. musculus*)	*RORC*	Dec. 2011(GRCm38/mm10)	NM_011281	Coordinates - chr3: 94,377,432-94,398,276 GenBank Accesion AJ132394
gene (*H. sapiens*)	*MIRLET7A1*	Dec. 2013 (GRCh38/hg38)	NR_029476.1	
gene (*H. sapiens*)	*MIRLET7A2*	Dec. 2013 (GRCh38/hg38)	NR_029477.1	
gene (*H. sapiens*)	*MIRLET7A3*	Dec. 2013 (GRCh38/hg38)	NR_029478.1	
gene (*H. sapiens*)	*RORA*	Dec. 2013 (GRCh38/hg38)	NM_134261	Coordinates - chr15: 60,488,284-61,229,302 GenBank Accesion AL832164, AK055969, BC008831
gene (*H. sapiens*)	*RORB*	Dec. 2013 (GRCh38/hg38)	NM_006914	Coordinates - chr9: 74,497,335-74,693,177 GenBank Accesion BX647070, AK125162
gene (*H. sapiens*)	*RORC*	Dec. 2013 (GRCh38/hg38)	NM_005060.3	Coordinates - chr1: 151,806,071-151,831,802 GenBank Accession - AL834219
gene (*H. sapiens*)	*PER2*	Dec. 2013 (GRCh38/hg38)	NM_022817.3	Coordinates - chr2: 238,244,044-238,288,610 GenBank Accession - AB002345
strain (*E. coli*)	OP50-1	*Caenorhabditis Genetics Center* (CGC)	*E. coli* OP50-1	
strain (*E. coli*)	HB101	*Caenorhabditis Genetics Center* (CGC)	*E . coli* HB101	
strain (*E. coli*)	DH5α	New England Biolabs	*E. coli* DH5α	
strain (*E. coli*)	vector only bacteria for RNAi; control	Julie Ahringer; PMID: 12529635	*E. coli* HT115(DE3) + pPD129.36	
strain (*E. coli*)	Transformed bacteria for RNAi of *nhr-23* ; *nhr-23(RNAi)*	Julie Ahringer; PMID: 12529635	*E. coli* HT115(DE3) + pPD129.36 with *nhr-23* insert	
strain (*C. elegans*)	wild type; N2	CGC	N2	wild type (Bristol)
genetic reagent (*C. elegans*)	*let-7(n2853)*	CGC	MT7626	*let-7(n2853) X* not out-crossed
genetic reagent (*C. elegans*)	*mir-48(Δ) mir-241(Δ); mir-84(n4037)* ; *let-7s* triple knockout	CGC	VT1066	*nDf51 V; mir-84(n4037) X*
genetic reagent (*C. elegans*)	*wgIs43[nhr-23* $^{++}$*]*; high-copy or increased dosage of *nhr-23*	CGC	OP43	*unc-119(ed3) III; wgIs43[nhr-23::TY1::EGFP::3xFLAG(92C12) + unc 119(+)]*
genetic reagent (*C. elegans*)	*mgIs49* ; *mlt-10* transcriptional reporter	Frand Lab; PMID: 16122351	GR1395	*mgIs49[mlt-10p::gfp-pest ttx-3p::gfp] IV*
genetic reagent (*C. elegans*)	*let-7(mg279)* ; partial loss-of-function *let-7* mutation	Frand Lab; PMID: 17065234	GR1436	*mgIs49[mlt-10p::gfp-pest ttx-3p::gfp] IV; let-7(mg279) X*
genetic reagent (*C. elegans*)	*let-7(mg279) mir-84(tm1304)*	Frand Lab; PMID: 17065234	ARF249	*mgIs49[mlt-10p::gfp-pest ttx-3p::gfp] IV; let-7(mg279) mir-84(tm1304) X*
genetic reagent (*C. elegans*)	*let-7p::nls-GFP* ; transcriptional reporter for *let-7*	Amy Pasquinelli; PMID: 23201578	PQ462	*apIs[let-7bp::NLS::gfp::let-858 3'UTR unc-119(+)] II; unc-119(ed9) III*
genetic reagent (*C. elegans*)	*let-7(n2853)* ; strong loss-of-function *let-7* mutation	Kim Lab	QK059	*let-7(n2853) X* out-crossed 3x
genetic reagent (*C. elegans*)	*nhr-23(aaa20-ΔLCS)*	This report	ARF413	*nhr-23(aaa20) I* not out-crossed. See "Editing the *C. elegans* Genome" in Method Details.
genetic reagent (*C. elegans*)	*nhr-23(aaa20-ΔLCS)*	This report	ARF414	*nhr-23(aaa20) I* out-crossed: 3x. See "Editing the *C. elegans* Genome" in Method Details.

Reagent type (species) or resource	Designation	Source or reference	Identifiers	Additional information
genetic reagent (*C. elegans*)	*nhr-23::3xflag* ; *nhr-23(xk22)*	This report	QK159	*nhr-23(xk22) I* out-crossed: 5x. See "Editing the *C. elegans* Genome" in Method Details.
genetic reagent (*C. elegans*)	*aaaEx97* ; *unc-54* 3'UTR reporter	This report	ARF370	*aaaEx97[dpy-7p::tdtomato::unc-54 3'UTR::SL2::gfp::unc-54 3'UTR ttx-3::gfp]* See "Construction of Fusion Genes and Transgenic Strains" in Method Details.
genetic reagent (*C. elegans*)	*aaaEx129* ; *nhr-23* 3'UTR reporter	This report	ARF372	*aaaEx129[dpy-7p::tdtomato::nhr-23 3'UTR::SL2::gfp::unc-54 3'UTR ttx-3::gfp].* See "Construction of Fusion Genes and Transgenic Strains" in Method Details.
genetic reagent (*C. elegans*)	*aaaEx146* ; *lin-41* 3'UTR reporter	This report	ARF399	*aaaEx146[dpy-7p::tdtomato::lin-41 3'UTR::SL2::gfp::unc-54 3'UTR ttx-3::gfp]* . See "Construction of Fusion Genes and Transgenic Strains" in Method Details.
genetic reagent (*C. elegans*)	*aaaEx131* ; *nhr-23* ΔLCS 3'UTR reporter	This report	ARF374	*aaaEx131[dpy-7p::tdtomato::nhr-23 3'UTR(ΔLCS)::SL2::gfp::unc-54 3'UTR ttx-3::gfp].* See "Construction of Fusion Genes and Transgenic Strains" in Method Details.
genetic reagent (*C. elegans*)	*aaaEx165* ; *nhr-23* Δ623-646 3'UTR reporter	This report	ARF400	*aaaEx165[dpy-7p::tdtomato::nhr-23 3'UTR(Δ623-646)::SL2::gfp::unc-54 3'UTR ttx-3::gfp].* See "Construction of Fusion Genes and Transgenic Strains" in Method Details.
genetic reagent (*C. elegans*)	*aaaEx166* ; *nhr-23* Δ227-249 3'UTR reporter	This report	ARF401	*aaaEx166[dpy-7p::tdtomato::nhr-23 3'UTR(Δ227-249)::SL2::gfp::unc-54 3'UTR ttx-3::gfp].* See "Construction of Fusion Genes and Transgenic Strains" in Method Details.
genetic reagent (*C. elegans*)	*aaaEx130* ; *nhr-23* Δ26-42 3'UTR reporter	This report	ARF373	*aaaEx130[dpy-7p::tdtomato::nhr-23 3'UTR(Δ26-42)::SL2::gfp::unc-54 3'UTR ttx-3::gfp].* See "Construction of Fusion Genes and Transgenic Strains" in Method Details.
genetic reagent (*C. elegans*)	"*wgIs43* ; *let-7(mg279) mir-84(tm1304)* "	This report	ARF422	*wgIs43[nhr 23::TY1::EGFP::3xFLAG(92C12) + unc 119(+)]; let-7(mg279) mir-84(tm1304) X* See "Construction of Fusion Genes and Transgenic Strains" in Method Details.
antibody	Monoclonal Anti-Flag M2 antibody	Sigma-Aldrich	F3165	
recombinant DNA reagent	*unc-54* 3'UTR reporter; negative control for set of bicistronic reporters	This report	pHR011	*dpy-7p::tdtomato::unc-54 3'UTR::SL2::gfp::unc-54 3'UTR* . See section titled "Construction of Fusion Genes and Transgenic Strains" in Methods.
recombinant DNA reagent	*nhr-23* 3'UTR reporter	This report	pHR017	*dpy-7p::tdtomato::nhr-23 3'UTR::SL2::gfp::unc-54 3'UTR* . See section titled "Construction of Fusion Genes and Transgenic Strains" in Methods.
recombinant DNA reagent	*lin-41* 3'UTR reporter; positive control for set of bicistronic reporters	This report	pHR023	*dpy-7p::tdtomato::lin-41 3'UTR::SL2::gfp::unc-54 3'UTR* . See section titled "Construction of Fusion Genes and Transgenic Strains" in Methods.
recombinant DNA reagent	*nhr-23* ΔLCS 3'UTR reporter	This report	pHR021	*dpy-7p::tdtomato::nhr-23 3'UTRΔLCS::SL2::gfp::unc-54 3'UTR* . See section titled "Construction of Fusion Genes and Transgenic Strains" in Methods.
recombinant DNA reagent	*nhr-23* Δ623-646 3'UTR reporter	This report	pHR022	*dpy-7p::tdtomato::nhr-23 3'UTRΔ623-646::SL2::gfp::unc-54 3'UTR* . See section titled "Construction of Fusion Genes and Transgenic Strains" in Methods.
recombinant DNA reagent	*nhr-23* Δ227-249 3'UTR reporter	This report	pHR026	*dpy-7p::tdtomato::nhr-23 3'UTRΔ227-249::SL2::gfp::unc-54 3'UTR* . See section titled "Construction of Fusion Genes and Transgenic Strains" in Methods.
recombinant DNA reagent	*nhr-23* Δ26-42 3'UTR reporter	This report	pHR020	*dpy-7p::tdtomato::nhr-23 3'UTRΔ26-42::SL2::gfp::unc-54 3'UTR* . See section titled "Construction of Fusion Genes and Transgenic Strains" in Methods.
peptide, recombinant protein	CAS9 protein	PNA Bio	CP01	
peptide, recombinant protein	1x HALT Protease and Phosphatase Inhibitor	ThermoFisher Scientific	78443	
peptide, recombinant protein	Proteinase K	ThermoFisher Scientific	25530015	
peptide, recombinant protein	RNase A	ThermoFisher Scientific	12091021	
peptide, recombinant protein	RNAsin Plus RNase inhibitor, 1 U/µL	Promega	N2611	
peptide, recombinant protein	Transcriptor Reverse Transcriptase, 0.5 U/µL	Roche	3531295001	
peptide, recombinant protein	KpnI-HF	New England Biolabs	R3142S	
peptide, recombinant protein	NotI-HF	New England Biolabs	R3189S	
commercial assay or kit	Gibson DNA Assembly Kit	New England Biolabs	E5510S	
commercial assay or kit	TOPO TA Cloning Kit	ThermoFisher Scientific	450641	
commercial assay or kit	Phusion High-Fidelity DNA Polymerase	New England Biolabs	M0530S	
commercial assay or kit	Q5 Site-Directed Mutagenesis Kit	New England Biolabs	E0554S	
commercial assay or kit	TURBO DNase Kit	ThermoFisher Scientific	AM1907	
commercial assay or kit	High-Capacity cDNA Reverse Transcription Kit	ThermoFisher Scientific	4368814	
commercial assay or kit	TaqMan Universal PCR Master Mix, no AmpErase UNG	ThermoFisher Scientific	4364341	
commercial assay or kit	TaqMan assay for *lin-42*	ThermoFisher Scientific	CE02593603_M1	
commercial assay or kit	TaqMan assay for *nhr-23*	ThermoFisher Scientific	CE02405513_G1	
commercial assay or kit	TaqMan assay for *mlt-10*	ThermoFisher Scientific	CE02426995_M1	
commercial assay or kit	TaqMan assay for *ama-1*	ThermoFisher Scientific	CE02462732_G1	
commercial assay or kit	TaqMan assay for primary *let-7*	ThermoFisher Scientific	AJ1RUH0	
commercial assay or kit	TaqMan assay for mature *let-7*	ThermoFisher Scientific	377	
commercial assay or kit	TaqMan assay for U18	ThermoFisher Scientific	1764	
chemical compound	Isopropyl β-D-1-thiogalactopyranoside (IPTG)	Laguna Scientific	6055-5	
chemical compound	TRIzol	ThermoFisher Scientific	15596026	
chemical compound	Chloroform: Isoamyl alcohol, 24:1	OmniPur	3160-450ML	
chemical compound	Acid Phenol: Chloroform, 5:1	ThermoFisher Scientific	AM9720	
chemical compound	Isopropanol, 100%	Sigma-Aldrich	I9516	
chemical compound	GlycoBlue	Sigma-Aldrich	AM9515	
chemical compound	Random primers, 25 ng/µL	Promega	C1181	

Reagent type (species) or resource	Designation	Source or reference	Identifiers	Additional information
chemical compound	dNTPs, 1 mM	New England Biolabs	N0446S	
chemical compound	Novex Tris- Glycine SDS Sample Buffer	ThermoFisher Scientific	LC2676	
chemical compound	Absolute Blue SYBR Green	ThermoFisher Scientific	AB4322B	
chemical compound	Dynabeads M-280 Streptavidin	ThermoFisher Scientific	11205D	
software or algorithm	Photoshop 21.0.1	Adobe	NA	
software or algorithm	Illustrator 24.0.1	Adobe	NA	
software or algorithm	NCBI BLAST	National Insitutes of Health	NA	
software or algorithm	ImageJ v2.0.0-rc-43/1.50e	National Insitutes of Health	NA	
software or algorithm	SnapGene	GSL Biotech LLC	NA	
software or algorithm	RNAhybrid	PMID: 15383676	NA	
software or algorithm	GraphPad Prism v6.0h	GraphPad Software, Inc.	NA	
software or algorithm	Volocity 6.3	Perkin Elmer	NA	
software or algorithm	R version 3.5.2	R Studio	NA	
software or algorithm	RStudio version 1.1.463	R Studio	NA	

Supplemental Table 4. Oligonucleotides used in this study

PCR Primer	Nucleotide Sequence (5' to 3')	Application
HM01	GAAGAACGCCTCACCGAAGGAAGGAAGCATGCGGGATTGGCCAAAGGACCCAAAGGTATGTTTCGAATGATACTAA CATAACATAGAACATTTTCAGGAGGACCCTTGGAGGGTAGAAAAAATGGTGAGCAAGGGCGAGGAGGTCATCAAAG	Construction of the bicistronic reporter for *cis*-regulatory elements in the 3' UTR of *unc-54* (pHR011 and *aaaEx97*)
HM04	ATGGTGAGCAAGGGCGAGG	
HM27	GCGGCCGCTTACTTGTACAGCTCGTCC	
HM28	GGACGAGCTGTACAAGTAAGCGGCCGCGTCCAATTACTCTTCAACATCCC	
HM37	GGTACCATGGTATTGAGCTGTCTCATCC	
HM29	CCGCGCACATTTCCCCGAAAAGTGCCACGGTACCCAAAAAAATTTATCAGAAG	Construction of pHR011 and *aaaEx97*
HM32	GTGGCACTTTTCGGGGAAATG	
HM34	CCTTTTCTGTACATGTCCTGGCCGGCCGGCCAGCAAAAGGCCAGGAACC	
RA31	GATGGCCGGCCTGATCGAAAGTCTCTCCGG	
RA32	CTAGTGATATCCATTTATCTGGAACAAAATGTAAG	
RA101	GGATCCCTGAATCCATATATCATC	Construction of *nhr-23* 3' UTR reporter (pHR017 and *aaaEx129*)
RA102	GGTACCGAGACGTTTTATCACTG	
RA190	GGATCCACACTTTCTTCTTGCTCTTTACC	Construction of *lin-41* 3' UTR reporter (pHR023 and *aaaEx146*)
RA191	GGTACCAATTTCGCAGTGAAATTTGCG	
RA169	TTAAAACTCGTATCATTCCAGTGTCTGC	Deletion of LCS from *nhr-23* 3' UTR reporter (pHR021 and *aaaEx131*)
RA170	TTAATAAAATAAAAATTAGTGCGCCTAGAAATCC	
RA171	TTTGATCCAACCATTTTCTCGTTTATGG	Deletion of nucleotides 623-646 from *nhr-23* 3' UTR reporter (pHR022 and *aaaEx165*)
RA172	GCAGACACTGGAATGATACGAGTTTTAA	
RA184	TTCTTTCTCTCCTTTTCCTGTTTTTAAAG	Deletion of nucleotides 227-249 from *nhr-23* 3' UTR reporter (pHR026 and *aaaEx166*)
RA185	GACTACAATTATTTTTCTATTAATTTTCTG	
RA168	AACTATTGATGATATATGGATTCAGGGATCC	Deletion of nucleotides 26-42 from *nhr-23* 3' UTR reporter (pHR020 and *aaaEx130*)
RA167	CCCTATCCCCGTCCATGAATC	
RA227	CACGGGTACAAAACCACAAATTTCC	Genotype *nhr-23(aaa20) I*
RA228	GCGACCACTACACCATAAACG	
RA272	AGATGAGATGACTAATGAAAGTCCTCG	Genotype *dpy-10 II*
RA273	AGTGAAGAAAGTCCTGCCTTATCC	
RA202	GGTGACAGCCCACTTGGTGCC	Genotype *let-7(n2853) X*
RA203	TCCTTCTAAATTCGTCTAGGCGTCG	
RA277	GGGATAAATGATAAAATGATAACG	Genotype *nDf51 V*
RA278	GGCCGAAAGGCTTCTTACAC	
RA246	GCTCAATTCTTGGAGCCAGC	Genotype *mir-84(n4037) X*
RA247	GATTTTCTGCTCCGACAGATTAACATG	
RA173	TGCCAGACGGCATTCCCTAG	Genotype *let-7(mg279) X*
RA174	AATCAAGTGTGCACTGACCACTC	
RA109	GCAACGGGAAGCTCTGTTACAGG	Genotype *mir-84(tm1304) X*
RA110	GTTCCTCCATTCGACCATAAAGCC	
oHG206	GCTCTTCAAAACTTCCGAATGTCTG	Genotype *nhr-23(xk22) I*
oHG207	AATAACCGGAGGAAACGAGATTCAT	
oHG227	ACTGCGTGACACCCGATTAAA	ChIP-qPCR for *let-7* promoter
oHG228	CAAAATCCAGGTCACCGCAA	
oHG235	TCCATCTCTCTTGGAAACACAT	ChIP-qPCR for *col-19* promoter
oHG236	ACACCTTCAAACCTAACCAGTGT	
oHG294	GCCTGACTCAGACTTCTCCATAGAT	ChIP-qPCR for *mir-84* promoter
oHG295	AGAAGAGGAAAGGAAAAAAACAAGTTA	
oHG298	GCTCGGTGCCGTGTACTTTTATA	ChIP-qPCR for *mir-241* promoter
oHG299	CCAACTTTCCATCTCTGTCGTCT	
oHG300	AAGCGGATCGAGGGAAAAGA	ChIP-qPCR for *mir-48* promoter
oHG301	CCTCTCTAGTTCCTTCTGACTCTCTTG	
CRISPR	**Nucleotide Sequence (5' to 3')**	**Application**
dpy-10 crRNA	GCUACCAUAGGCACCACGAGGUUUUAGAGCUAUGCUGUUUUG	Edit the *dpy-10* locus
RA226	CACTTGAACTTCAATACGGCAAGATGAGAATGACTGGAAACCGTACCGCATGCGGTGCCTATGGTAGCGGAGCTTCACATGGCTTCAGACCAACAGCCTAT	*dpy-10* ssODN
nhr-23 crRNA	GAGUUUUAAAAGGCAAUAAAGUUUUAGAGCUAUGCUGUUUUG	Edit the 3' UTR of *nhr-23*
tracrRNA	AACAGCAUAGCAAGUUAAAAUAAGGCUAGUCCGUUAUCAACUUGAAAAAGUGGCACCGAGUCGGUGCUUUUUUU	Trans-activation of CAS9
RA225	CTGGATTTCTAGGCGCACTAATTTTTATTTTATTAATTAAAACTCGTATCATTCCAGTGTCTGCGCTTTAA	Repair template (ssODN) for excision of the LCS from 3' UTR of *nhr-23*
oHG202 crRNA	AUGAUAUAUGGAUUCAGUCA	Edit the final exon of *nhr-23*
oHG257	TAGGGAAGGAGAGCATGGATAAAACTATTGATGATATATGGATTCAGTCATCCCTTGTCGTCGTCGTCCTTGTAGTCGATATCATGGTCCTTGTAATCTCCGT(GTGATCTTTATAGTCCGATCCCGATCCTCCTGAGCCTCCAGGCCGATCTGCAGTGAATAGCTCTTTGTAGAGGGCAGGAAGCTTTTCAG	Repair template (ssODN) for insertion of the coding sequence for 3xFLAG between the last coding codon and the stop codon of *nhr-23*

Supplemental Table 4. Oligonucleotides used in this study.

The unique identifier for each DNA or RNA molecules appears in the first column. Suppliers of specific oligonucleotides are identified in the Method Details. For those primers used to construct a particular bicistronic reporter for *cis*-regulatory elements in a 3′ UTR of interest, the resulting plasmid and corresponding extrachromosomal array are identified in the "application" column. All seven reporters and respective transgenic strains of *C. elegans* are further described in The Key Resources Table.

REFERENCES

Abbott, A.L., Alvarez-Saavedra, E., Miska, E.A., Lau, N.C., Bartel, D.P., Horvitz, H.R., and Ambros, V. (2005). The let-7 MicroRNA family members mir-48, mir-84, and mir-241 function together to regulate developmental timing in Caenorhabditis elegans. Dev Cell *9*, 403-414.

Aguinaldo, A.M., Turbeville, J.M., Linford, L.S., Rivera, M.C., Garey, J.R., Raff, R.A., and Lake, J.A. (1997). Evidence for a clade of nematodes, arthropods and other moulting animals. Nature *387*, 489-493.

Alvarez-Saavedra, M., Antoun, G., Yanagiya, A., Oliva-Hernandez, R., Cornejo-Palma, D., Perez-Iratxeta, C., Sonenberg, N., and Cheng, H.Y. (2011). miRNA-132 orchestrates chromatin remodeling and translational control of the circadian clock. Hum Mol Genet *20*, 731-751.

Ambros, V., and Horvitz, H.R. (1984). Heterochronic mutants of the nematode Caenorhabditis elegans. Science *226*, 409-416.

Ambros, V., and Ruvkun, G. (2018). Recent Molecular Genetic Explorations of Caenorhabditis elegans MicroRNAs. Genetics *209*, 651-673.

Antebi, A. (2015). Nuclear receptor signal transduction in C. elegans. WormBook, 1-49.

Benazeraf, B., and Pourquie, O. (2013). Formation and segmentation of the vertebrate body axis. Annu Rev Cell Dev Biol *29*, 1-26.

Bethke, A., Fielenbach, N., Wang, Z., Mangelsdorf, D.J., and Antebi, A. (2009). Nuclear hormone receptor regulation of microRNAs controls developmental progression. Science *324*, 95-98.

Bouchard-Cannon, P., Mendoza-Viveros, L., Yuen, A., Kaern, M., and Cheng, H.Y. (2013). The circadian molecular clock regulates adult hippocampal neurogenesis by controlling the timing of cell-cycle entry and exit. Cell Rep *5*, 961-973.

Bracht, J., Hunter, S., Eachus, R., Weeks, P., and Pasquinelli, A.E. (2004). Trans-splicing and polyadenylation of let-7 microRNA primary transcripts. RNA *10*, 1586-1594.

Broughton, J.P., Lovci, M.T., Huang, J.L., Yeo, G.W., and Pasquinelli, A.E. (2016). Pairing beyond the Seed Supports MicroRNA Targeting Specificity. Mol Cell *64*, 320-333.

Celniker, S.E., Dillon, L.A., Gerstein, M.B., Gunsalus, K.C., Henikoff, S., Karpen, G.H., Kellis, M., Lai, E.C., Lieb, J.D., MacAlpine, D.M.*, et al.* (2009). Unlocking the secrets of the genome. Nature *459*, 927-930.

Chen, R., D'Alessandro, M., and Lee, C. (2013). miRNAs are required for generating a time delay critical for the circadian oscillator. Curr Biol *23*, 1959-1968.

Chisholm, A.D., and Hsiao, T.I. (2012). The Caenorhabditis elegans epidermis as a model skin. I: development, patterning, and growth. Wiley Interdiscip Rev Dev Biol *1*, 861-878.

Cook, D.N., Kang, H.S., and Jetten, A.M. (2015). Retinoic Acid-Related Orphan Receptors (RORs): Regulatory Functions in Immunity, Development, Circadian Rhythm, and Metabolism. Nucl Receptor Res *2*.

Du, N.H., Arpat, A.B., De Matos, M., and Gatfield, D. (2014). MicroRNAs shape circadian hepatic gene expression on a transcriptome-wide scale. Elife *3*, e02510.

Ecsedi, M., Rausch, M., and Grosshans, H. (2015). The let-7 microRNA directs vulval development through a single target. Dev Cell *32*, 335-344.

Edelman, T.L., McCulloch, K.A., Barr, A., Frokjaer-Jensen, C., Jorgensen, E.M., and Rougvie, A.E. (2016). Analysis of a lin-42/Period Null Allele Implicates All Three Isoforms in Regulation of Caenorhabditis elegans Molting and Developmental Timing. G3 (Bethesda).

Esperk, T., Tammaru, T., and Nylin, S. (2007). Intraspecific variability in number of larval instars in insects. J Econ Entomol *100*, 627-645.

Frand, A.R., Russel, S., and Ruvkun, G. (2005). Functional genomic analysis of C. elegans molting. PLoS Biol *3*, e312.

Galles, C., Prez, G.M., Penkov, S., Boland, S., Porta, E.O.J., Altabe, S.G., Labadie, G.R., Schmidt, U., Knolker, H.J., Kurzchalia, T.V.*, et al.* (2018). Endocannabinoids in Caenorhabditis elegans are essential for the mobilization of cholesterol from internal reserves. Sci Rep *8*, 6398.

Giguere, V., Tini, M., Flock, G., Ong, E., Evans, R.M., and Otulakowski, G. (1994). Isoform-specific amino-terminal domains dictate DNA-binding properties of ROR alpha, a novel family of orphan hormone nuclear receptors. Genes Dev *8*, 538-553.

Grishok, A., Pasquinelli, A.E., Conte, D., Li, N., Parrish, S., Ha, I., Baillie, D.L., Fire, A., Ruvkun, G., and Mello, C.C. (2001). Genes and mechanisms related to RNA interference regulate expression of the small temporal RNAs that control C. elegans developmental timing. Cell *106*, 23-34.

Gupta, B.P., Hanna-Rose, W., and Sternberg, P.W. (2012). Morphogenesis of the vulva and the vulval-uterine connection. WormBook, 1-20.

Hammell, C.M., Karp, X., and Ambros, V. (2009). A feedback circuit involving let-7-family miRNAs and DAF-12 integrates environmental signals and developmental timing in Caenorhabditis elegans. Proc Natl Acad Sci U S A *106*, 18668-18673.

Hayes, G.D., Frand, A.R., and Ruvkun, G. (2006). The mir-84 and let-7 paralogous microRNA genes of Caenorhabditis elegans direct the cessation of molting via the conserved nuclear hormone receptors NHR-23 and NHR-25. Development *133*, 4631-4641.

Hayes, G.D., and Ruvkun, G. (2006). Misexpression of the Caenorhabditis elegans miRNA let-7 is sufficient to drive developmental programs. Cold Spring Harb Symp Quant Biol *71*, 21-27.

Hendriks, G.J., Gaidatzis, D., Aeschimann, F., and Grosshans, H. (2014). Extensive oscillatory gene expression during C. elegans larval development. Mol Cell *53*, 380-392.

Iwanir, S., Tramm, N., Nagy, S., Wright, C., Ish, D., and Biron, D. (2013). The microarchitecture of C. elegans behavior during lethargus: homeostatic bout dynamics, a typical body posture, and regulation by a central neuron. Sleep *36*, 385-395.

Janich, P., Pascual, G., Merlos-Suarez, A., Batlle, E., Ripperger, J., Albrecht, U., Cheng, H.Y., Obrietan, K., Di Croce, L., and Benitah, S.A. (2011). The circadian molecular clock creates epidermal stem cell heterogeneity. Nature *480*, 209-214.

Jeon, M., Gardner, H.F., Miller, E.A., Deshler, J., and Rougvie, A.E. (1999). Similarity of the C. elegans developmental timing protein LIN-42 to circadian rhythm proteins. Science *286*, 1141-1146.

Johnson, M.H., and Day, M.L. (2000). Egg timers: how is developmental time measured in the early vertebrate embryo? Bioessays *22*, 57-63.

Johnson, S.M., Lin, S.Y., and Slack, F.J. (2003). The time of appearance of the C. elegans let-7 microRNA is transcriptionally controlled utilizing a temporal regulatory element in its promoter. Dev Biol *259*, 364-379.

Kai, Z.S., Finnegan, E.F., Huang, S., and Pasquinelli, A.E. (2013). Multiple cis-elements and trans-acting factors regulate dynamic spatio-temporal transcription of let-7 in Caenorhabditis elegans. Dev Biol *374*, 223-233.

Kallen, J.A., Schlaeppi, J.M., Bitsch, F., Geisse, S., Geiser, M., Delhon, I., and Fournier, B. (2002). X-ray structure of the hRORalpha LBD at 1.63 A: structural and functional data that cholesterol or a cholesterol derivative is the natural ligand of RORalpha. Structure *10*, 1697-1707.

Kamath, R.S., and Ahringer, J. (2003). Genome-wide RNAi screening in Caenorhabditis elegans. Methods *30*, 313-321.

Katz, S.S., Maybrun, C., Maul-Newby, H.M., and Frand, A.R. (2018). Non-canonical apical constriction shapes emergent matrices in C. elegans. bioRxiv preprint.

Kessenbrock, K., Wang, C.Y., and Werb, Z. (2015). Matrix metalloproteinases in stem cell regulation and cancer. Matrix Biol *44-46*, 184-190.

Keyte, A.L., and Smith, K.K. (2014). Heterochrony and developmental timing mechanisms: changing ontogenies in evolution. Semin Cell Dev Biol *34*, 99-107.

Kim, D., Grun, D., and van Oudenaarden, A. (2013). Dampening of expression oscillations by synchronous regulation of a microRNA and its target. Nat Genet *45*, 1337-1344.

Kostrouchova, M., Krause, M., Kostrouch, Z., and Rall, J.E. (1998). CHR3: a Caenorhabditis elegans orphan nuclear hormone receptor required for proper epidermal development and molting. Development *125*, 1617-1626.

Kostrouchova, M., Krause, M., Kostrouch, Z., and Rall, J.E. (2001). Nuclear hormone receptor CHR3 is a critical regulator of all four larval molts of the nematode Caenorhabditis elegans. Proc Natl Acad Sci U S A *98*, 7360-7365.

Kouns, N.A., Nakielna, J., Behensky, F., Krause, M.W., Kostrouch, Z., and Kostrouchova, M. (2011). NHR-23 dependent collagen and hedgehog-related genes required for molting. Biochem Biophys Res Commun *413*, 515-520.

Martin, A.C., and Goldstein, B. (2014). Apical constriction: themes and variations on a cellular mechanism driving morphogenesis. Development *141*, 1987-1998.

Matsu-Ura, T., Dovzhenok, A., Aihara, E., Rood, J., Le, H., Ren, Y., Rosselot, A.E., Zhang, T., Lee, C., Obrietan, K.*, et al.* (2016). Intercellular Coupling of the Cell Cycle and Circadian Clock in Adult Stem Cell Culture. Mol Cell *64*, 900-912.

McCulloch, K.A., and Rougvie, A.E. (2014). Caenorhabditis elegans period homolog lin-42 regulates the timing of heterochronic miRNA expression. Proc Natl Acad Sci U S A *111*, 15450-15455.

Meli, V.S., Osuna, B., Ruvkun, G., and Frand, A.R. (2010). MLT-10 defines a family of DUF644 and proline-rich repeat proteins involved in the molting cycle of Caenorhabditis elegans. Mol Biol Cell *21*, 1648-1661.

Monsalve, G.C. (2013). Unifying mechanisms of developmental timing genetic and molecular analysis of the molting cycle timer of Caenorhabditis elegans. In Biological Chemistry (Los Angeles: University of California, Los Angeles,), pp. 1 online resource (xiv, 96 p).

Monsalve, G.C., Van Buskirk, C., and Frand, A.R. (2011). LIN-42/PERIOD controls cyclical and developmental progression of C. elegans molts. Curr Biol *21*, 2033-2045.

Novak, B., and Tyson, J.J. (2008). Design principles of biochemical oscillators. Nat Rev Mol Cell Biol *9*, 981-991.

Oyama, Y., Bartman, C.M., Gile, J., and Eckle, T. (2017). Circadian MicroRNAs in Cardioprotection. Curr Pharm Des *23*, 3723-3730.

Page, A.P., and Johnstone, I.L. (2007). The cuticle. WormBook, 1-15.

Paix, A., Folkmann, A., Rasoloson, D., and Seydoux, G. (2015). High Efficiency, Homology-Directed Genome Editing in Caenorhabditis elegans Using CRISPR-Cas9 Ribonucleoprotein Complexes. Genetics *201*, 47-54.

Partch, C.L., Green, C.B., and Takahashi, J.S. (2014). Molecular architecture of the mammalian circadian clock. Trends Cell Biol *24*, 90-99.

Patke, A., Murphy, P.J., Onat, O.E., Krieger, A.C., Ozcelik, T., Campbell, S.S., and Young, M.W. (2017). Mutation of the Human Circadian Clock Gene CRY1 in Familial Delayed Sleep Phase Disorder. Cell *169*, 203-215 e213.

Perales, R., King, D.M., Aguirre-Chen, C., and Hammell, C.M. (2014). LIN-42, the Caenorhabditis elegans PERIOD homolog, negatively regulates microRNA transcription. PLoS Genet *10*, e1004486.

Pourquie, O. (2011). Vertebrate segmentation: from cyclic gene networks to scoliosis. Cell *145*, 650-663.

Puram, R.V., Kowalczyk, M.S., de Boer, C.G., Schneider, R.K., Miller, P.G., McConkey, M., Tothova, Z., Tejero, H., Heckl, D., Jaras, M.*, et al.* (2016). Core Circadian Clock Genes Regulate Leukemia Stem Cells in AML. Cell *165*, 303-316.

Raizen, D.M., Zimmerman, J.E., Maycock, M.H., Ta, U.D., You, Y.J., Sundaram, M.V., and Pack, A.I. (2008). Lethargus is a Caenorhabditis elegans sleep-like state. Nature *451*, 569-572.

Rehmsmeier, M., Steffen, P., Hochsmann, M., and Giegerich, R. (2004). Fast and effective prediction of microRNA/target duplexes. RNA *10*, 1507-1517.

Reinhart, B.J., Slack, F.J., Basson, M., Pasquinelli, A.E., Bettinger, J.C., Rougvie, A.E., Horvitz, H.R., and Ruvkun, G. (2000). The 21-nucleotide let-7 RNA regulates developmental timing in Caenorhabditis elegans. Nature *403*, 901-906.

Roenneberg, T., and Merrow, M. (2016). The Circadian Clock and Human Health. Curr Biol *26*, R432-443.

Rougvie, A.E. (2001). Control of developmental timing in animals. Nat Rev Genet *2*, 690-701.

Santori, F.R., Huang, P., van de Pavert, S.A., Douglass, E.F., Jr., Leaver, D.J., Haubrich, B.A., Keber, R., Lorbek, G., Konijn, T., Rosales, B.N.*, et al.* (2015). Identification of natural RORgamma ligands that regulate the development of lymphoid cells. Cell Metab *21*, 286-298.

Sarrazin, A.F., Peel, A.D., and Averof, M. (2012). A segmentation clock with two-segment periodicity in insects. Science *336*, 338-341.

Shaner, N.C., Steinbach, P.A., and Tsien, R.Y. (2005). A guide to choosing fluorescent proteins. Nat Methods *2*, 905-909.

Singh, K., Chao, M.Y., Somers, G.A., Komatsu, H., Corkins, M.E., Larkins-Ford, J., Tucey, T., Dionne, H.M., Walsh, M.B., Beaumont, E.K.*, et al.* (2011). C. elegans Notch signaling regulates adult chemosensory response and larval molting quiescence. Curr Biol *21*, 825-834.

Singh, R.N., and Sulston, J.E. (1978). Some observations on moulting in Caenorhabditis elegans. Nematologica *24*, 63-71.

Sparrow, D.B., Chapman, G., Turnpenny, P.D., and Dunwoodie, S.L. (2007). Disruption of the somitic molecular clock causes abnormal vertebral segmentation. Birth Defects Res C Embryo Today *81*, 93-110.

Stiernagle, T. (2006). Maintenance of C. elegans. WormBook, 1-11.

Takahashi, J.S. (2016). Molecular Architecture of the Circadian Clock in Mammals. In A Time for Metabolism and Hormones, P. Sassone-Corsi, and Y. Christen, eds. (Cham (CH)), pp. 13-24.

Takahashi, J.S. (2017). Transcriptional architecture of the mammalian circadian clock. Nat Rev Genet *18*, 164-179.

Takeda, Y., Jothi, R., Birault, V., and Jetten, A.M. (2012). RORgamma directly regulates the circadian expression of clock genes and downstream targets in vivo. Nucleic Acids Res *40*, 8519-8535.

Takeda, Y., Kang, H.S., Lih, F.B., Jiang, H., Blaner, W.S., and Jetten, A.M. (2014). Retinoid acid-related orphan receptor gamma, RORgamma, participates in diurnal transcriptional regulation of lipid metabolic genes. Nucleic Acids Res *42*, 10448-10459.

Trojanowski, N.F., and Raizen, D.M. (2016). Call it Worm Sleep. Trends Neurosci *39*, 54-62.

Uriu, K. (2016). Genetic oscillators in development. Dev Growth Differ *58*, 16-30.

Van Buskirk, C., and Sternberg, P.W. (2007). Epidermal growth factor signaling induces behavioral quiescence in Caenorhabditis elegans. Nat Neurosci *10*, 1300-1307.

Van Wynsberghe, P.M., Finnegan, E.F., Stark, T., Angelus, E.P., Homan, K.E., Yeo, G.W., and Pasquinelli, A.E. (2014). The Period protein homolog LIN-42 negatively regulates microRNA biogenesis in C. elegans. Dev Biol *390*, 126-135.

Van Wynsberghe, P.M., Kai, Z.S., Massirer, K.B., Burton, V.H., Yeo, G.W., and Pasquinelli, A.E. (2011). LIN-28 co-transcriptionally binds primary let-7 to regulate miRNA maturation in Caenorhabditis elegans. Nat Struct Mol Biol *18*, 302-308.

Wang, D.J., Legesse-Miller, A., Johnson, E.L., and Coller, H.A. (2012). Regulation of the let-7a-3 promoter by NF-kappaB. PLoS One *7*, e31240.

Woltering, J.M. (2012). From lizard to snake; behind the evolution of an extreme body plan. Curr Genomics *13*, 289-299.

You, Y.J., Kim, J., Raizen, D.M., and Avery, L. (2008). Insulin, cGMP, and TGF-beta signals regulate food intake and quiescence in C. elegans: a model for satiety. Cell Metab *7*, 249-257.

Zhang, Y., Papazyan, R., Damle, M., Fang, B., Jager, J., Feng, D., Peed, L.C., Guan, D., Sun, Z., and Lazar, M.A. (2017). The hepatic circadian clock fine-tunes the lipogenic response to feeding through RORalpha/gamma. Genes Dev.

Zhao, C., Sun, G., Ye, P., Li, S., and Shi, Y. (2013). MicroRNA let-7d regulates the TLX/microRNA-9 cascade to control neural cell fate and neurogenesis. Sci Rep *3*, 1329.

CHAPTER III

Molecules and Pathways that Impinge on the Balance between NHR-23/ROR and *let-7* microRNAs to Regulate Number of Molts

ABSTRACT

C. elegans molt four times before transitioning into adulthood. Forced expression of NHR-23 in otherwise wild-type animals can trigger extra molts. Genetic inactivation of *let-7* and its paralogs is also associated with supernumerary molts, in part because NHR-23 is re-expressed in adult animals. Thus, the expression levels of both *nhr-23* and *let-7s* are important factors that determine entry into a supernumerary molt. I sought to identify additional factors that promote extra molts by acting upstream of NHR-23 and *let-7s*. Using longitudinal studies of behavior and genetic techniques, I showed that exogenous supplies of cholesterol were necessary for the extra molts observed in *nhr-23(gf)* and *let-7(lf) mir-84(lf)* mutants. I also found that specific inverse agonists of RORα prevented the supernumerary molts of *let-7(lf) mir-84(lf)* mutants. By using bio-informatics, I found that key amino acid residues in RORα that mediate binding with cholesterol and oxysterols appeared conserved to NHR-23. These data implied that an unidentified, steroid-based molecule might bind to NHR-23 and modulate activity. Towards identifying genes that synthesize or regulate bioavailability of the ligand, I conducted a reverse genetic screen for suppressors of the supernumerary molts of *let-7(lf) mir-84(lf)* mutants, using RNA-interference (RNAi) to inactivate the cytochrome P450s, other sterol-modifying enzymes and a few predicted peptide hormones. I identified twenty-seven knockdowns that suppressed the supernumerary molts of *let-7(lf) mir-84(lf)* mutants. Further characterization of the hits from the RNAi screen could lead to identification of neuroendocrine pathways that control molting in *C. elegans*.

INTRODUCTION

The research described in Chapter II showed that the relative and interdependent levels of NHR-23 and *let-7s* regulate the number of molts in *C. elegans* (Chapter II). In my model, NHR-23 works as a pro-molt factor, whereas the *let-7s* work as anti-molt factors. Extra molts are triggered in *wgIs43[nhr-23^{++}]*, *nhr-23(aaa20ΔLCS)* and *let-7(mg279) mir-84 (tm1304)* adults, as previously described (Hayes et al., 2006). Both *nhr-23(aaa20ΔLCS)* and *let-7(mg279) mir-84 (tm1304)* adults have abnormally high expression of *nhr-23*. Moreover, knockdown of *nhr-23* suppresses the supernumerary molts of *let-7(mg279) mir-84 (tm1304)* mutants (Hayes et al., 2006). The *let-7s* restrain the levels of NHR-23 in adult animals by dampening expression of *nhr-23* over the course of larval development. However, the extent to which additional factors – the availability of an as-yet-unidentified hormone for NHR-23 or transcription factors that promote expression of *let-7s* – impinge on the balance in activity between NHR-23 versus *let-7s* to control the number of molts is not well understood (Figure 1A).

C. elegans require dietary supplementation of cholesterol because animals cannot synthesize the molecule *de novo* (Hieb and Rothstein, 1968). At least one enzyme involved in the cholesterol biosynthetic pathway – squalene synthase – is undetectable in the worm genome by bioinformatic analysis (Kurzchalia and Ward, 2003). In the absence of an exogenous source, the maternal supply of cholesterol is sufficient to support growth and development for one generation but not further (Yochem et al., 1999).

An unknown ligand is thought to bind to NHR-23 and alter the ability to transactivate gene expression. This theory is due to gene identity of NHR-23, and the observation that *C. elegans* deprived of external supplies of cholesterol for two consecutive generations undergo molting defects (Yochem et al., 1999). Likewise, genetic inactivation of LRP-1, which is similar to the

mammalian low density lipoprotein receptor-related protein Megalin, is also associated with molting defects (Yochem et al., 1999). Antibody staining showed that LRP-1 is detectable in the hypodermis, where NHR-23 is also expressed. Thus, perhaps the LRP-1 protein acts in the hypodermis to endocytose ligands for NHR-23 (Yochem et al., 1999).

Mammalian RORs bind cholesterol, cholesterol-derivatives and small molecules. The ligand-binding domain (LBD) of *H. sapiens* RORα was previously isolated in complex with cholesterol when overexpressed in SF-9 insect cells, suggesting that cholesterol might be a native ligand for RORα (Kallen et al., 2002). Mutation of amino acid residues of RORα that mediate interactions with cholesterol interfere with the ability of the nuclear receptor to transactivate reporter gene expression. Likewise, substitution of residues within the LBD that interact with each other to stabilize RORα in the ligand-bound conformation also reduce transactivation. Furthermore, RORα can also bind to cholesterol sulfate, although the extent to which this molecule acts as an endogenous ligand remains unclear (Kallen et al., 2004). All trans-retinoic acid is a potent antagonist of RORβ but has not been shown to be an endogenous ligand (Stehlin-Gaon et al., 2003). Intermediates of the biosynthetic pathway for cholesterol are natural agonists of RORγ (Santori et al., 2015). Knockdown of enzymes such as SC4MOL (Sterol-C4-methyl oxidase-like) and NSDHL (NAD(P) dependent steroid dehydrogenase-like), which both catalyze reactions in the pathway, reduces the expression of a reporter gene that is normally transactivated by RORγ in control cells (Santori et al., 2015).

Hormones regulate development, molting, metamorphosis and puberty in many model organisms, and in humans. In *C. elegans*, the bile acid-like hormones Δ^4- and Δ^7- dafachronic acid together with the nuclear receptor DAF-12 control the choice between continuous versus discontinuous development (Lee and Schroeder, 2012). In insects such as *D. melanogaster*, the

steroid hormone ecdysone and the Ecdysone Receptor together promote molting and associated behaviors (Di Cara and King-Jones, 2013). Ecdysone also promotes molting in crustaceans like the blue crab *Callinectes sapidus*, and synthesis of ecdysone is negatively regulated by a neuropeptide called molt-inhibiting hormone (MIH) (Hyde et al., 2019; Lee et al., 1998). In *Xenopus*, thyroid hormone and the thyroid hormone receptor promote metamorphosis (Shi, 2013). In humans, steroid hormones such as estrogen, progesterone and testosterone are necessary for development of the reproductive system (DeMayo et al., 2002). However, analogous molecules that control either molting in *C. elegans* larvae or cessation of the cycle in adulthood are yet to be identified.

Pathways for biosynthesis and degradation of steroid hormones usually consist of multiple steps, which are catalyzed by enzymes such as Rieske Oxygenases, cytochrome P450s, 3β-hydroxysteroid dehydrogenase (3β-HSD) and 17β-HSD (Cui et al., 2013; Yoshiyama-Yanagawa et al., 2011). The Rieske oxygenases DAF-36 in *C. elegans* and Neverland in *D. melanogaster* convert cholesterol to 7-dehydrocholesterol in the respective organisms (Yoshiyama-Yanagawa et al., 2011). The formation of 7-dehydrocholesterol is the first step in the pathways for synthesis of dafachronic acid in *C. elegans* and ecdysone in *D. melanogaster* (Markov et al., 2009). Cytochrome P450 enzymes are oxygenases that use heme as a cofactor. One example is the cytochrome P450 Aromatase, which converts testosterone into 17β-estradiol in humans (Cui et al., 2013). The enzyme 3β-HSD is an oxidoreductase that catalyzes reactions such as the conversion of pregnenolone to progesterone. However, the anticipated enzymes that act in biosynthetic pathways for molting-related hormones in *C. elegans* are not known.

Here, I show evidence that either cholesterol or a derivative of cholesterol is necessary for the initiation of supernumerary molts in adult animals, likely by promoting the activity of NHR-23.

I find that several key residues that mediate binding sterol-based ligands are conserved between *H. sapiens* RORα and NHR-23. By utilizing a reverse genetic approach, I identify genes that encode P450 enyzmes, 3β-HSDs, as well as putative neuropeptides whose activity enables supernumerary molts of *let-7 mir-84* mutants. The enzymes likely act in pathways that synthesize the ligand for NHR-23. I also uncover a novel transcription factor that prevents molts in *let-7 mir-84* mutants, possibly by promoting expression of the *let-7s*. Going further, analysis of the genes that I have uncovered in my screens may lead to identification of steroid hormones that promote molting in *C. elegans*.

RESULTS

Molecules that enable supernumerary molts in *nhr-23(gf)* and *let-7(lf) mir-84(lf)* mutants

I hypothesized that the activity of NHR-23 is dependent upon a ligand, which is either cholesterol itself or derived from cholesterol (Figure 1A). As an initial test of this hypothesis, I asked whether supernumerary molts triggered by high-copy *nhr-23* depended upon an exogenous supply of cholesterol (Figure 1B). To test this hypothesis, I scored the penetrance of quiescence among synchronized populations of *wgIs43[nhr-23^{++}]* adults grown in the absence or presence of exogenous cholesterol. In parallel, I also tracked the behavior of synchronized populations of wild-type adults grown in standard culture conditions. Repeated instances of adult quiescence were not detectable among populations of *wgIs43[nhr-23^{++}]* adults cultured on media lacking exogenous cholesterol, in contrast to standard culture conditions. Furthermore, comparable proportions of lethargic adults were observed among both *wgIs43[nhr-23^{++}]* animals cultured on media lacking exogenous cholesterol and wild-type animals on standard media at all but three time-points. These data imply that cholesterol regulates the ability of NHR-23 to promote extra molts.

To further investigate the mechanism by which cholesterol enables extra molts in *C. elegans*, I asked whether the supernumerary molts observed among *let-7(mg279) mir-84(tm1304)* mutants were also dependent upon exogenous cholesterol (Figure 1C). I scored the penetrance of molting – defined as quiescence, bagging or a visible Mlt phenotype – among synchronized populations of *let-7(mg279) mir-84(tm1304)* mutants that were cultured for 72 h on media that either lacked or contained cholesterol. Supernumerary molts were detected in 2 ± 2% (mean ± s.d.) of the animals cultivated without cholesterol, as compared with 98 ± 2% of the control animals. Going further, I asked whether inverse agonists of ROR likewise suppress the supernumerary

molts of *let-7(mg279) mir-84(tm1304)* mutants. SR1001 and SR2211 reduced the penetrance of the supernumerary molt phenotype detected in the mutants to 48% and 15%, respectively, as compared with 71% detected among vehicle-only control animals. Notably, all three culture conditions had regular amounts of cholesterol. Perhaps then both inverse agonists could outcompete the native ligand for binding with NHR-23.

Taken together, these findings show that cholesterol, together with the gene dosage of *nhr-23* and *let-7s* controls the total number of molts.

Key amino acids that compose the ligand-binding pocket of mammalian ROR are conserved in *C. elegans* NHR-23

To further examine whether cholesterol or a cholesterol-derivative is a ligand for NHR-23, I aligned the amino acid sequences of the ligand-binding domains (LBD) of NHR-23 and mammalian RORα (Figure 2).

The residues Q328 and Y329 in NHR-23 aligned with two residues in RORα that form hydrogen-bonds with cholesterol and cholesterol-sulfate—Q289 and Y290 (Figure 2). The residues W387 and L394 in NHR-23 aligned with two residues in RORα that form van der Waals contacts with cholesterol and derivatives, W320 and I327. In NHR-23, Y579 and H557 aligned perfectly with counterparts in RORα that likely stabilize the conformation of the LBD when bound to an agonist. Additionally, K406 and E581 in NHR-23 were perfectly conserved with residues in RORα that mediate interactions with coactivators.

Thus, my sequence analysis shows that cholesterol and its derivatives could be native ligands for NHR-23. Additionally, I identified specific residues that could mediate the interaction between the ligand(s) and NHR-23. Going further, substitution of these residues to generate mutant

NHR-23 proteins that mimic conformations of either constitutively ligand-bound or constitutively ligand-free receptors would help discern different the roles of NHR-23 in regulation of the molting cycle.

RNAi screen reveals genes that potentiate supernumerary molts in *let-7 mir-84* mutants

Thus far, my findings strongly suggest that a steroid-based ligand may bind to and control the ability of NHR-23 to promote extra molts. The anticipated pathways for synthesis and degradation of the ligand have not been identified. To address this question, I performed an RNAi screen for suppression of the supernumerary molts of *let-7(mg279) mir-84(tm1304)* mutants and focused on the P450 genes as targets. I chose the *let-7(mg279) mir-84(tm1304)* mutants because knockdown of *nhr-23* almost completely suppresses the supernumerary molt, implying that derepression of NHR-23 drives the additional molt in this background (Hayes et al., 2006). Briefly, I fed synchronized hatchlings with 91 distinct clones of bacteria that express dsRNAs complementary to 69 of the 81 known P450s in *C. elegans*, as well as homologs of 22 additional genes involved in synthesis of dafachronic acid in *C. elegans*, ecdysone in insects, steroid hormones in mammals and thyroid hormone in frogs (Figure 3A). I also used RNA-interference to target one homolog of a gene that encodes MIH in blue crabs. I then scored the penetrance of molting among adults 72 h after plating, as described earlier.

The chart in Figure 3B shows 27 gene-specific knockdowns that significantly and reproducibly suppressed detection of the supernumerary molt phenotype to 3 ± 1% – 64 ± 1% (mean ± s.d.), on average, in *let-7(mg279) mir-84(tm1304)* mutants (Table 1). In contrast, 81 ± 1% of the mock-treated adults were detected in a molt. The top hit, *daf-36*, suppressed the supernumerary molt phenotype of the mutants to the same extent as the positive control *nhr-23*. The gene *daf-36*

encodes an enzyme that converts cholesterol to 7-dehydrocholesterol, which is a precursor for synthesis of both dafachronic acid in *C. elegans* and ecdysone in *D. melanogaster* (Yoshiyama-Yanagawa et al., 2011) (Table 2). Thus, 7-dehydrocholesterol may either be a native ligand for NHR-23 or be at the top of the pathway for synthesis of the ligand.

The second topmost hit, *cyp-29A2* was reported to cycle in expression throughout larval development, and expression was detectable in tissues such as the intestine, unidentified neurons in the head, and the hypodermis—one site of expression of NHR-23 expression ((Hendriks et al., 2014; Kim et al., 2013). The predicted homolog of *cyp-29A2* in humans oxidizes molecules that are precursors for fatty acids; perhaps *cyp-29A2* in *C. elegans* oxidizes the sterol backbone in cholesterol, similar to initial steps in the pathway for synthesis of dafachronic acid.

Knockdown of the gene F13D11.4 in *let-7(mg279) mir-84(tm1304)* mutants reduced the penetrance of extra molts to 53 ± 11 %. F13D11.4 undergoes cyclical expression (Hendriks et al., 2014; Kim et al., 2013) and sequence alignments using BLAST indicated that F13D11.4 was similar to *H. sapiens* NSDHL. NSDHL encodes an enzyme that catalyzes one step in the pathway for cholesterol synthesis (Nes, 2011). As stated previously, intermediates of the cholesterol biosynthetic pathway promote activity of RORγ, and knockdown of NSDHL reduces activity of RORγ (Santori et al., 2015). Additionally, BLASTP analysis showed that F13D11.4 was also similar in sequence to *H. sapiens* 3β-HSD—an enzyme that catalyzes reactions such as conversion of pregnenolone to progesterone (Cui et al., 2013). Thus, F13D11.4 might be an important candidate gene for further analysis.

BLASTP searches indicated that *cyp-35A1*, *cyp-33C11*, *cyp-34A2*, *daf-9*, *cyp-33C8*, *cyp-34A8*, *cyp-35A4*, *cyp-33B1* and *cyp-34A9* were similar in sequence to the gene phantom in *D. melanogaster*, which is part of the enzymatic pathway for synthesis of ecdysone (data not shown).

The same genes were also similar to the gene *cyp18a1* from *D. melanogaster*, which modifies ecdysone (Table 2). Interestingly, five of the ten potential homologs of phantom were previously found to oscillate in expression throughout larval development (Hendriks et al., 2014; Kim et al., 2013). Going further, prioritization of analysis of the ten genes may lead to identification of the elusive ligand for NHR-23.

Knockdown of the gene T10G3.1 also significantly suppressed the supernumerary molt phenotype of *let-7(mg279) mir-84(tm1304)* mutants—the detected penetrance of extra molts was 45 ± 16%. A BLASTP search showed that T10G3.1 was 24% identical to the molt-inhibiting hormone of blue crab. In crustaceans, MIH is a neuropeptide that normally inhibits molts by inhibiting synthesis of ecdysone; ecdysone titers rise when the levels of MIH are low (Lee et al., 1998). In *C. elegans*, however, the T10G3.1 was necessary for supernumerary molts of *let-7 mir-84* mutants. Thus, the gene may encode a neuropeptide that normally promotes synthesis of the ligand for NHR-23, similar to the function of the neuropeptide PTTH in insects (Di Cara and King-Jones, 2013). Alternatively, T10G3.1 may potentiate the extra molts of *let-7(mg279) mir-84(tm1304)* mutants by parallel pathways.

The sites of expression of only 12 of the hits are described in the literature (Wormbase WS274). Nine of these twelve genes were previously detected in the nervous system and five in the intestine, suggesting that both tissues play an important role in endocrine regulation of the molting cycle.

I also found that RNAi of 4 genes: *homt-1*, *npp-24*, *ref-1* and *daf-7* modestly but significantly increased the penetrance of the supernumerary molt phenotype of *let-7 mir-84* mutants to 90 ± 1% – 98 ± 1% (Figure 3C). The gene *ref-1* encodes a transcription factor containing two bHLH domains (Alper and Kenyon, 2001). Loss-of-function mutations in *ref-1* are associated with gaps

in the alae. Alae are also missing or gapped in retarded heterochronic mutants such as *let-7(n2853)*, wherein the epidermis fails to terminally differentiate at the L4-to-A transition (Reinhart et al., 2000). Thus, it is possible that knockdown of *ref-1* enhances the supernumerary molt phenotype of *let-7 mir-84* mutants because *ref-1* normally promotes the expression of *let-7s*. The gene *daf-7* encodes a homolog of TGF-β (Ren et al., 1996); *homt-1* encodes an enzyme in the pathway for synthesis of melatonin in *C. elegans* (Hobert, 2013) and *npp-24* is predicted to encode a nucleoporin (WS274). These genes might act in signaling pathways that normally enhance the activity of *let-7s*. Further characterization of how these genes regulate the activity of *let-7* might lead to the identification of novel transcriptional and post-transcriptional regulators of *let-7* expression. Alternatively, *homt-1*, *npp-24*, *ref-1* and *daf-7* may constrain the number of molts by inhibiting the activity of NHR-23, or by unknown parallel pathways. For example, the genes might normally drive maturation of the endocrine tissues at the L4-to-A transition, such as the nervous system, that synthesize and secrete the hormone for NHR-23.

Forward genetic screen for additional pathways that control the total number of molts

To identify additional genes that control the number of molts, either through regulating NHR-23, *let-7s*, or via a parallel pathway, I mapped and identified mutations from a forward genetic screen for adult animals that molt. Briefly, a transgenic strain containing the *mlt-10p::gfp-pest* fusion gene, which is a marker for molting larvae, was exposed to EMS (Russel et al., 2011). Among the descendants, animals that reanimate the reporter while gravid were cloned and propagated, resulting in 90 mutant strains. In fifteen of these strains, the proportion of adults that underwent molts was at least 58%, comparable to the penetrance of supernumerary molts among asynchronous populations of mutants such as *pqn-47(mg412)* and *let-7(mg279) mir-84(tm1304)*.

After one round of outcrossing, I then crossed seven strains to *C. elegans* CB4856 and mapped and identified missense and nonsense mutations using one-step whole genome sequencing and SNP mapping (Doitsidou et al., 2010).

Table 3 lists the resulting candidate genes. Two of the seven strains had mutations – one missense and one nonsense – in the gene *alg-1*, which encodes a *C. elegans* Argonaute protein that associates with the microRNA-induced silencing complex (RISC) to catalyze RNA degradation and silence gene expression (Grishok et al., 2001). One strain had a nonsense mutation in *ain-1*, which encodes a GW182 protein that operates within the miRISC to promote target silencing (Ding et al., 2005; Ding and Grosshans, 2009). Another strain had a nonsense mutation in *nhl-2*, which encodes a protein that enhances the repressive activity of the miRISC (Hammell et al., 2009; Karp and Ambros, 2012). Thus, these four strains likely undergo additional molts because *let-7s* are unable to effectively dampen the expression of *nhr-23*. Going forward, complementation and rescue experiments might verify that the observed supernumerary molt phenotype was caused by mutations in each of the candidate genes.

DISCUSSION

Based on my findings, I propose that two major factors – bioavailability of cholesterol and the abundance of NHR-23 – together regulate entry into a molt in *C. elegans*. Both *nhr-23(gf)* single and *let-7(lf) mir-84(lf)* double mutants undergo extra molts in a manner dependent on the exogenous supply of cholesterol. Furthermore, the observation that inverse agonists of ROR can prevent extra molts of *let-7 mir-84* mutants strongly implies that a ligand is necessary for NHR-23 to activate gene expression cascades that culminate in execution of the molt.

I hypothesize that cholesterol is modified by enzymes such as *daf-36* and F13D11.4 within foraging worms to produce a pro-molt hormone, similar to the production of ecdysone in insects. Going forward, mass spectrometric analysis of extracts from worm strains that overexpress the candidate genes from my RNAi screen may lead to identification of the elusive ligand(s) for NHR-23. The candidate molecules could be tested one at a time for ability to restore the supernumerary molts of *let-7(mg279) mir-84 (tm1304)* animals that are cultivated on media lacking cholesterol. Molecules could also be tested for ability to promote the activity of NHR-23 by using transactivation reporter assays in mammalian cell lines.

I also anticipate that levels of the hormone(s) that binds NHR-23 fluctuate throughout larval development, similar to the 24-h rhythm in abundance of ecdysone in insects (Di Cara and King-Jones, 2013). Thus, as an alternative approach to identifying the hormone, I would collect samples of synchronized populations of *let-7(mg279) mir-84 (tm1304)* adults, either cultivated on media lacking or containing cholesterol, at 2 – 3 h intervals from young adulthood until the time of the supernumerary molt. I would then use mass-spectrometry to compare the extracts and identify molecules that are enriched specifically among animals grown in media lacking cholesterol. The candidate molecules would be tested using the approaches described above—

ability to restore supernumerary molts to *let-7(mg279) mir-84(tm1304)* mutants grown without dietary cholesterol supplementation and the ability to promote activity of NHR-23.

I found that knockdown of twenty-three P450s, one Rieske oxygenase and one 3 β-HSD decreased the penetrance of supernumerary molts in *let-7(mg279) mir-84(tm1304)* mutants. The observation that knockdown of the gene *daf-36*, which encodes a Rieske oxygenase, almost completely suppressed the supernumerary molts suggests that it is likely at the top of the pathway that produces molting-related hormone(s). It is possible that certain P450s act in parallel, independent pathways to produce multiple hormones that regulate the activity of NHR-23, similar to the model that has been proposed for production of dafachronic acid (Rottiers et al., 2006). Alternatively, the possibility exists that the triggers used for RNAi were complementary to a domain that is present in multiple P450s. Analysis of the phenotypes of single mutations in candidate P450s uncovered from this screen would reveal false positive hits. Furthermore, characterization of the phenotypes of double mutants, such as *daf-9(-) cyp-34A9(-)*, and comparison with each single mutant would organize and rank genes in one or more pathways.

By using a forward genetics approach, I uncovered several genes that are necessary to prevent molting in adult animals. As described, I uncovered some novel alleles of *alg-1* and *ain-1*, which encode components of the miRISC, as well *nhl-2*, which is a positive modulator of the activity of the miRISC. Further analysis of the mutations uncovered from this screen would lead to identification of genes that control cessation of the molts either upstream of NHR-23 and *let-7s*, or in parallel pathways.

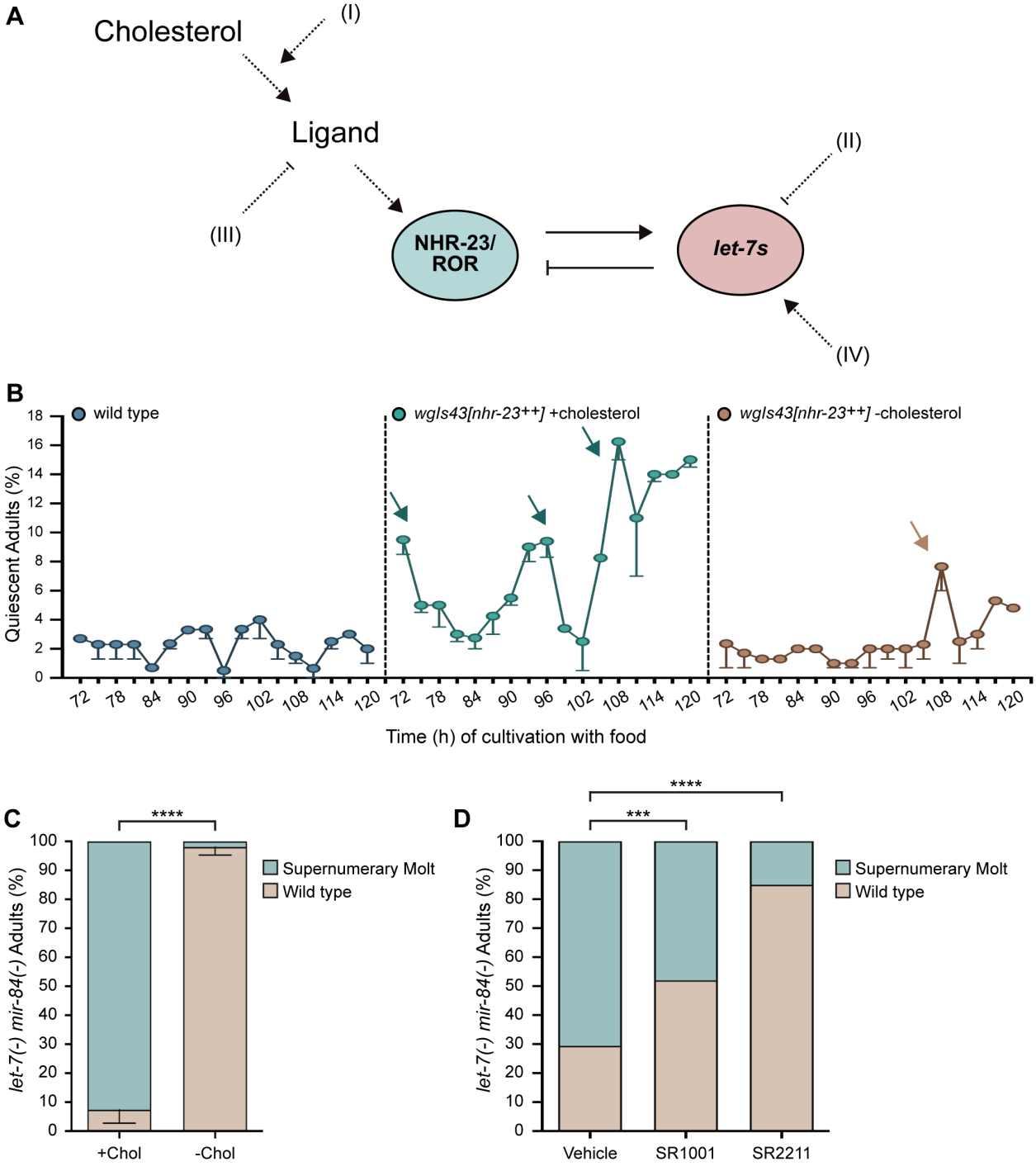
A
Cholesterol
(I)
Ligand
(II)
(III)
NHR-23/
ROR
let-7s
(IV)
B
wild type
wgIs43[nhr-23++] +cholesterol
wgIs43[nhr-23++] -cholesterol
Quiescent Adults (%)
Time (h) of cultivation with food
C
****
let-7(-) mir-84(-) Adults (%)
Supernumerary Molt
Wild type
+Chol
-Chol
D
****
***
let-7(-) mir-84(-) Adults (%)
Supernumerary Molt
Wild type
Vehicle
SR1001
SR2211

Figure 1. Factors that Regulate the Number of Molts in *C. elegans*. **A)** Model of the negative feedback loop described in Chapter II of this thesis. Factors that may function upstream to regulate the balance in activity between NHR-23 and *let-7s* are also depicted. Such factors might synthesize (I) or degrade (III) an as-yet-unidentified ligand for NHR-23, or repress (II) or promote (IV) activity of *let-7s*. **B)** Charts depict the percentage of adult quiescence detected among populations of wild-type adults, and *wgIs43[nhr-23^{++}]* adults that were cultivated on media either containing a regular concentration cholesterol, or the equivalent amount of ethanol only. Time post-release from starvation-induced L1-diapause is depicted on the x-axis in hours. The datasets for both wild-type and *wgIs43[nhr-23^{++}]* adults cultivated in standard culture conditions are exact replicates of those depicted in Chapter II, Figure 6A. Arrows point to time-points at which a significant enrichment of lethargic animals were detected relative to wild type, based on a chi-square test ($p<0.0001$). n = 150 – 200 worms per time-point. **C)** Quantitation of supernumerary molts among *let-7(mg279) mir-84(tm1304)* adults, cultivated with or without exogenous cholesterol. Error bars represent the mean minus s.d. from two independent trials, with a cumulative sample size of 200 worms from both trials. ****$p<0.0001$, chi-square test. **D)** Similar to C, except that either SR1001, SR2211 or DMSO were incorporated in the culture media. Graph depicts results from a single trial, n = 20 – 25 animals per condition. ****$p<0.0001$, ***$p<0.001$, chi-square test.

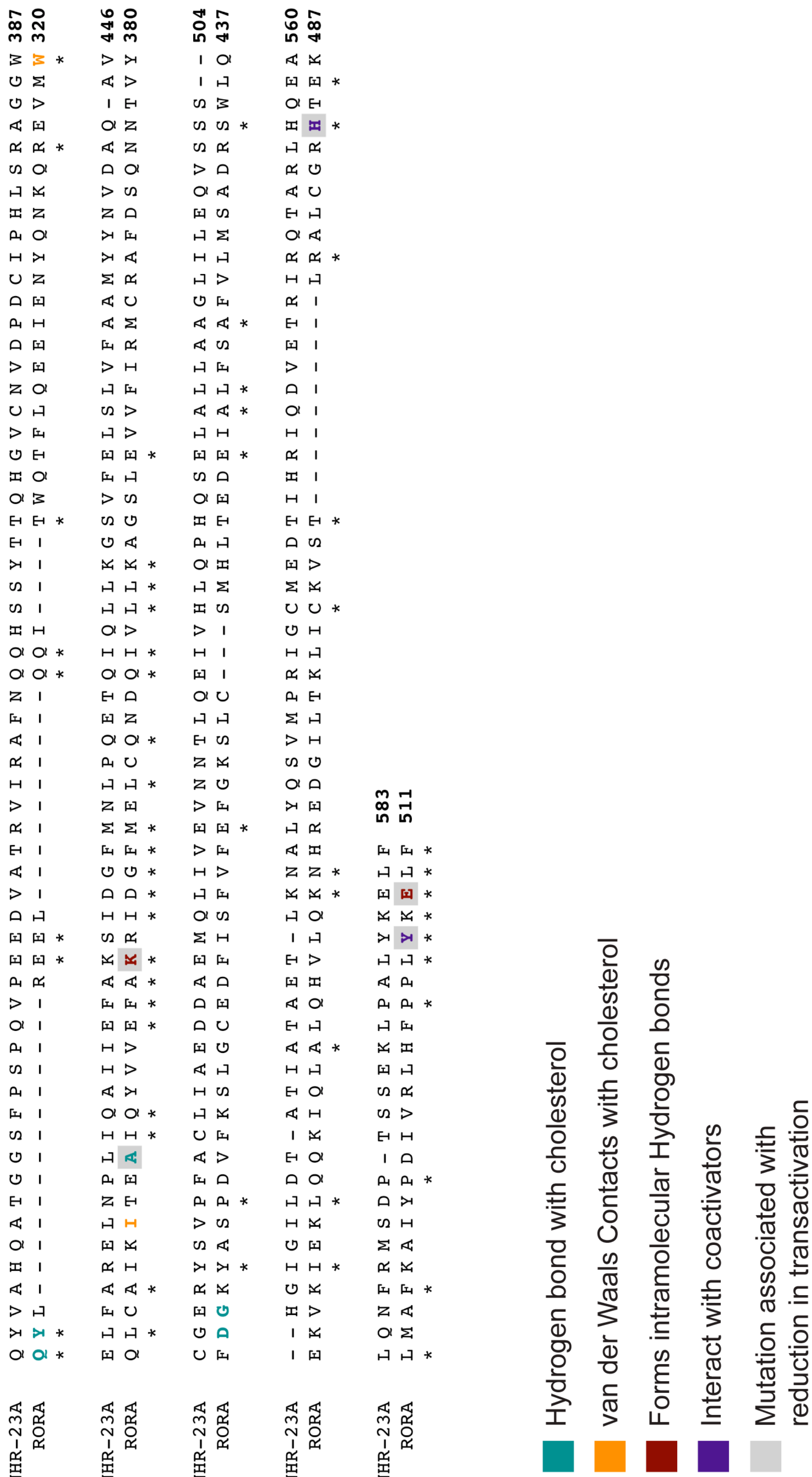
Hydrogen bond with cholesterol
van der Waals Contacts with cholesterol
Forms intramolecular Hydrogen bonds
Interact with coactivators
Mutation associated with reduction in transactivation

Figure 2. Conservation of essential residues that interact with cholesterol, cholesterol sulfate and coactivators, and stabilize the ligand-bound conformation of RORα. Alignment of sequence of the LBD of NHR-23 Isoform A with that of RORα Isoform 1. Residues in RORα that form hydrogen bonds with a ligand are colored in teal; those that form van der Waals contacts colored in orange; those that form intramolecular hydrogen bonds to stabilize RORα in the ligand-bound conformation are colored red; and those that interact with coactivator molecules are colored purple (Kallen et al., 2004; Kallen et al., 2002). Additionally, grey boxes indicate residues, which when mutated, reduce the activity of RORα in a transactivation assay. The symbol * marks perfectly identical residues.

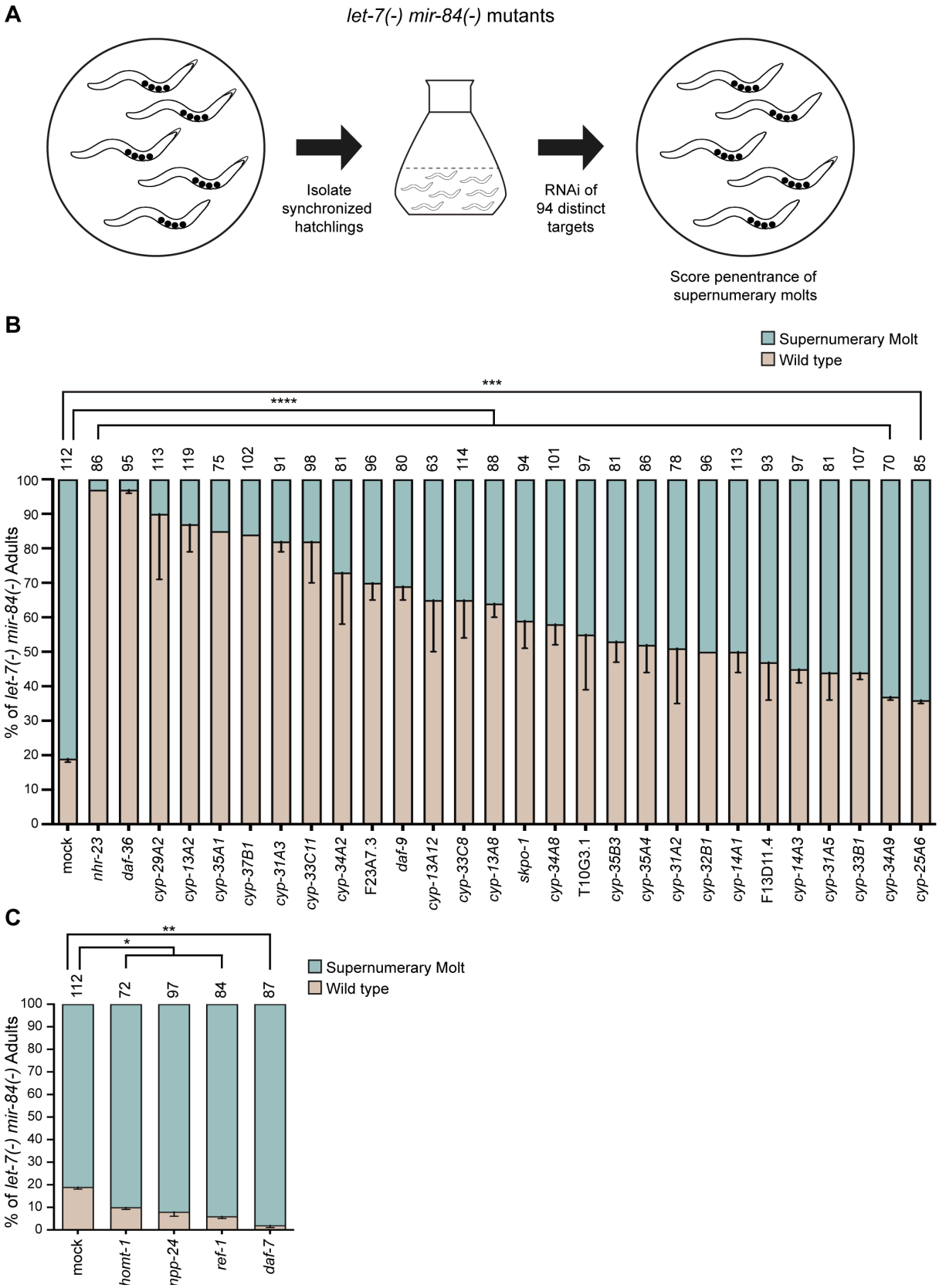
A
let-7(-) mir-84(-) mutants
Isolate synchronized hatchlings
RNAi of 94 distinct targets
Score penentrance of supernumerary molts
B
Supernumerary Molt
Wild type
***
****
% of let-7(-) mir-84(-) Adults
112 86 95 113 119 75 102 91 98 81 96 80 63 114 88 94 101 97 81 86 78 96 113 93 97 81 107 70 85
mock
nhr-23
daf-36
cyp-29A2
cyp-13A2
cyp-35A1
cyp-37B1
cyp-31A3
cyp-33C11
cyp-34A2
F23A7.3
daf-9
cyp-13A12
cyp-33C8
cyp-13A8
skpo-1
cyp-34A8
T10G3.1
cyp-35B3
cyp-35A4
cyp-31A2
cyp-32B1
cyp-14A1
F13D11.4
cyp-14A3
cyp-31A5
cyp-33B1
cyp-34A9
cyp-25A6
C
**
*
Supernumerary Molt
Wild type
% of let-7(-) mir-84(-) Adults
112 72 97 84 87
mock
homt-1
npp-24
ref-1
daf-7

Figure 3. An RNAi screen uncovers modifiers of extra molts in *let-7(mg279) mir-84(tm1304)* mutants. **A)** Experimental design for isolating genes that suppress or enhance the supernumerary molt phenotype of *let-7(mg279) mir-84(tm1304)* mutants. **B)** Knockdown of the indicated genes significantly suppressed the supernumerary molts of *let-7(mg279) mir-84(tm1304)* mutants. Graph depicts the percentage of *let-7(mg279) mir-84(tm1304)* adults, fed bacterial clones that express dsRNAs complementary to the indicated gene, that were detected as either undergoing a molt or superficially wild type. Error bars represent the mean minus s.d. from two independent trials, with cumulative sample sizes indicated above the chart. ****$p<0.0001$, ***$p<0.001$ chi-square test. **C)** Knockdown of the indicated genes significantly enhanced the supernumerary molt phenotype of *let-7(mg279) mir-84(tm1304)* mutants. Graph is the same as described in B. **$p<0.01$, *$p<0.05$, chi-square test.

Table 1. List of genes that prevent or promote supernumerary molts of *let-7(mg279) mir-84(tm1304)* mutants.

SUPPRESSORS OF SUPERNUMERARY MOLTS										
Gene	TRIAL 1			TRIAL 2			%WT (WEIGHTED AVG)	%SM (WEIGHTED AVG)	N (BOTH TRIALS)	P-value
	% WT	% SM	N	% WT	% SM	N				
mock	20	80	25	18	82	87	19	81	112	n.s.
nhr-23	96	4	25	97	3	61	97	3	86	<0.0001
daf-36	95	5	19	97	3	76	97	3	95	<0.0001
cyp-29A2	38	62	13	97	3	100	90	10	113	<0.0001
cyp-13A2	68	32	19	91	9	100	87	13	119	<0.0001
cyp-35A1	86	14	14	85	15	61	85	15	75	<0.0001
cyp-37B1	84	16	25	84	16	77	84	16	102	<0.0001
cyp-31A3	88	12	17	81	19	74	82	18	91	<0.0001
cyp-33C11	59	41	22	88	12	76	82	18	98	<0.0001
cyp-34A2	100	0	19	65	35	62	73	27	81	<0.0001
F23A7.3	56	44	9	71	29	87	70	30	96	<0.0001
daf-9	75	25	20	67	33	60	69	31	80	<0.0001
cyp-13A12	30	70	10	72	28	53	65	35	63	<0.0001
cyp-33C8	36	64	14	69	31	100	65	35	114	<0.0001
cyp-13A8	50	50	8	65	35	80	64	36	88	<0.0001
skpo-1	41	59	17	62	38	77	59	41	94	<0.0001
cyp-34A8	44	56	16	61	39	85	58	42	101	<0.0001
T10G3.1	83	17	23	46	54	74	55	45	97	<0.0001
cyp-35B3	40	60	15	56	44	66	53	47	81	<0.0001
cyp-35A4	69	31	16	49	51	70	52	48	86	<0.0001
cyp-31A2	86	14	14	44	56	64	51	49	78	<0.0001
cyp-32B1	50	50	10	50	50	86	50	50	96	<0.0001
cyp-14A1	37	63	19	52	48	94	50	50	113	<0.0001
F13D11.4	26	74	19	53	47	74	47	53	93	<0.0001
cyp-14A3	53	47	19	44	56	78	45	55	97	<0.0001
cyp-31A5	64	36	11	41	59	70	44	56	81	<0.0001
cyp-33B1	48	52	21	43	57	86	44	56	107	<0.0001
cyp-34A9	38	62	13	37	63	57	37	63	70	<0.0001
cyp-25A6	33	67	12	37	63	73	36	64	85	<0.001

ENHANCERS OF SUPERNUMERARY MOLTS										
Gene	TRIAL 1			TRIAL 2			WT (WEIGHTED AVG)	SM (WEIGHTED AVG)	N (BOTH TRIALS)	P-value
	% WT	% SM	N	% WT	% SM	N				
homt-1	11	89	9	10	90	63	10	90	72	<0.05
ZK177.4	4	96	23	9	91	74	8	92	97	<0.05
ref-1	7	93	14	6	94	70	6	94	84	<0.01
daf-7	0	100	18	3	97	69	2	98	87	<0.01

Table 1. List of genes that prevent or promote the supernumerary molts of *let-7(mg279) mir-84(tm1304)* mutants. Column 1 shows the gene targeted by RNAi; mock-treated animals were used as the negative control. The orange (columns 2 and 5) and green columns (columns 3 and 6) show the percentage of adults detected as wild type or in a molt, respectively, for each trial. The weighted average in percentage of wild-type and molting adults across both trials are shown in columns 9 and 10, respectively—the same values are plotted in graphs in Figures 3C and D. "N" denotes the sample size for each trial (columns 5 and 8), or the cumulative sample size (column 11). A chi-square test was used to compute p-values for pairwise comparisons between animals treated with dsRNAs complementary to a candidate gene versus animals that were treated with control bacteria.

Table 2. Expression profiles and putative homologs of hits from RNAi screen for suppressors of supernumerary molts.

Gene	Accession Number	Site of Expression	Cyclical Expression (Y/N)	Function	*D. melongaster*				*H. sapiens*				
					Gene	Accession	E-value	Function	Gene	Accession	E-value	Function	Diseases
daf-36	C12D8.5	XXXL/XXXR, intestine, seam cells, hypodermis	N	Conversion of cholesterol to 7-dehydrocholesterol	neverland	NP_001097670.1	6E-70	Synthesis of ecdysone	-				
cyp-29A2	T19B10.1	Body wall muscle, head neurons, hypodermis, intestine, pharynx, tail neuron	Y	-	Cyp4c3	NP_524598.1	8E-105	-	CYP4V2	NP_997235.3	5E-97	Metabolism of fatty acid precursors into polyunsaturated fatty acids	Bietti crystalline corneoretinal dystrophy
cyp-13A2	T10B9.7	-	Y	-	Cyp6a18	NP_001287562.1	4E-49	-	TBXAS1	NP_001052.3	2E-62	Converts prostglandin H2 to thromboxane A2	Stroke, cardiovascular disease
cyp-35A1	C03G6.14	-	N	Metabolism of xenobiotics	Cyp18a1	NP_728191.1	2E-37	Degradation of ecdysone	CYP2C8	NP_001185784.1	9E-59	Synthesis of 17beta-estradiol and estrone	Congenital Adrenal Hyperplasia
cyp-37B1	F28G4.1	Intestine, phasmid neuron	N	Defense against bacterial infections	Cyp4c3	NP_524598.1	3E-123	-	CYP4V2	NP_997235.3	5E-123	Metabolism of fatty acid precursors into polyunsaturated fatty acids	Bietti crystalline corneoretinal dystrophy
cyp-31A3	Y17G9B.3	Gonad, oocyte	N	-	Cyp4c3	NP_524598.1	8E-131	-	CYP4V2	NP_997235.3	7E-144	Metabolism of fatty acid precursors into polyunsaturated fatty acids	Bietti crystalline corneoretinal dystrophy
cyp-33C11	Y49C4A.9	Pan-neuronal in embryo	N	-	Cyp18a1	NP_728191.1	1E-74	Degradation of ecdysone	CYP2C8	NP_001185784.1	9E-81	Synthesis of 17beta-estradiol and estrone	Congenital Adrenal Hyperplasia
cyp-34A2	T10H4.11	-	Y	-	Cyp18a1	NP_728191.1	4E-46	Degradation of ecdysone	CYP2C8	NP_001185784.1	3E-72	Synthesis of 17beta-estradiol and estrone	Congenital Adrenal Hyperplasia
	F23A7.3	Coelomyocyte, ventral nerve cord, neurons	N	-	-				-				

Gene	Accession Number	Site of Expression	Cyclical Expression (Y/N)	Function	*D. melongaster*				*H. sapiens*				
					Gene	Accession	E-value	Function	Gene	Accession	E-value	Function	Diseases
daf-9	T13C5.1	XXXL/XXXR, hypodermis, head neurons, vulval muscle, spermatheca	N	-	Cyp18a1	NP_728191.1	3E-52	Degradation of ecdysone	CYP2W1	NP_060251.2	1E-61	-	Hereditary spastic paraplegia, lung cancer and rickets
cyp-13A12	F14F7.3	Marginal cell	N	-	Cyp9C1	NP_523850.1	8E-53	-	CYP3A4	NP_059488.2	4E-71	-	-
cyp-33C8	R08F11.3	-	Y	-	Cyp18a1	NP_728191.1	3E-75	Degradation of ecdysone	CYP2J2	NP_000766.2	2E-86	Metabolism of polyunsaturated fatty acids	Cardiovascular disease
cyp-13A8	T10B9.4	-	N	-	Cyp6a8	NP_523749.2	8E-47	-	CYP3A4	NP_059488.2	1E-68	-	-
skpo-1	F49E12.1	-	N	Defense against bacterial infections	Pxn	NP_001260573.1	7E-115	Basement membrane synthesis, collagen fibril organization, ECM organization	PXDN	NP_036425.1	2E-109	Peroxidase, secreted into ECM, matrix assembly	Ocular anomalies, microphthalmia
cyp-34A8	B0213.14	-	Y	-	Cyp18a1	NP_728191.1	5E-51	Degradation of ecdysone	CYP2A6	NP_000753.3	3E-74	Metabolism of xenobiotics	-
	T10G3.1	OLL, PVD	N	-	-				-				
cyp-35B3	K07C6.2	-	N	-	Cyp18a1	NP_728191.1	2E-37	Degradation of ecdysone	CYP2C8	NP_001185784.1	4E-61	Synthesis of 17beta-estradiol and estrone	Congenital Adrenal Hyperplasia
cyp-35A4	C49G7.8	-	Y	-	Cyp18a1	NP_728191.1	6E-39	Degradation of ecdysone	CYP2C8	NP_001185784.1	6E-39	Synthesis of 17beta-estradiol and estrone	Congenital Adrenal Hyperplasia

Gene	Accession Number	Site of Expression	Cyclical Expression (Y/N)	Function	*D. melongaster*				*H. sapiens*				
					Gene	Accession	E-value	Function	Gene	Accession	E-value	Function	Diseases
cyp-31A2	H02I12.8	Motor neurons in embryos	N	-	Cyp4c3	NP_524598.1	8E-133	-	CYP4V2	NP_997235.3	1E-144	Metabolism of fatty acid precursors into polyunsaturated fatty acids	Bietti crystalline corneoretinal dystrophy
cyp-32B1	Y5H2B.5	-	N	-	Cyp4c3	NP_524598.1	7E-105	-	CYP4V2	NP_997235.3	1E-120	Metabolism of fatty acid precursors into polyunsaturated fatty acids	Bietti crystalline corneoretinal dystrophy
cyp-14A1	K09A11.2	-	Y	-	Cyp18a1	NP_728191.1	2E-51	Degradation of ecdysone	CYP2C8	NP_001185784.1	5E-79	Synthesis of 17beta-estradiol and estrone	Congenital Adrenal Hyperplasia
	F13D11.4	-	Y	-	Uxs	NP_648182.1	0.00002	UDP-glucuronate decarboxylase activity	NSDHL	NP_001123237.1	3E-13	Biosynthesis of cholesterol	-
cyp-14A3	K09A11.4	PVT, head neuron, intestine, tail neuron, nervous system	N	-	Cyp18a1	NP_728191.1	1E-54	Degradation of ecdysone	CYP2J2	NP_000766.2	2E-78	Metabolism of polyunsaturated fatty acids	Cardiovascular disease
cyp-31A5	Y62E10A.15	-	N	-	Cyp4c3	NP_524598.1	1E-51	-	CYP4V2	NP_997235.3	1E-62	Metabolism of fatty acid precursors into polyunsaturated fatty acids	Bietti crystalline corneoretinal dystrophy
cyp-33B1	C25E10.2	-	N	-	Cyp18a1	NP_728191.1	3E-54	Degradation of ecdysone	CYP2C8	NP_001185784.1	2E-69	Synthesis of 17beta-estradiol and estrone	Congenital Adrenal Hyperplasia
cyp-34A9	B0213.15	Intestine	Y	-	Cyp18a1	NP_728191.1	2E-46	Degradation of ecdysone	CYP2A6	NP_000753.3	3E-66	Metabolism of xenobiotics	-
cyp-25A6	K06B9.1	-	Y	-	Cyp6a18	NP_001287562.1	2E-23	-	CYP3A4	NP_059488.2	8E-19	-	-

Table 2. Expression profiles and putative homologs of hits from RNAi screen for suppressors of supernumerary molts. Column 1 lists the gene name and Column 2 shows the WormBase WS274 accession number. Column 3 shows the tissue of expression and Column 5 shows functions of the protein product – known or predicted – as listed in WormBase WS274. A "Y" in Column 4 indicates that the gene is known to undergo cyclical expression; an "N" indicates that it is not (Hendriks et al., 2014; Kim et al., 2013). Columns 6 and 10 shows putative homologs in *D. melanogaster* and *H. sapiens*, respectively, detected by BLASTP searches and listed in WormBase 274. Related E-values are listed in Columns 8 and 12. Columns 7 and 11 show the RefSeq accession number of the protein product encoded by each predicted homolog in fly and human, respectively. Column 9 lists functions of the putative fly homolog, as listed in FlyBase FB2020_01. Columns 13 and 14 list the functions and diseases associated with the putative human homolog, as listed in GeneCards version 4.13.

Table 3. Candidate genes uncovered from a forward genetic screen for adults that molt.

Strain Name		Penetrance of Supernumerary molts (%)		Allele Name	Candidate Genes
Original Isolate	1x out-cross	Original Isolate	1x out-cross		
GR1490	RA08	79	38	*aaa7*	*alg-1*, K04C1.5, *ram-5*
GR1554	RA19	60	67	*aaa10*	*alg-1*
GR1498	RA25	81	32	*aaa11*	*rpt-3*, *hmg-4*, *pat-2*
GR1480	RA33	60	49	*aaa16*	*ain-1*
GR1487	RA35	-	61	*aaa17*	*cbs-2*, Y94A7B.11
GR1491	RA37	58	61	*aaa18*	F21H7.2
GR1502	RA41	13	25	*aaa19*	*nhl-2*, *mdt-30*, *mdt-29*, C30A5.10, *emb-9*, *dcn-1*, *alx-1*

Table 3. Candidate genes uncovered from a forward genetic screen for adults that molt. Columns 1 lists the name of the original isolate and Column 2 lists the name of the strain obtained after one outcross. Column 3 lists the percentage of gravid animals that were molting – i.e. expressing the *mlt-10p::gfp-PEST* transcriptional reporter in the epidermis or quiescent or bagging – for the original isolate. Column 4 lists the same metric for the outcrossed strain. Column 5 lists allele names that were assigned to mutations that cause the supernumerary molt phenotype. Column 6 lists all genes with missense and nonsense mutations within genomic regions that had a negligible frequency of recombination.

MATERIALS AND METHODS

Working with *C. elegans*

C. elegans were cultivated, preserved, observed, and transformed using standard methods (Stiernagle, 2006). Strains were cultivated at 20°C unless otherwise specified. Newly-hatched worms were developmentally synchronized by passage through starvation-induced, L1-stage diapause. Briefly, eggs were isolated by lysis of gravid hermaphrodites in sodium hypochlorite, suspended in M9 buffer supplemented with 5 µg/mL cholesterol, and incubated for 24 h with rotational aeration. Hatchlings were then plated on solid nematode growth medium (NGM) seeded with *Escherichia coli* strain OP50-1 or HT115(DE3), as indicated. To culture animals in the absence of supplementary cholesterol, hatchlings were plated on NGM plates lacking cholesterol, but containing an equivalent concentration of ethanol. Fifteen to twenty-five hatchlings were routinely plated on 24-well NGM plates supplemented with isopropyl β-D-1-thiogalactopyranoside (IPTG, Laguna Scientific); thirty to forty hatchlings on 6-well NGM plates; one to two hundred hatchlings on 6 cm NGM plates; and ten to fifteen thousand hatchlings on 10 cm NGM plates seeded with 10-fold concentrated bacteria.

To determine the extent to which cholesterol supplementation in the culture media was necessary for supernumerary molts of *let-7(mg279) mir-84(tm1304)* mutants, 6 cm NGM plates supplemented with 8 mM IPTG and seeded with *E. coli* HT115(DE3) were used.

To score the penetrance of lethargy among synchronized populations of *wgIs43[nhr-23^{++}]* and wild-type adults, 10 cm NGM plates seeded with *E. coli* OP50-1 were used. Vehicle-only control plates were seeded with cultures of OP50-1 that had been washed thrice with M9 buffer.

Pharmacological inhibition of ROR

To determine the effect of inverse agonists of ROR, SR1001 and SR2211 (Sigma-Aldrich) on the penetrance of supernumerary molts, 6-well NGM plates supplemented with 8 mM IPTG and seeded with *E. coli* HT115(DE3) were used. Synchronized hatchlings were plated on media that either contained 5 uM SR1001, 10 uM SR2211 or an equivalent concentration of DMSO, based on prior reports of studies on ROR (Kumar et al., 2012; Solt et al., 2011).

Detection and characterization of supernumerary lethargi and molts

To score quiescence among populations of young adults, synchronized hatchlings were released from starvation-induced diapause by plating on 10-fold concentrated lawns of *E. coli* OP50-1 at a density of 200-400 worms per 10 cm NGM plate. For each strain of interest, four distinct clutches were plated at 12 h intervals, facilitating the later evaluation of time samples covering a 72-h interval. As described, worms were observed by light microscopy and scored as quiescent or active at regular 3 h intervals, 72 to 120 h post-release from diapause.

To score the penetrance of supernumerary molts among populations of adults, synchronized hatchlings were plated on either 6-well NGM plates or 6 cm NGM plates supplemented with 8 mM IPTG. Each well of the 6-well plate either had SR1001/SR2211 or DMSO; each 6 cm plate either had cholesterol or ethanol only. Gravid animals were observed by light microscopy 72 h after cultivation and scored as undergoing a molt if they were quiescent, bagging or trapped in cuticle.

Comparison between amino acid sequences of the LBDs of NHR-23 and ROR

The amino acid sequence of NHR-23 Isoform A (C01H6.5a) was retrieved from WormBase WS274. The amino acid sequence of RORA Isoform 1 was retrieved from UniProt KB (Accession Number P35398-2). The LBD was annotated by comparison with known ligand-binding domains of nuclear hormone receptors using the Conserved Domain Database (Marchler-Bauer et al., 2015). Then, the LBDs of both NHR-23 and RORA were aligned using Clustal Omega (Madeira et al., 2019). The resulting alignments were evaluated by directed inspection of the sequences and refined to include obvious segments of high similarity or identity.

Targeted, RNAi-based screen for genes that restrict the number of molts

Relevant clones of *E. coli* HT115(DE3) were cultured, plated on solid NGM supplemented with 8 mM IPTG, and incubated for 24 h at 25°C, allowing for IPTG-induced expression of dsRNAs. The following 92 genes were targeted by RNA-interference: 69 of the 81 known *C. elegans* P450s, including predicted homologs of genes encoding distinct enzymes that catalyze synthesis of dafachronic acid, ecdysone, estrogen, progesterone, testosterone and cortisol; homologs of 4 genes that encode 3-β-hydroxysteroid dehydrogenases and homologs of 4 genes that encode 17-β-hydroxysteroid dehydrogenases; homologs of 3 genes that synthesize thyroid hormone in *Xenopus*; 4 genes that encode enzymes that synthesize melatonin (Hobert, 2013); 3 genes that encode protein products that regulate synthesis of dafachronic acid in *C. elegans*; 1 gene with a protein product that is homologous to molt-inhibiting hormone of *C. sapidus* (Uniprot ID:P55321); and 4 additional genes: *unc-13*, *npp-24*, *aha-1* and *ref-1*. Worms used as negative controls were fed bacteria transformed with the empty vector pPD129.36 (a gift from Andy Fire); positive controls were fed bacteria transformed with a derivative of the same vector with an inserted *nhr-23*

sequence. The penetrance of supernumerary molts was scored among synchronized populations of adults cultivated for 72 h after release from starvation-induced L1-diapause, either on 24-well or 6 cm plates, as previously described. Additionally, each plate was scored blind to the identity of the bacterial clone. The range of cumulative sample sizes, across two independent trials, was 63 – 124.

Information on the site of expression and homology for each genetic suppressor obtained from the screen was retrieved from Wormbase WS274. Additionally, genes that are cyclically expressed were identified from previously published RNA-Seq datasets (Hendriks et al., 2014; Kim et al., 2013). Accession Numbers were retrieved from RefSeq. The functions of putative fly and human homologs were retrieved from FlyBase FB2020_01 and GeneCards version 4.13, respectively.

Forward genetic screen for mutants that molt as sexually mature animals

Ninety mutant strains were previously isolated from a forward genetic screen for adults that re-express the *mlt-10p::gfp-pest* transcriptional reporter, which is normally only expressed in molting larvae (Russel et al., 2011). The proportion of molting adults was scored among asynchronous populations of each mutant strain. Molting adults were defined by simultaneous observation of embryos in the uterus and expression of *mlt-10p::gfp-pest* in the epidermis or partly shed cuticle over the head or bagging, which is the presence of live hatchlings within the body. For fifteen of the ninety strains, the proportion of adults that were scored as molting was at least 58%, comparable to the penetrance of supernumerary molts among asynchronous populations of mutants such as *pqn-47(mg412)* and *let-7(mg279) mir-84(tm1304)*. For one additional strain, the proportion of molting adults was only 13%, however, the phenotype persisted through two generations and

therefore the mutant was retained for further analysis. Each of the sixteen mutant strains was then outcrossed once.

Mapping and identification of potential causal mutations was done essentially as described (Doitsidou et al., 2010). Briefly, hermaphrodites from seven of the sixteen outcrossed strains were crossed to CB4856 males. F1 cross-progeny were allowed to self-fertilize. Thirty to fifty animals that were both fluorescent and gravid were picked from the F2 generation and singled onto 6 cm NGM plates. All plates were allowed to starve. Then, for each strain, F3 and F4 progeny from all plates were pooled and genomic DNA was harvested. The genomic DNA was used for library preparation followed by Whole Genome Sequencing by the BSCRC Sequencing Core (Bentley et al., 2008). The resulting dataset was analyzed using the software MAQGene (Bigelow et al., 2009). Genomic regions wherein the relative ratio of SNPs from the Bristol strain to SNPs from CB4856 strain was close to 1 were identified. Annotated genes within these regions that had either missense or nonsense mutations were prioritized for further analysis.

STATISTICAL ANALYSES

The software GraphPad Prism v8.0 was used for all statistical tests done in this chapter.

REFERENCES

Alper, S., and Kenyon, C. (2001). REF-1, a protein with two bHLH domains, alters the pattern of cell fusion in C. elegans by regulating Hox protein activity. Development *128*, 1793-1804.

Bentley, D.R., Balasubramanian, S., Swerdlow, H.P., Smith, G.P., Milton, J., Brown, C.G., Hall, K.P., Evers, D.J., Barnes, C.L., Bignell, H.R.*, et al.* (2008). Accurate whole human genome sequencing using reversible terminator chemistry. Nature *456*, 53-59.

Bigelow, H., Doitsidou, M., Sarin, S., and Hobert, O. (2009). MAQGene: software to facilitate C. elegans mutant genome sequence analysis. Nat Methods *6*, 549.

Cui, J., Shen, Y., and Li, R. (2013). Estrogen synthesis and signaling pathways during aging: from periphery to brain. Trends Mol Med *19*, 197-209.

DeMayo, F.J., Zhao, B., Takamoto, N., and Tsai, S.Y. (2002). Mechanisms of action of estrogen and progesterone. Ann N Y Acad Sci *955*, 48-59; discussion 86-48, 396-406.

Di Cara, F., and King-Jones, K. (2013). How clocks and hormones act in concert to control the timing of insect development. Curr Top Dev Biol *105*, 1-36.

Ding, L., Spencer, A., Morita, K., and Han, M. (2005). The developmental timing regulator AIN-1 interacts with miRISCs and may target the argonaute protein ALG-1 to cytoplasmic P bodies in C. elegans. Mol Cell *19*, 437-447.

Ding, X.C., and Grosshans, H. (2009). Repression of C. elegans microRNA targets at the initiation level of translation requires GW182 proteins. EMBO J *28*, 213-222.

Doitsidou, M., Poole, R.J., Sarin, S., Bigelow, H., and Hobert, O. (2010). C. elegans mutant identification with a one-step whole-genome-sequencing and SNP mapping strategy. PLoS One *5*, e15435.

Grishok, A., Pasquinelli, A.E., Conte, D., Li, N., Parrish, S., Ha, I., Baillie, D.L., Fire, A., Ruvkun, G., and Mello, C.C. (2001). Genes and mechanisms related to RNA interference regulate expression of the small temporal RNAs that control C. elegans developmental timing. Cell *106*, 23-34.

Hammell, C.M., Lubin, I., Boag, P.R., Blackwell, T.K., and Ambros, V. (2009). nhl-2 Modulates microRNA activity in Caenorhabditis elegans. Cell *136*, 926-938.

Hayes, G.D., Frand, A.R., and Ruvkun, G. (2006). The mir-84 and let-7 paralogous microRNA genes of Caenorhabditis elegans direct the cessation of molting via the conserved nuclear hormone receptors NHR-23 and NHR-25. Development *133*, 4631-4641.

Hendriks, G.J., Gaidatzis, D., Aeschimann, F., and Grosshans, H. (2014). Extensive oscillatory gene expression during C. elegans larval development. Mol Cell *53*, 380-392.

Hieb, W.F., and Rothstein, M. (1968). Sterol requirement for reproduction of a free-living nematode. Science *160*, 778-780.

Hobert, O. (2013). The neuronal genome of Caenorhabditis elegans. WormBook, 1-106.

Hyde, C.J., Elizur, A., and Ventura, T. (2019). The crustacean ecdysone cassette: A gatekeeper for molt and metamorphosis. J Steroid Biochem Mol Biol *185*, 172-183.

Kallen, J., Schlaeppi, J.M., Bitsch, F., Delhon, I., and Fournier, B. (2004). Crystal structure of the human RORalpha Ligand binding domain in complex with cholesterol sulfate at 2.2 A. J Biol Chem *279*, 14033-14038.

Kallen, J.A., Schlaeppi, J.M., Bitsch, F., Geisse, S., Geiser, M., Delhon, I., and Fournier, B. (2002). X-ray structure of the hRORalpha LBD at 1.63 A: structural and functional data that cholesterol or a cholesterol derivative is the natural ligand of RORalpha. Structure *10*, 1697-1707.

Karp, X., and Ambros, V. (2012). Dauer larva quiescence alters the circuitry of microRNA pathways regulating cell fate progression in C. elegans. Development *139*, 2177-2186.

Kim, D., Grun, D., and van Oudenaarden, A. (2013). Dampening of expression oscillations by synchronous regulation of a microRNA and its target. Nat Genet *45*, 1337-1344.

Kumar, N., Lyda, B., Chang, M.R., Lauer, J.L., Solt, L.A., Burris, T.P., Kamenecka, T.M., and Griffin, P.R. (2012). Identification of SR2211: a potent synthetic RORgamma-selective modulator. ACS Chem Biol *7*, 672-677.

Kurzchalia, T.V., and Ward, S. (2003). Why do worms need cholesterol? Nat Cell Biol *5*, 684-688.

Lee, K.J., Watson, R.D., and Roer, R.D. (1998). Molt-inhibiting hormone mRNA levels and ecdysteroid titer during a molt cycle of the blue crab, Callinectes sapidus. Biochem Biophys Res Commun *249*, 624-627.

Lee, S.S., and Schroeder, F.C. (2012). Steroids as central regulators of organismal development and lifespan. PLoS Biol *10*, e1001307.

Madeira, F., Park, Y.M., Lee, J., Buso, N., Gur, T., Madhusoodanan, N., Basutkar, P., Tivey, A.R.N., Potter, S.C., Finn, R.D*., et al.* (2019). The EMBL-EBI search and sequence analysis tools APIs in 2019. Nucleic Acids Res *47*, W636-W641.

Marchler-Bauer, A., Derbyshire, M.K., Gonzales, N.R., Lu, S., Chitsaz, F., Geer, L.Y., Geer, R.C., He, J., Gwadz, M., Hurwitz, D.I*., et al.* (2015). CDD: NCBI's conserved domain database. Nucleic Acids Res *43*, D222-226.

Markov, G.V., Tavares, R., Dauphin-Villemant, C., Demeneix, B.A., Baker, M.E., and Laudet, V. (2009). Independent elaboration of steroid hormone signaling pathways in metazoans. Proc Natl Acad Sci U S A *106*, 11913-11918.

Nes, W.D. (2011). Biosynthesis of cholesterol and other sterols. Chem Rev *111*, 6423-6451.

Reinhart, B.J., Slack, F.J., Basson, M., Pasquinelli, A.E., Bettinger, J.C., Rougvie, A.E., Horvitz, H.R., and Ruvkun, G. (2000). The 21-nucleotide let-7 RNA regulates developmental timing in Caenorhabditis elegans. Nature *403*, 901-906.

Ren, P., Lim, C.S., Johnsen, R., Albert, P.S., Pilgrim, D., and Riddle, D.L. (1996). Control of C. elegans larval development by neuronal expression of a TGF-beta homolog. Science *274*, 1389-1391.

Rottiers, V., Motola, D.L., Gerisch, B., Cummins, C.L., Nishiwaki, K., Mangelsdorf, D.J., and Antebi, A. (2006). Hormonal control of C. elegans dauer formation and life span by a Rieske-like oxygenase. Dev Cell *10*, 473-482.

Russel, S., Frand, A.R., and Ruvkun, G. (2011). Regulation of the C. elegans molt by pqn-47. Dev Biol *360*, 297-309.

Santori, F.R., Huang, P., van de Pavert, S.A., Douglass, E.F., Jr., Leaver, D.J., Haubrich, B.A., Keber, R., Lorbek, G., Konijn, T., Rosales, B.N.*, et al.* (2015). Identification of natural RORgamma ligands that regulate the development of lymphoid cells. Cell Metab *21*, 286-298.

Shi, Y.B. (2013). Unliganded thyroid hormone receptor regulates metamorphic timing via the recruitment of histone deacetylase complexes. Curr Top Dev Biol *105*, 275-297.

Solt, L.A., Kumar, N., Nuhant, P., Wang, Y., Lauer, J.L., Liu, J., Istrate, M.A., Kamenecka, T.M., Roush, W.R., Vidovic, D.*, et al.* (2011). Suppression of TH17 differentiation and autoimmunity by a synthetic ROR ligand. Nature *472*, 491-494.

Stehlin-Gaon, C., Willmann, D., Zeyer, D., Sanglier, S., Van Dorsselaer, A., Renaud, J.P., Moras, D., and Schule, R. (2003). All-trans retinoic acid is a ligand for the orphan nuclear receptor ROR beta. Nat Struct Biol *10*, 820-825.

Stiernagle, T. (2006). Maintenance of C. elegans. WormBook, 1-11.

Yochem, J., Tuck, S., Greenwald, I., and Han, M. (1999). A gp330/megalin-related protein is required in the major epidermis of Caenorhabditis elegans for completion of molting. Development *126*, 597-606.

Yoshiyama-Yanagawa, T., Enya, S., Shimada-Niwa, Y., Yaguchi, S., Haramoto, Y., Matsuya, T., Shiomi, K., Sasakura, Y., Takahashi, S., Asashima, M.*, et al.* (2011). The conserved Rieske oxygenase DAF-36/Neverland is a novel cholesterol-metabolizing enzyme. J Biol Chem *286*, 25756-25762.

CHAPTER IV

Concluding Remarks and Future Directions

This thesis has refined our understanding of the gene regulatory networks and molecules that together govern the molting cycle of *C. elegans*. In Chapter II, I described a negative feedback loop between the conserved nuclear hormone receptor NHR-23 and the *let-7* family of miRNAs that controls both the pace of the molting cycle and the total number of molts. Reciprocal interactions between NHR-23 and *let-7s*, during larval development, schedule the timing of repeated transitions from episodes of quiescence to episodes of wakefulness and vice versa. The *let-7* mediated decline in the amplitude of *nhr-23* expression, over the course of larval development, schedules the extinction of the molting cycle in adult animals.

The molting cycle timer is a complex genetic oscillator that likely consists of multiple core components. The nuclear hormone receptor NHR-25 and the transcription factor BLMP-1 are two more candidate components of the molting cycle timer. The mRNA levels of both genes cycle throughout larval development; peaks in expression of both *blmp-1* and *nhr-25* are observed 2 – 3 h after peak levels of *nhr-23* transcripts, and around the same time as peak levels of both *lin-42* and *let-7s* transcripts (Hendriks et al., 2014; Kim et al., 2013). Genetic inactivation of *nhr-25* is associated with the molting defective phenotype (Gissendanner and Sluder, 2000). Preliminary data from the Frand lab indicate that genetic inactivation of *blmp-1* by RNA-interference is also associated with molting defects. Going further, I mined the ChIP-Seq datasets of fusion genes consisting of GFP::3XFLAG fused either with NHR-23, NHR-25 or BLMP-1, generated by the modENCODE consortium (Celniker et al., 2009). ChIP-Seq signal showed that all three proteins were enriched among the upstream regulatory regions of each of the three genes, as well as *lin-42*. Thus, NHR-23, NHR-25 and BLMP-1 likely regulate their own expression, expression of each other and expression of *lin-42*. Moreover, NHR-23 and BLMP-1 likely share several target genes, as ChIP-Seq signal for both proteins were detected at forty out of a set of sixty genes (67%) that

are linked to molting and undergo cyclical expression. Therefore, I propose that feedback loops among NHR-23, NHR-25, LIN-42, BMLP-1 and *let-7s* shape the oscillatory expression curves of both core clock genes and many CCGs and thereby fine-tune the speed and rhythm of molting. In this model, NHR-23 and NHR-25 act as transcriptional activators, whereas as LIN-42 and *let-7s* act as repressors—consistent with my findings and prior reports on the activities of these molecules (Frand et al., 2005; Hada et al., 2010; Kouns et al., 2011; McCulloch and Rougvie, 2014; Perales et al., 2014; Van Wynsberghe et al., 2014). On the other hand, the function of BLMP-1 in the molting cycle timer might be dependent on the target gene, as the protein was previously reported to act both as an activator and a repressor of transcription (Su et al., 2009; Yang et al., 2015).

The molting cycle timer likely regulates the metabolism and bioenergetics of the epidermis of *C. elegans* and possibly the entire organism, analogous to the control of mammalian metabolism by components of the circadian clock (Reinke and Asher, 2019). ChIP-Seq data from the modENCODE consortium shows that NHR-23 is bound in the upstream regulatory regions of *idh-1* and *idh-2*, genes that cycle in expression throughout larval development (Celniker et al., 2009; Hendriks et al., 2014; Kim et al., 2013). Both *idh-1* and *idh-2* are predicted to encode isocitrate dehydrogenase, an enzyme that catalyzes the formation of α-Ketoglutarate. The metabolite α-Ketoglutarate promotes autophagy in adult *C. elegans* by inhibiting the TOR pathway (Chin et al., 2014). Furthermore, unpublished data from the Frand lab shows an increased expression of markers of autophagosomes during the molts. I propose that cyclical expression of isocitrate dehydrogenase might drive cycles in the level of α-Ketoglutarate in the epidermis, leading to increased autophagy in molting animals. Autophagy is one mechanism for degradation of components of the ECM that are internalized into cells (Kawano et al., 2017). It is therefore possible that increased autophagy during the molts is necessary for degradation and recycling of

components of the old cuticle. In this manner, the metabolic status of the epidermis would directly control remodeling of the ECM.

Nutrient levels could also act as an input into the molting cycle timer by controlling synthesis of hormones necessary for molting. In insects such as *Manduca sexta and Drosophila melanogaster*, the checkpoint for critical weight couples the nutritional status of the organism to molting and metamorphosis. Starvation of insects below but not above critical weight delays entry into metamorphosis. Critical weight is sensed by the insulin and TOR signaling pathways—the nutrient sensing pathways then regulate entry into a molt by controlling synthesis of the pro-molt hormones PTTH and ecdysone (Danielsen et al., 2013; Di Cara and King-Jones, 2013; Mirth and Riddiford, 2007; Nijhout et al., 2014; Rewitz et al., 2013; Yamanaka et al., 2013). A similar checkpoint for critical weight exists in *C. elegans*, wherein starvation of larvae before the checkpoint prevents entry into the molt; this phenotype can be suppressed by overexpression of DAF-9, a cytochrome P450 (Schindler et al., 2014). Interestingly, knockdown of *daf-9* suppresses the supernumerary molts of *let-7(mg279) mir-84(tm1304)* mutants, possibly because the enzyme catalyzes synthesis of a ligand for NHR-23 (Chapter III).

Another potential input to the molting cycle timer is pressure or force from the cuticle. *C. elegans* larvae grow continuously in volume during each intermolt (Knight et al., 2002). It is reasonable to speculate that the stiffness of the cuticle changes over the course of a larval stage because of growth of just the body and not the exoskeleton. A prior study proposed that *C. elegans* larvae will enter a molt only if they surpass a critical threshold in size that is typical of each larval stage (Uppaluri and Brangwynne, 2015). Although size and nutritional state of an organism are likely tightly linked, size may specifically be sensed and transduced by mechanosensory neurons that lie in close contact with both the cuticle and the epidermis (Goodman, 2006). In this model,

the mechanosensory neurons would detect pressure from the cuticle on the growing animal and signal to the epidermis, where the molting cycle timer acts. Alternatively, integrins in the plasma membrane of the epidermis itself may sense the strain or stress from the cuticle and transduce the information to the molting cycle timer. The stiffness of the extra-cellular matrix (ECM) regulates the cyclical expression of *Per2* in primary mammary epithelial cells of mice (Yang et al., 2017).

In Chapter III, I uncovered additional genes and molecules that control the onset of supernumerary molts in *C. elegans*. First, I showed that the ability of NHR-23 to promote extra molts depends upon either cholesterol itself or a derivative of cholesterol. I uncovered genes that may act in pathways that synthesize and degrade such a ligand.

The gene *lrp-2*, which is similar in sequence to mammalian low-density lipoprotein receptor related protein 1 LRP-1, was uncovered from the screen for animals that molt as adults (Monsalve, 2013). Mutants that are defective in LRP-2 activity undergo supernumerary molts. In *D. melanogaster*, Megalin, a member of the family of low-density lipoprotein receptor related proteins, endocytoses the protein Yellow and targets it for degradation (Riedel et al., 2011). I propose that in *C. elegans*, LRP-2 prevents additional molts by endocytosing and clearing the hormone for NHR-23 from the pseudocoelomic fluid.

In summary, this thesis shows that a negative feedback loop links two distinct timekeeping mechanisms: a genetic oscillator (the molting cycle timer) and an hourglass timer (the heterochronic pathway). If the principle applies broadly, then the intersection of oscillators and temporal cell-fate pathways may be a general mechanism for shut-off of developmental timers such as the segmentation clock. Conversely, molecular imbalance in core components during aging may be an explanation for the age-related deterioration of physiologic clocks like circadian clock (Weinert et al., 2001). Furthermore, I show that both sterol-based molecules and several conserved

sterol-modifying enzymes are necessary for the onset of extra molts, implying that similar molecules and genes could govern circadian rhythms in mammals.

REFERENCES

Celniker, S.E., Dillon, L.A., Gerstein, M.B., Gunsalus, K.C., Henikoff, S., Karpen, G.H., Kellis, M., Lai, E.C., Lieb, J.D., MacAlpine, D.M.*, et al.* (2009). Unlocking the secrets of the genome. Nature *459*, 927-930.

Chin, R.M., Fu, X., Pai, M.Y., Vergnes, L., Hwang, H., Deng, G., Diep, S., Lomenick, B., Meli, V.S., Monsalve, G.C.*, et al.* (2014). The metabolite alpha-ketoglutarate extends lifespan by inhibiting ATP synthase and TOR. Nature *510*, 397-401.

Danielsen, E.T., Moeller, M.E., and Rewitz, K.F. (2013). Nutrient signaling and developmental timing of maturation. Curr Top Dev Biol *105*, 37-67.

Di Cara, F., and King-Jones, K. (2013). How clocks and hormones act in concert to control the timing of insect development. Curr Top Dev Biol *105*, 1-36.

Frand, A.R., Russel, S., and Ruvkun, G. (2005). Functional genomic analysis of C. elegans molting. PLoS Biol *3*, e312.

Gissendanner, C.R., and Sluder, A.E. (2000). nhr-25, the Caenorhabditis elegans ortholog of ftz-f1, is required for epidermal and somatic gonad development. Dev Biol *221*, 259-272.

Goodman, M.B. (2006). Mechanosensation. WormBook, 1-14.

Hada, K., Asahina, M., Hasegawa, H., Kanaho, Y., Slack, F.J., and Niwa, R. (2010). The nuclear receptor gene nhr-25 plays multiple roles in the Caenorhabditis elegans heterochronic gene network to control the larva-to-adult transition. Dev Biol *344*, 1100-1109.

Hendriks, G.J., Gaidatzis, D., Aeschimann, F., and Grosshans, H. (2014). Extensive oscillatory gene expression during C. elegans larval development. Mol Cell *53*, 380-392.

Kawano, S., Torisu, T., Esaki, M., Torisu, K., Matsuno, Y., and Kitazono, T. (2017). Autophagy promotes degradation of internalized collagen and regulates distribution of focal adhesions to suppress cell adhesion. Biol Open *6*, 1644-1653.

Kim, D., Grun, D., and van Oudenaarden, A. (2013). Dampening of expression oscillations by synchronous regulation of a microRNA and its target. Nat Genet *45*, 1337-1344.

Knight, C.G., Patel, M.N., Azevedo, R.B., and Leroi, A.M. (2002). A novel mode of ecdysozoan growth in Caenorhabditis elegans. Evol Dev *4*, 16-27.

Kouns, N.A., Nakielna, J., Behensky, F., Krause, M.W., Kostrouch, Z., and Kostrouchova, M. (2011). NHR-23 dependent collagen and hedgehog-related genes required for molting. Biochem Biophys Res Commun *413*, 515-520.

McCulloch, K.A., and Rougvie, A.E. (2014). Caenorhabditis elegans period homolog lin-42 regulates the timing of heterochronic miRNA expression. Proc Natl Acad Sci U S A *111*, 15450-15455.

Mirth, C.K., and Riddiford, L.M. (2007). Size assessment and growth control: how adult size is determined in insects. Bioessays *29*, 344-355.

Monsalve, G.C. (2013). Unifying mechanisms of developmental timing genetic and molecular analysis of the molting cycle timer of Caenorhabditis elegans (Los Angeles: University of California, Los Angeles,), pp. 1 online resource (xiv, 96 p.

Nijhout, H.F., Riddiford, L.M., Mirth, C., Shingleton, A.W., Suzuki, Y., and Callier, V. (2014). The developmental control of size in insects. Wiley Interdiscip Rev Dev Biol *3*, 113-134.

Perales, R., King, D.M., Aguirre-Chen, C., and Hammell, C.M. (2014). LIN-42, the Caenorhabditis elegans PERIOD homolog, negatively regulates microRNA transcription. PLoS Genet *10*, e1004486.

Reinke, H., and Asher, G. (2019). Crosstalk between metabolism and circadian clocks. Nat Rev Mol Cell Biol *20*, 227-241.

Rewitz, K.F., Yamanaka, N., and O'Connor, M.B. (2013). Developmental checkpoints and feedback circuits time insect maturation. Curr Top Dev Biol *103*, 1-33.

Riedel, F., Vorkel, D., and Eaton, S. (2011). Megalin-dependent yellow endocytosis restricts melanization in the Drosophila cuticle. Development *138*, 149-158.

Schindler, A.J., Baugh, L.R., and Sherwood, D.R. (2014). Identification of late larval stage developmental checkpoints in Caenorhabditis elegans regulated by insulin/IGF and steroid hormone signaling pathways. PLoS Genet *10*, e1004426.

Su, S.T., Ying, H.Y., Chiu, Y.K., Lin, F.R., Chen, M.Y., and Lin, K.I. (2009). Involvement of histone demethylase LSD1 in Blimp-1-mediated gene repression during plasma cell differentiation. Mol Cell Biol *29*, 1421-1431.

Uppaluri, S., and Brangwynne, C.P. (2015). A size threshold governs Caenorhabditis elegans developmental progression. Proc Biol Sci *282*, 20151283.

Van Wynsberghe, P.M., Finnegan, E.F., Stark, T., Angelus, E.P., Homan, K.E., Yeo, G.W., and Pasquinelli, A.E. (2014). The Period protein homolog LIN-42 negatively regulates microRNA biogenesis in C. elegans. Dev Biol *390*, 126-135.

Weinert, H., Weinert, D., Schurov, I., Maywood, E.S., and Hastings, M.H. (2001). Impaired expression of the mPer2 circadian clock gene in the suprachiasmatic nuclei of aging mice. Chronobiol Int *18*, 559-565.

Yamanaka, N., Rewitz, K.F., and O'Connor, M.B. (2013). Ecdysone control of developmental transitions: lessons from Drosophila research. Annu Rev Entomol *58*, 497-516.

Yang, J., Fong, H.T., Xie, Z., Tan, J.W., and Inoue, T. (2015). Direct and positive regulation of Caenorhabditis elegans bed-3 by PRDM1/BLIMP1 ortholog BLMP-1. Biochim Biophys Acta *1849*, 1229-1236.

Yang, N., Williams, J., Pekovic-Vaughan, V., Wang, P., Olabi, S., McConnell, J., Gossan, N., Hughes, A., Cheung, J., Streuli, C.H.*, et al.* (2017). Cellular mechano-environment regulates the mammary circadian clock. Nat Commun *8*, 14287.